Peptide channel redesign: mutations of gramicidin A at membrane-water interface

Author: Fang Wang

Boston College

The Graduate School of Arts and Sciences

Department of chemistry

PEPTIDE CHANNEL REDESIGN: MUTATIONS OF GRAMICIDIN A AT MEMBRANE-WATER INTERFACE

a dissertation

by

FANG WANG

submitted in partial fulfillment of the requirements

for the degree of

Doctor of Philosophy

December 2012

Peptide Channel Redesign: Mutations of Gramicidin A at the Membrane-Water Interface

Fang Wang **Dr. Jianmin Gao**

Dec 14th 2012 Research Advisor

Abstract

My graduate research focuses on engineering and characterizing gramicidin A (gA), a natural fifteen-residue transmembrane channel peptide. It consists of D- and L- amino acids at alternate positions. gA is believed to fold into a β-helix in membranes, and two folded monomers at each leaflet of the lipid bilayer dimerize to form a transmembrane channel. gA shares the common features of other known membrane channels: a well defined structure that only allows the passage of specific ions, a gating mechanism, and a high abundance of aromatic residues. This dissertation includes two subprojects:

I. Understanding Channel Formation: Aromatic Modifications of Gramicidin A Channel

Ion channels are key elements in signaling and molecule transport, and therefore crucial for normal function of cells. Defective ion channels are known to be responsible for a number of diseases. Although hundreds of crystallographic structures of membrane proteins have been deposited into the PDB in the past few decades, our knowledge on this large family of proteins is still limited and mostly descriptive. Study of small peptides in model membranes is a good simplification of the more complex biological systems. In **chapter 1**, I will introduce my research using gA as a model system to understand the significant role of aromatic residues in membrane channel structure formation. Channel activities of these gA-Ar mutants were evaluated by ion leakage assays. The structure activity relationship of a library of gA mutants was discussed. The

alternating chirality of amino acids was proven to be essential for gA channel activity. Several additional interesting observations are discussed.

II. Towards Bacterium Specific Ion Channels: Solublized Gramicidin A as Potential Systemic Antibiotics

The rapid development of multidrug resistance by pathogenic bacteria poses a serious threat to society and demands new antibiotics with different mechanisms. Often considered as a model transmembrane channel, gA also has proven antibiotic activities. The gA channel facilitates passive diffusion of water and monovalent cations (e.g. H^+, Na^+, K^+) thus killing bacteria by disrupting the ion gradient across the cell membrane. However because of its poor solubility and high toxicity, its medicinal application as an antibiotic has been limited to topical reagents. A detailed understanding of gA allows rational optimization of the gA-WT to potential systemic antibiotics.

Bacterial membranes are composed of a large fraction of anionic species, therefore, we hypothesize that strategic incorporation of cationic residues into gA will afford bacterium-specific toxicities. In addition, the charged residues will greatly improve the water solubility of gA. In **chapter 2**, I will introduce my research on developing soluble and bacterium specific gA as a potential systemic antibiotic. We firstly incorporated D-Lys at the C-terminus to obtain our first generation of gA based antibiotics. The best candidate (D-Leu10,12,14D-Lys gA) shows significantly increased water solubility (~ 1, 000 times) and therapeutic index (> 50 times). Modifications on the Lys side chain were then carried out to fine tune the antibiotic activities of these cationic gA. My research has pointed out a possible strategy to convert hydrophobic membrane channel peptides into potential systemic antibiotics.

In addition to targeting the negative charges of bacterial membranes with cationic gA mutants, we proposed a novel strategy in which boronic acid is used to chase after the 1,2-diol

substructure in the PG headgroup through boronate ester formation. Polyvalent display of boronic acids on a peptide scaffold results in enhanced binding with diols, showing promise of the boronate approach in the development of bacterium specific reagents.

Acknowledgements

First of all I would like to especially thank my advisor Prof. Jianmin Gao for his education, support, and help during my Ph.D. studies. He has been always encouraging and supportive, giving me confidence and has inspired me in the research. I am so lucky to have him as my advisor. His great personality and habits as a scientist will influence me for the rest of my life.

I would like to thank the members of my thesis defense committee: Prof. Mary Roberts, Prof. Eranthie Weerapana, and Prof. Kian Tan for taking time to critically read my thesis and to attend my defense. I would like to thank Prof. Jianmin Gao again for his help in finishing my thesis.

I would like to thank Christopher Pace for carefully reviewing my thesis and for the great collaboration experience; Prof. Eranthie Weerapana for teaching me handling cells; Dr. Luoheng Qin for the help in organic synthesis; Yue for making the azatryptophan; Patrick Wong for his help in several subprojects. These nice and smart people helped me a lot in my graduate studies.

I would like to thank my parents for everything they have done for me, for their love and care during my whole life. I would to thank my husband for his love and support; my friends for their friendship.

Finally, I would like to thank all the current and past group members of the Gao lab. I have enjoyed graduate study largely because of these people around me.

Table of Contents

List of Abbreviations:

7-AW	L-7-azatryptophan
AES	Atomic emission spectroscopy
AMPs	Antimicrobial peptides
Ar	Aromatic amino acids
Arg, R	Arginine
ARS	Alizarin Red S
AW	7-azatryptophan
B. subtilis	*Bacillus. Subtilis*
Boc	tert-Butoxycarbonyl
Bpa, B	Boronophenylalanine
BSA	Bovine serum albumin
CD	Circular dichroism spectra
CL	Cardiolipin
Dab	2,4-Diaminobutyric acid
Dap	2,3-Diaminopropionic acid
DBU	1,8-Diazabicyclo[5.4.0]undec-7-ene
DCM	Dichloromethane
DIC	*N,N′*-Diisopropylcarbodiimide
DIPEA	Diisopropylethylamine
DLS	Dynamic light scattering
DMAP	4-Dimethylaminopyridine
DMF	Dimethylformamide
DMSO	Dimethylsulfoxide

DPA	Dipicolinic acid
DPC	Fos-Choline-12
dppf	1,1'-Bis(diphenylphosphino)ferrocene
E.coli	*Escherichia coli*
EDTA	Ethylenediaminetetraacetic acid
ESI	Electrospray ionization
EYPC	Egg yolk phosphatidylcholine
f4Y	tetraflurophenylalanine
FBS	Fetal bovine serum
Fmoc	Fluorenylmethyloxycarbonyl
Fmoc-Cl	Fluorenylmethyloxycarbonyl chloride
Fmoc-OSU	N-(9-Fluorenylmethoxycarbonyloxy) succinimide
gA	Gramicidin A
Gly, G	Glycine
HATU	*O*-(7-azabenzotriazol-1-yl)-*N*,*N*,*N*′,*N*′-tetramethyluronium hexafluorophosphate
HBTU	O-BenzotriazoleN,N,N’,N’-tetramethyl-uronium-hexafluoro-phosphate
HC_{50}	50% hemoglobin release from human red blood cells concentration
HEPES	4-(2-hydroxyethyl)-1-piperazineethanesulfonic acid
HOAt	1-Hydroxy-7-azabenzotriazole
HOBt	Hydroxybenzotriazole
HPTS	8-hydroxy-1, 3, 6-pyrenetrisulfonate
hRBCs	human red blood cells
KC_{50}	Half potassium release from human red blood cells

K_d	Dissociation constant
K-ISE	Potassium ion selective electrode
L/P ratio	lipid/peptides ratio
LC_{50}	50% leakage concentration
LC-MS	Liquid chromatography – mass spectrometry
Leu. L	Leucine
LP3B	lipid binding peptide with 3 PBA
LUVs	Large unilamellar vesicles
Lys, K	Lysine
MeOH	Methanol
MIC	Minimum inhibitory concentration
MOPS	3-(N-morpholino)propanesulfonic acid
MTT	3-(4,5-Dimethylthiazol-2-yl)-2,5-diphenyltetrazolium bromide
NMR	Nuclear magnetic resonance
OD	Optical density
Orn	Ornithine
Pal	Pyridyl alanine
PBA	Phenylboronic acid
PBS	Phosphate buffer solution
PC	Phosphatidylcholine
PDB	Protein data bank
PE	Phosphatidylethanolamine
pen	Pencillin
PESF	Phenylmethylsulfonyl fluoride

PG	Phosphatidylglycerol
Phe, F	Phenylalanine
pin	Pinacol
PLP	Pyridoxal 5'-phosphate
POPC	1-Palmitoyl-2-oleoylphosphatidylcholine
POPG	1-Palmitoyl-2-oleoyl-*sn*-glycero-3-phospho-(1'-*rac*-glycerol) (sodium salt)
RP-HPLC	Reverse phase – high pressure liquid chromatography
RT	Room temperature
S. aureus	*Staphylococcus aureus*
S. pyogenes	*Streptococcus pyogenes*
SAR	structure activity relationship
SBFI	Sodium-binding benzofuran isophthalate
SDS	Sodium dodecyl sulfate
SEC-HPLC	Size exclusion high performance liquid chromatography
SM	Sphingomyelin
SPPS	Solid phase peptide synthesis
strep	Streptomycin
SUVs	Small unilamellar vesicles
TES	2-[[1,3-dihydroxy-2-(hydroxymethyl)propan-2-yl]amino]ethanesulfonic acid
TFA	Trifluoroacetic acid
THF	Tetrahydrofuran
Trp	Trptophan
Tyr, Y	Tyrosine

UV	Ultra violet
Vis	Visible light
⊃	Encapsulating

List of Tables:

List of Figures:

Chapter 1. Understanding Channel Formation: Aromatic Modifications of Gramicidin A Channel

1.1 Introduction

1.1.1 Membrane channels

The cell membrane is not an inert physical barrier but rather a complex and dynamic environment that affects the functions and activities of a cell. The basic composite units of a cellular membrane include a variety of lipids, which form a diffusion barrier to ions and polar signaling molecules. Transport of these important species is facilitated by a battery of carriers and channels. Membrane carriers and ion channels are encoded by numerous gene families, comprising about 4% of the genes in the human genome. Approximately 406 genes are known to encode ion channels, and 883 to encode a broad variety of carriers, of which 350 are classified as intracellular transporters. [1] Most carriers are substrate specific and undergo a series of conformational changes to move their substrates across the lipid bilayer. Channels function by permitting the passive flow of ions across the membrane at a speed close to the diffusion limit. Ion specificities are controlled by the channel diameter or other gating mechanisms. Ion channels are found to be responsible for signaling in the nervous system, coordinating muscle contraction, and transport of messenger molecules. Defective ion channels are known to be responsible for diseases such as cystic fibrosis, renal disorders, and certain types of hypertension, osteoporosis, and conditions such as deafness and reduced sleep.[2,3] Because of their important biological functions, they have become important drug targets. In the past few decades, great efforts have been made to understand the structure, the biochemical function and mechanisms of these channels. Recent success in the crystallographic analyses of ion channels, such as the KscA potassium channel, has provided exciting insights into ion channel structures and functions.

However, it is becoming increasingly clear that the static structures obtained by crystallography may not be sufficient to represent proteins, especially the conformational changes in a functional channel.

The use of model membranes allows for simplification of the biological membrane, while still providing a dynamic environment for detailed characterization of ion channels. As recombinant membrane proteins are often difficult to be produced in its active conformation in high yield and purity, small peptide channels are also considered to be attractive models due to their simplicity in synthesis and purification.

1.1.2 Aromatic residues in membrane proteins

Long before the first high resolution structure of a membrane channel was obtained, the availability of amino acid sequences for many membrane channel proteins opened up the possibility of structural and functional studies through computational modeling and topology prediction. As the number of available structures in the Protein Data Bank increases, more is learnt through rigorous statistical analyses. In general, membrane proteins are divided into two basic structural categories: helical bundle and β-barrel. Nevertheless, membrane proteins share common characteristics of a belt of hydrophobic (mainly aliphatic) amino acids in the middle, buried in the hydrophobic core of the lipid bilayer and flanked by two "aromatic girdles" composed of tryptophan (Trp) and tyrosine (Tyr) residues around the membrane-water interfaces. This presents a hydrophobic match of the protein architecture and the membrane environment.[4,5] It has been proposed that the aromatic residues can participate in cation-π interactions, polar-polar interactions, and hydrogen bonding interactions with the lipid head-groups, water molecules, or with each other. Therefore, they can promote protein association and lock the protein structure by anchoring around the membrane-water interfaces. Mutagenesis studies have also suggested

the importance of these aromatic residues in terms of protein stability and activity.[4,6,7] In summary, aromatic residues (Trp and Tyr) appear to be important and special among the twenty natural amino acids. We intend to probe the chemical basis of aromatic residues as membrane anchors and further propose that unnatural amino acids could serve as powerful tools in this investigation.

1.1.3 Gramicidin A channel

Gramicidin is a heterogeneous mixture, with gramicidin A, B, and C making up 80%, 6% and 14% respectively. It was first identified as an antibiotic produced by a culture of *B. brevis* isolated from soil samples by Dubos et al.[8] Among the mixture, gramicidin A (gA), the peptide of interest, has fifteen amino acids, consisting of D- and L- amino acids at alternate positions (formyl-L-Val-Gly-L-Ala-D-Leu-L-Ala-D-Val-L-Val-D-Val-L-Trp-D-Leu-L-Trp-D-Leu-L-Trp-D-Leu-L-Trp-ethanolamine). It is one of the most hydrophobic sequences reported and is essentially insoluble in aqueous solution (< 50 nM). [9] In a lipid bilayer, the peptide folds into a β-helix. Due to the alternating D- and L- residues, all side chains project to the same side of the peptide strand, which, upon peptide folding, becomes the exterior of gA channel and interacts with the hydrophobic core of the bilayer. The interior of the β-helix is formed by the polar peptide backbone hydrogen bonding network. Two folded monomers in the two leaflets of a membrane bilayer dimerize to form a head-to-head transmembrane channel (Figure 1-1). This dimeric channel is stabilized by six intermolecular hydrogen bonds and the channel is gated by the association and dissociation of the monomers (Figure 1-1b).[10] The size of the channel pore (diameter about 4 Å) is only large enough to accommodate monovalent cations (Cs^+, Rb^+, K^+, Na^+, Li^+, NH_4^+, H^+) and water molecules but not cations with higher oxidation state or anions. [11,12,13]

The vertical length of the dimer is about 26 Å, which is long enough to span most lipid bilayer (Figure 1-1).[14]

Besides the β-helical channel conformation found in membranes, other conformations have been observed when the gA peptide is dissolved in a variety of organic solvents.[15,16] Among them, the most dominant and stable one is an intertwined double helix (ds-dimer), known as the non-channel conformation. This ds-dimer is stabilized by 28 intermolecular hydrogen bonds (Figure 1-2).[5] It was found that polar solvents promote the monomer formation, while the ds-dimer is favored in most nonpolar solvent.[17] Interestingly, upon binding and insertion into a lipid bilayer, the peptide conformation is determined by the solvent in which the peptide is dissolved prior to mixing with lipids. As described above, the gA channel can only be formed by the monomers. Therefore, the amount of monomers, in a peptide stock solution determines the amount of peptides available for potential channel formation.

gA has four Trp residues at positions 9, 11, 13 and 15. In the ds-dimer non-channel conformation, Trp residues are more evenly distributed along the vertical axis of the membrane whereas in the β-helical channel, Trp residues are clustered at the end of the β-helix and towards the membrane-water interface (Figure 1-2). Early studies suggested that these Trp residues were critical for maintaining the structure and function of the channels. For example, the channel conductance decreases upon substitution of one or all of the Trp residues by glycine, phenylalanine, or naphthylalanine.[17,18,19] These mutations also promote the non-channel conformation.

As described above, gA shares several important features with other channels from natural sources: (1) it possesses a well-defined structure that allows for the rapid passage of specific ions; (2) it presents a high abundance of aromatic residues, Trp to be specific, which locate at the membrane-water interfaces; (3) it has a known gating mechanism. Compared to

other membrane channels, gA offers several experimental advantages because of its small size, easy accessibility, and a well characterized structure and mechanism of action. We therefore chose gA as a model peptide, from which we learned useful information that could be applicable to the understanding of more complex membrane channels, and to future efforts in membrane channel engineering.

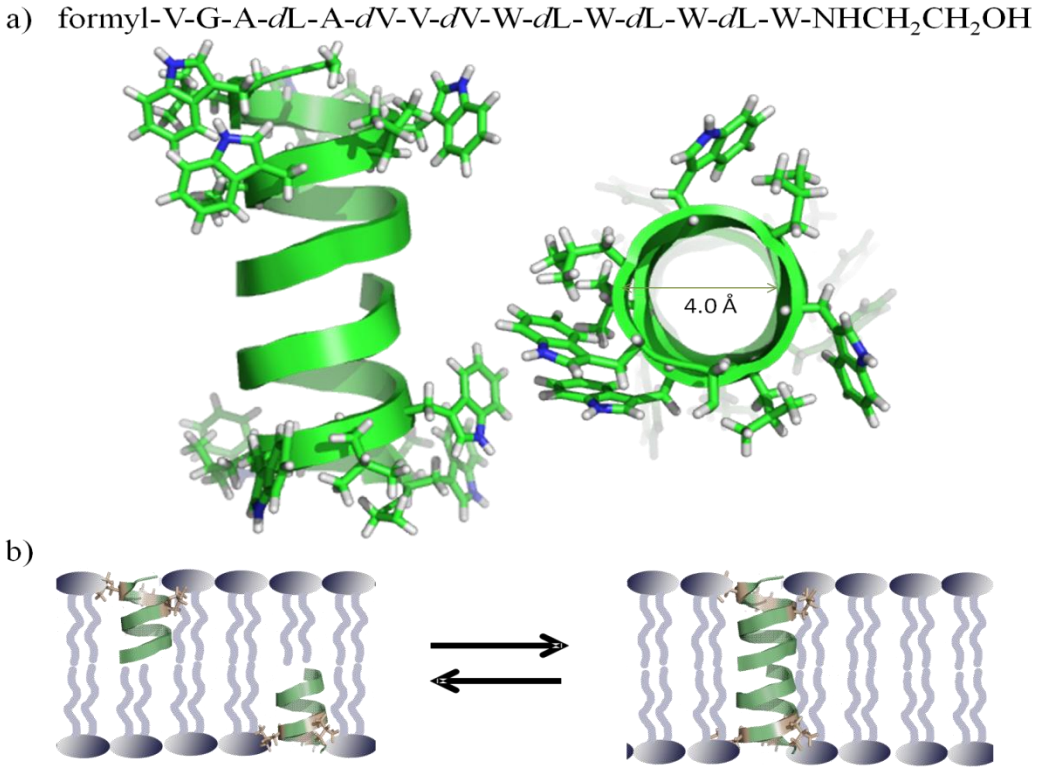

Figure 1-1. a) Sequence of gA in single letter code (the D-amino acids were labeled by the italic "*d*") and cartoon representations of the β-helical dimeric channel (bottom, PDB: 1MAG, derived from solid-state NMR data in lipid bilayer, side view on the left and top view on the right); b) the gating and channel formation equilibration. A cartoon representation showing the peptide in a lipid bilayer can be found in Figure 1-2.

Earlier studies using gA as a model peptide are rather limited, as the reported modification on gA only substituted the Trp residues with simple hydrophobic amino acids. While Trp has the largest nonpolar surface area among the twenty natural amino acids, it possesses a polar NH moiety that can serve as hydrogen bond donor. This unique amphipathic character may account for its preference for the membrane-water interface. To test our hypothesis, a series of amphipathic aromatic amino acids were chosen to be incorporated into the gA peptides. The channel activities of these gA mutants were determined by ion leakage assay. Activity comparison and detailed analyses were performed to understand the structure activity relationship of gA channel formation.

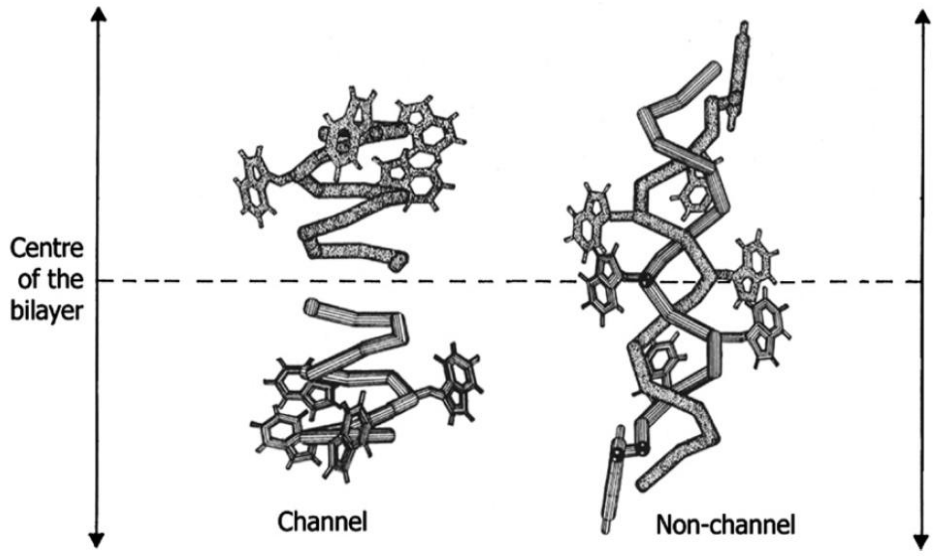

Figure 1-2. A schematic representation of the channel (β-helical dimer, left) and non-channel (intertwined double helix, ds-dimer, right) conformations of gA, indicating the location of Trp residues in a membrane bilayer. The membrane axis is represented by double headed arrows and the center of the bilayer is marked by a dotted line. The graph is reconstructed from reference 5.

1.1.4 Membrane channel characterization

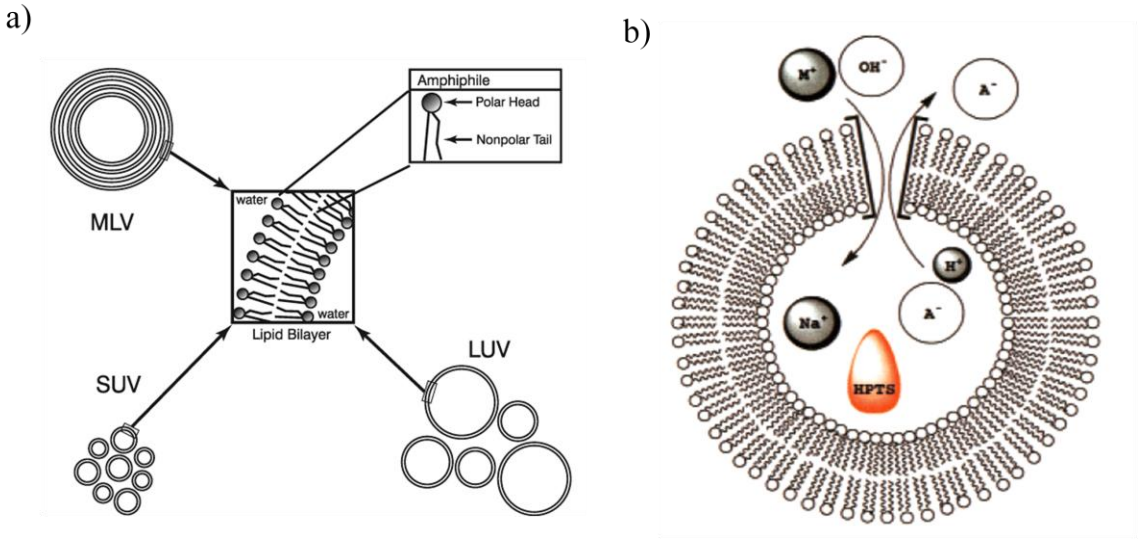

Figure 1-3. a) Schematic representations of different vesicles; b) schematic representation of ion channel leakage experiments. A pH gradient results from addition of extravesicular NaOH solution. The charge caused by H^+ efflux or OH^- influx is compensated by anion influx or proton efflux, mediated by a transmembrane channel such as gA. The increase in intravesicular pH, monitored by the entrapped pH-sensitive fluorophore, HPTS, reflects the electrolyte exchange rate. Figure b was reconstructed from reference 20.

Characterization of membrane proteins is generally more complicated then soluble ones due to peptide/protein aggregation and the heterogeneity introduced by the mixture of membranes and aqueous solution. Model membranes have been widely used as mimics of the native membrane environment. There are two main experimental approaches to the study of ion channels: vesicles and planar bilayer membranes. Vesicles (or liposomes) are prepared by dispersion of lipids in an aqueous buffer to form spherical closed-shell structures ranging from

below 20 nm to above 1 μm in diameter. They can have one (unilamellar, SUV and LUV) or more layers (multi-lamellar, MLV) of bilayer membrane(Figure 1-3a).[21] The internal aqueous volume is therefore fixed and separated from the external medium. A wide range of membrane impermeable reporters can be trapped in the interior of this robust vesicle structure. The external environment can be readily adjusted by size-exclusion gel filtration. The size of the vesicles can be dictated by the pore size of the filtering membrane, through which the vesicles pass repetitively. The vesicles can be composed of various lipids and in different ratios as designed, to mimic the lipid composition of cells of interest. [22,23]

Membrane channels promote the translocation of ions from one side of a membrane to the other. The interior volume of a typical vesicle is on the order of femtoliters, much smaller than the bulk exterior solution. Therefore gain or loss of a relatively small amount of ions is sufficient to produce a very large change in the concentration of compound inside the vesicle. Consequently, any techniques that can measure ionic concentrations on one or both sides of the vesicles can be used to determine the activity of an ion channel. Several ion selective fluorescence probes have been developed for this purpose, examples including the pH- sensitive probe HPTS (8-hydroxypyrene-1,3,6-trisulfonic acid, Figure 1-3b) and sodium sensitive probes.[20,24,25,26,27] In addition, ^{23}Na-NMR can be used to determine the translocation rate through a line-shape analysis.[28]

Planar bilayers can be formed across a small aperture in a glass barrier between two aqueous electrolyte solutions. Planar bilayer membranes are ideal for the study of the ion channel conductance using a technique known as voltage clamp, developed by Erwin Neher and Bert Sakmann in the late 1970s early 1980s . In this technique, a constant transmembrane potential is applied and the resultant current changes are monitored as a function of time (Figure 1-4). The membrane itself is a good resistor. Therefore, in the absence of an open channel, very little

current is observed. When a single ion channel opens, the ion flux in response to the applied potential produces a current in the range of pico- to nanoamps. This ‘‘opening’’ appears as a step-change in the conductance of the membrane. When an active channel ceases to function, the ionic current falls abruptly back to the baseline of the unaltered bilayer membrane. This step-change behavior is a unique and unmistakable signature of a single ion channel. The voltage clamp technique directly observes redundant ion channels individually. The collective properties of channels are assessed by statistical techniques to determine the specific conductance of the channel, its open probability, the voltage-dependence of the conductance, and the ionic selectivity of the transport. Due to the requirement of the high resistance membrane to achieve a low background signal, the lipid composition is limited to lipids with branched tails.

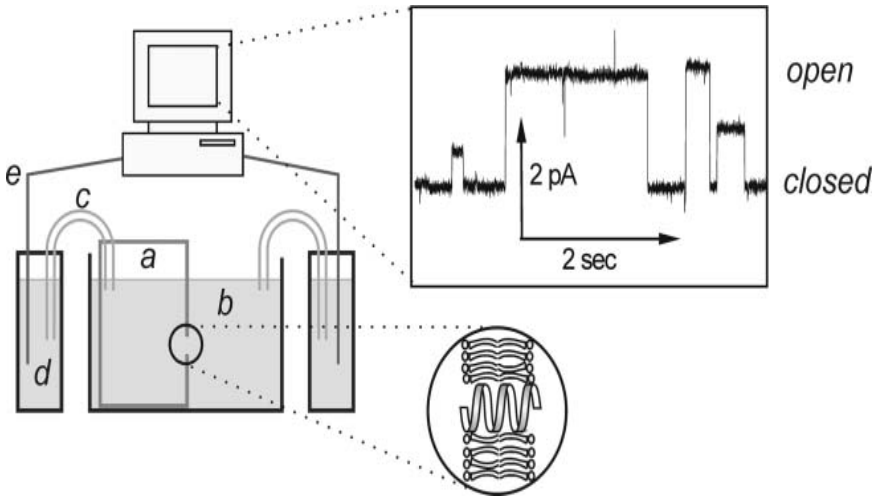

Figure 1-4. Schematic representation of a voltage clamp experiment. A cuvette (a), with a small hole cut into one face, is immersed in an electrolyte (b) and the bilayer is formed by painting lipid across the hole. Electrical contact with Ag/AgCl reference electrodes (e) in a reference electrolyte (d) is via Agar salt-bridges (c). A potential is applied and the current measured as a function of time. Channels appear as abrupt transitions. Figures reconstructed from reference 21.

In summary, the patch clamp technique focuses more on the characterization of individual ion channels embedded in the planar lipid bilayer. It requires experienced personnel, special equipments, and a low noise environment. In contrast, the vesicle-based leakage technique focuses more on the bulk properties and the average effects of thousands of channel forming molecules, and importantly the assay is much more applicable and flexible.

In my project, we are trying to identify better ion channels that can cause ion leakage and ion equilibration induced cell death more efficiently. Therefore, in the characterization of our gA mutants, the vesicles based ion leakage assay is used primarily.

1.2 Synthesis and characterization of aromatic mutations of gA channel

1.2.1 Selection of aromatic residues and peptide synthesis

A library of natural and unnatural aromatic amino acids was chosen to substitute the Trp residues in the wild-type gA. In contrast to early reported mutations, in which Trp was substituted by nonpolar amino acids (Phe, naphthylalanine, Ala, Gly), the aromatic amino acids we have tested possess amphiphilic side chains (Table 1-1). Among them, the phenylalanine modification has been heavily characterized and serves as a control peptide in our system. It was suggested that the more Trp residues were substituted with Phe, the more channel conductance decreased.[29] In our designed gA mutants, the Trp at position 15 was kept as a reporter for peptide concentration calibration, and binding constant determination. It also simplifies the peptide synthesis, as all peptides can be loaded on Fmoc-Trp-Wang resin. Substitutions of the other three Trp residues at positons 9, 11, 13 would provide a wide window for characterization and comparison. Important properties of these amino acids were calculated by computational simulation in Spartan (Table 1-1). While similar in size, these aromatic residues varied in electronic properties, which were proposed to be important for the preferential interface localization of aromatic residues.[9,30] The wild-type gA is commercially available and other mutants were synthesized through solid phase

peptide synthesis (SPPS) using the standard Fmoc/HBTU chemistry. DMF was used as solvent. The N-terminal formyl-valine was pre-made and used as a building block in SPPS. gA has one of the most hydrophobic sequences known. Linear synthesis of the whole peptide was found to be

Table 1-1. Structures and important properties of the aromatic residues used in modification

Peptide	Aromatic residues	Sovaltion energy (kJ/mol)	Dipole moment (Deby)	Log P	Dipole direction(degree)
gA-WT	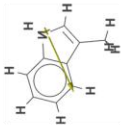 W	-26.89	1.86	1.81	110
gA-Ar-2	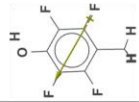 f4Y	-7.61	1.88	2.76	60
gA-Ar-3	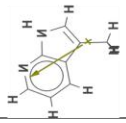 AW	-37.87	1.87	1.47	32
gA-Ar-4	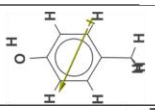 Y	-23.74	1.67	2.31	70
gA-Ar-5	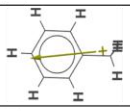 F	-2.62	0.33	2.52	8
gA-Ar-6	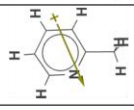 2Pal	-20.13	2.08	0.9	110
gA-Ar-7	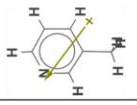 3Pal	-21.96	2.62	1.18	55
gA-Ar-8	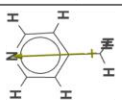 4Pal	-22.61	2.84	1.18	0

The properties were calculated by computational simulation in Sparten using the PM3 model as neutral molecules, the direction of dipole moment is represented by the angle between the dipole moment and the bond Cβ-Cγ, the dipole vector was labeled by the arrow in the amino acid structure

problematic. Except the 7-azatryptophan (AW) containing mutant (**gA-Ar-3**), a mixture of fragments was observed in the LC-MS analysis for all other gA mutants (data not shown). Therefore, a fragment condensation method was applied instead (Scheme 1-1). To be more specific, two fragments of the peptide were synthesized through SPPS, in which the N-fragment contains the first 10 amino acids (formyl-L-Val1 to D-Leu10) and the C-fragment contains the remaining five amino acids (Ar11 to Trp15-ethanolamine). The N-fragment was cleaved off the Fmoc-D-Leu Wang resin by reagent K to expose a free carboxylic acid. The C-fragment was cleaved off the resin by ethanolamine. Both fragments were then precipitated from the cleavage solution by water. The two fragments were then dissolved into a solvent of DCM/DMF (v/v: 3/1), and the amide bond formation was accomplished by using HATU/HOAt activation. When the reaction is complete, DCM was removed and the full sequence peptide was precipitated from DMF with water. The crude material was purified by RP-HPLC and confirmed by LC-MS.

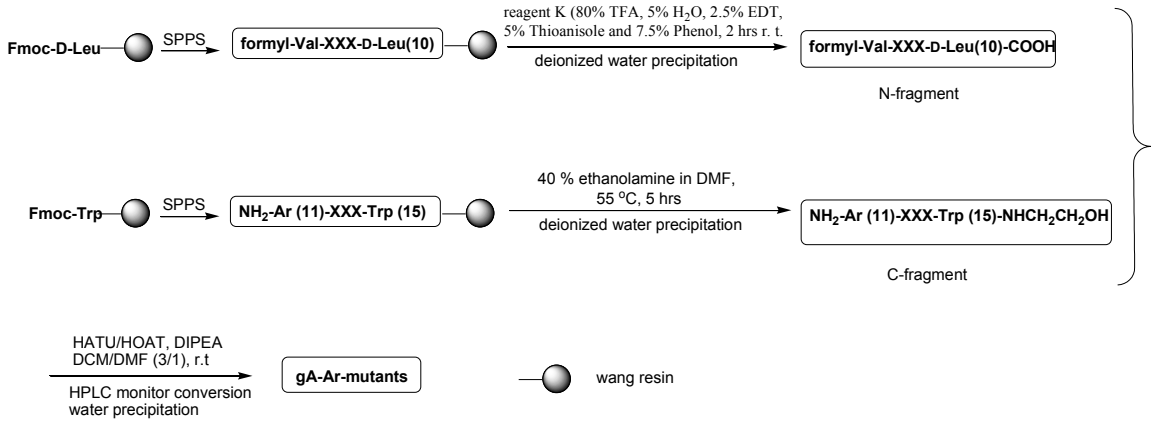

Scheme 1-1. Synthesis of gA mutants through a fragment condensation method.

There is a possibility of racemization when fragment condensation happens between two polypeptide fragments through amide bond formation between the activated carboxylic acid and

amine. To confirm the success of our method, two variants of **gA-Ar-8** with D-Leu (**gA-Ar-8**) and L-Leu (**gA-Ar-8**L) at position 10 respectively were made under the exact same conditions and analyzed with LC-MS. Racemization in our ligation reaction is negligible. The two peptides were well resolved on the C4 column (retention times 17.87 mins for **gA-Ar-8** and 19.15 mins for **gA-Ar-8**L) and only one dominant peak was observed in each reaction (Figure 1-5).

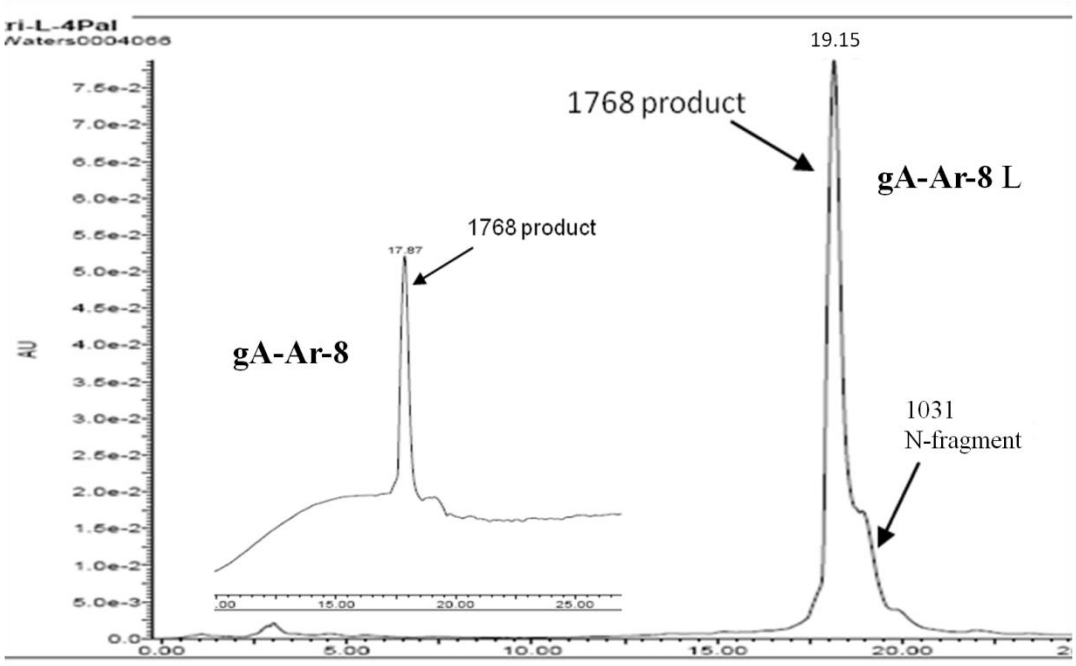

Figure 1-5. Analytical HPLC traces of the two **gA-Ar-8** variants **gA-Ar-8** (insert graph, D-Leu10) and **gA-Ar-8**L (L-Leu10). The mass of the species represented by each peak is marked in the figure.

1.2.2 Characterization of gA mutants with aromatic modifications

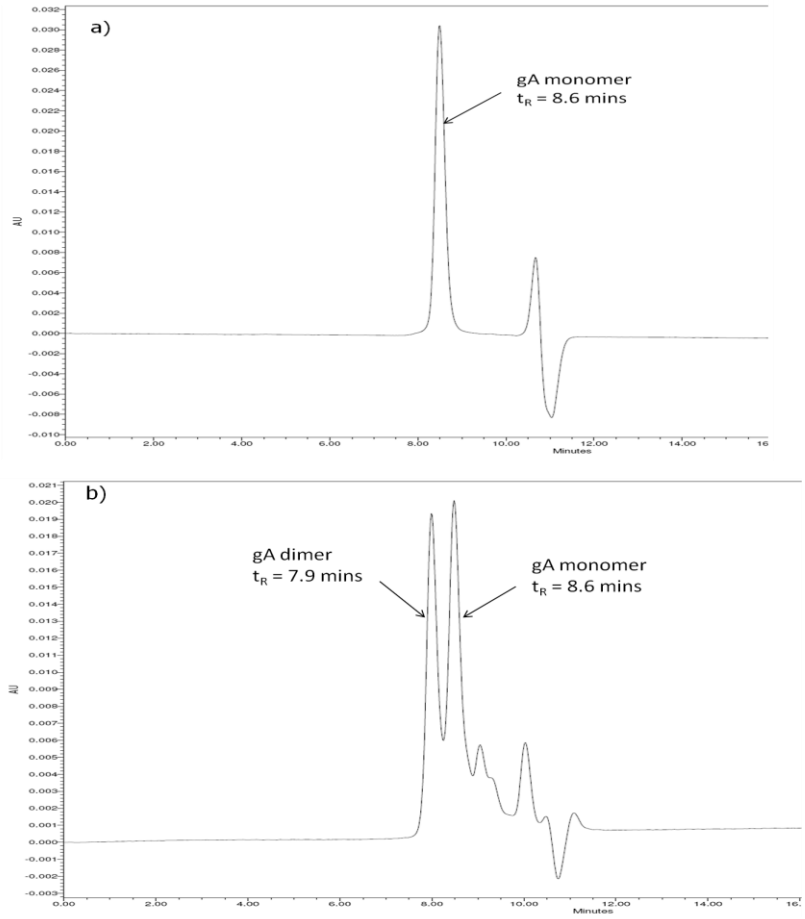

Figure 1-6. Representative SEC-HPLC traces separating the monomer and the ds-dimer (a) **gA-WT** incubated in MeOH reported as monomer; b) **gA-WT** incubated in THF for two days, reported as a mixture of monomer and dimer.

Firstly, the peptide conformation (monomer vs ds-dimer) in DMSO was determined by size exclusion high performance liquid chromatography (SEC-HPLC). A solution of a peptide in DMSO was injected onto the SEC column and then eluted with THF isochromatically with a flow rate of 1 mL/min. The interconversion between the two conformations (monomer and ds-dimer) is too slow to be noticed on the experimental time-scale.[31] The percentages of the ds-dimers and

β-helical monomers eluted from the column do not differ from the values originally present in the solution.[17] The eluting peptides were detected at two wavelengths (280 nm and 254 nm) and the relative amount was calculated by the integration area of each peak. [17] The retention time of the gA monomer and ds-dimer was calibrated by that of **gA-WT** (Figure 1-6, Table 1-2). Our results were consistent with previous reports: **gA-WT** dissolved in MeOH exists as monomers, and when **gA-WT** is incubated in THF, the peptide exists as a mixture of monomers and ds-dimers. Based on the mechanism of size exclusion chromatography, we assigned the first peak as the ds-dimer, which is larger and less likely to be trapped into the pore of the solid phase. The retention times for the ds-dimer and monomer are 7.9 minutes and 8.6 minutes respectively. In DMSO, all gA mutants we made exist as a monomer.

Table 1-2: The retention times of gA mutants off the SEC-HPLC

peptide	Retention Time (t_R/mins)	Area %	peptide	Retention Time (t_R/mins)	Area %
gA-WT	8.7	100%	**gA-Ar-5** [a]	8.8	95%
gA-Ar-2	8.7	100%	**gA-Ar-6**	8.7	100%
gA-Ar-3	8.5	100%	**gA-Ar-7**	8.6	100%
gA-Ar-4	8.5	100%	**gA-Ar-8**	8.5	100%

[a] about 5% of the ds-dimer, which had a retention time of 8 mins, was observed in the **gA-Ar-5** DMSO solution

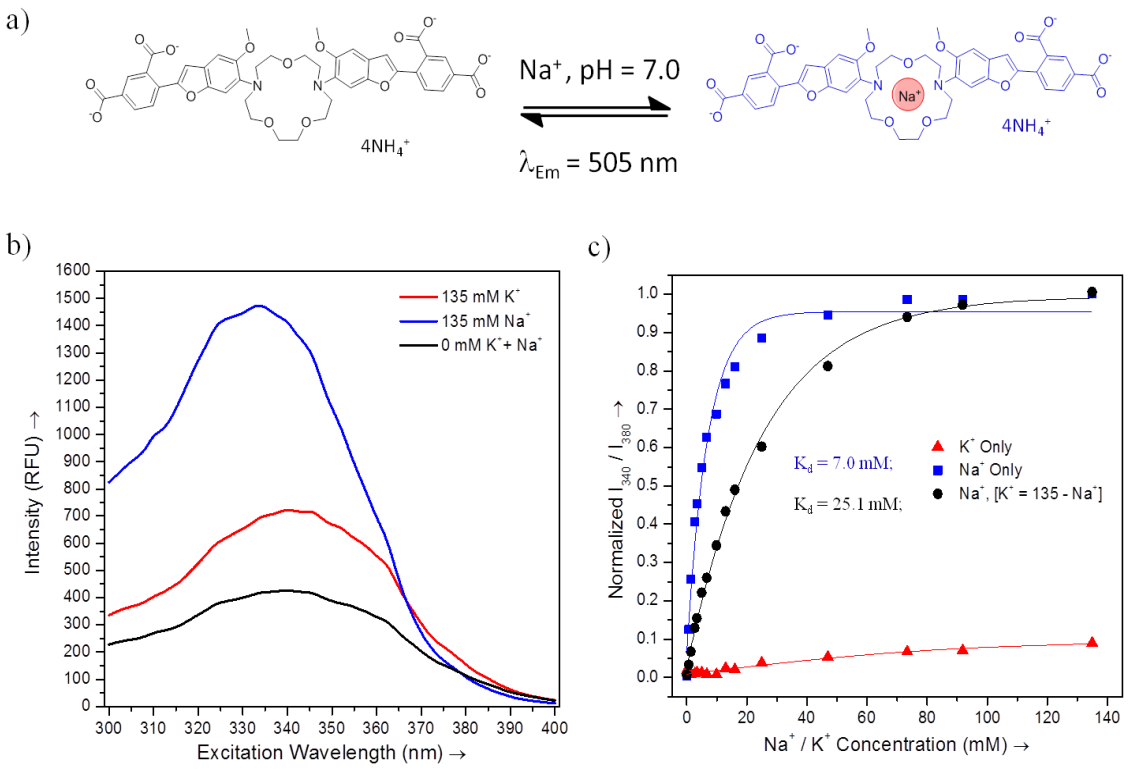

Figure 1-7. Na^+ ion detection with the sodium sensitive fluorescence probe SBFI. a) Binding mechanism of SBFI and Na^+ ion; b) Excitation spectra of SBFI (5 µM in 10 mM MOPS buffer, pH 7.05), in the absence of monovalent ions (black), in the presence of 135 mM Na^+ ions (blue) or 135 mM K^+ ions (red); c) Determination of the SBFI-Na^+ dissociation constant in absence (blue) or presence (black) of K^+ ions. The y-axis represents the fluorescence ratio of 340 nm over 380 nm in the excitation spectra(λem = 505 nm).

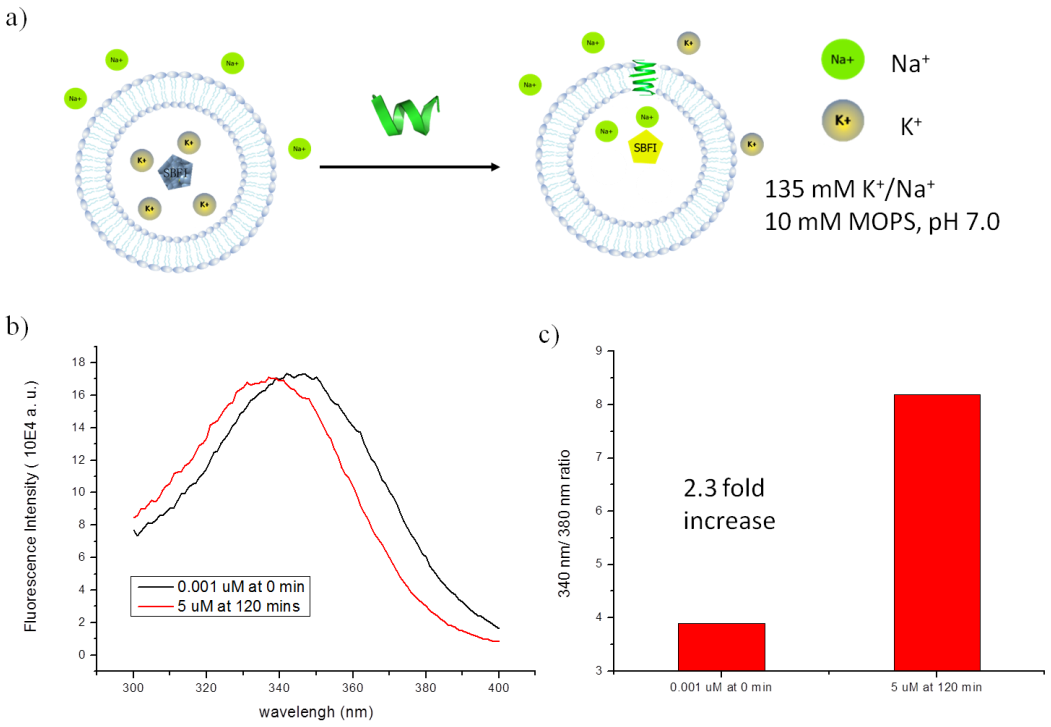

Figure 1-8. Determination of gA channel activity. a) Representative scheme of the ion leakage assay. The counter ions Cl^- are not shown in the graphs. b) fluorescence detection of Na^+ transport. Condition: 500 μM LUVs POPC ⊃ 20 μM SBFI, 135 mM KCl, 10 mM MOPS buffer, pH 7.0, in which symbol⊃ means encapsulating; outside buffer: 10 mM MOPS, 135 mM NaCl Fluorescence spectra of 1 nM (black) **gA-WT** addition (known to have no effect on liposomes) and 5 μM (red) **gA-WT** addition, which is known to induce complete ion leakage from liposome. The spectra were recorded at 505 nm; c) ratio of I_{340}/I_{380} in the excitation spectra shown in b.

To test channel activities of these gA mutants, a leakage assay was established. In the assay, a sodium sensitive fluorescent dye (SBFI, sodium-binding benzofuran isophthalate) was encapsulated inside the large unilamellar vesicles (LUVs) to report interior Na^+ concentration (Figure 1-8). SBFI (Figure 1-7a) is a membrane impermeable sodium indicator consisting of fluorophores linked to the nitrogens of a crown ether, with a cavity size that confers selectivity

for Na^+. Upon sodium binding, the excitation peak narrows significantly and blue shifted, causing a large change in the ratio of 340nm/380nm at the excitation spectra (λ_{em} = 505 nm, about 2.5 fold increases at 135 mM Na^+, Figure 1-7b). This assay provides sufficient spatial and temporal resolution of Na^+ concentration under physiological conditions.[27,31] Furthermore, the interfering effect of K^+ ion in solution was evaluated. In contrast to the Na^+ addition, the effect of 135 mM K^+ ions added to the SBFI solution is minimal (Figure 1-7c). The presence of K^+ ions only shifts the dissociation constant from 7.0 mM to 25.1 mM, which guarantees 100% occupation of SBFI when 135 mM Na^+ is used in the leakage experiments even in presence of K^+ (< 135 mM).

In the leakage assay (Figure 1-8), a solution of SBFI (20 μM and 135 mM K^+ ion in 10 mM MOPS, pH = 7.0) was encapsulated into POPC LUVs, which are suspended in a buffer containing 135 mM Na^+ (10 mM MOPS, pH = 7.0). As a result, there would be no osmotic pressure while a Na^+/K^+ ion gradient is built across the lipid bilayer. When a gA mutant is added into the solution, the active peptide binds onto the lipid bilayer and forms a channel. Upon channel formation, Na^+ ion diffuses across the lipid bilayer along the ion gradient (from the outside to the inside), and binds with the encapsulated SBFI, eliciting a shift of the SBFI fluorescence excitation spectrum (Figure 1-8b) and a 2.3 fold increase in the $I_{340}/I_{380\ nm}$ ratio (Figure 1-8c).

To further confirm the reliability of this leakage assay in terms of measuring ion diffusion through stable membrane channels, we performed the assay following two protocols with different orders of peptide addition and Na^+ ion gradient formation. Liposomes encapsulating SBFI (20 μM) and KCl (135 mM) were suspended in a MOPS buffer containing either 135 mM NaCl (system I) or 135 mM KCl (system II). In system I, a transmembrane Na^+ gradient exists before gA peptide addition. In contrast, NaCl was added to generate the transmembrane Na^+ ion gradient in system II 2 hours after the peptide addition, at which point the peptide folding and

translocation is complete. We would expect similar observations in both systems when stable channels, like **gA-WT**, are formed. In system I, **gA-WT** addition induced Na^+ ion leakage and changed the excitation spectrum. A concentration profile of **gA-WT** was generated (Figure 1-9a). In system II, however, upon peptide addition, no change in the fluorescence spectra was observed due to the absence of Na^+ ions. This result suggests that encapsulated SBFI reports Na^+ ion specifically, and a high concentration of K^+ ion does not affect the fluorescence signal. A similar concentration profile was then observed in system II upon NaCl addition (Figure 1-9b). Moreover, similar LC_{50} (the peptide concentration required to induce 50% of ion leakage) values were obtained in the two systems. If ion equilibration is only caused by membrane disturbance during peptide binding and/or translocation, there would be negligible fluorescence change in the system II.

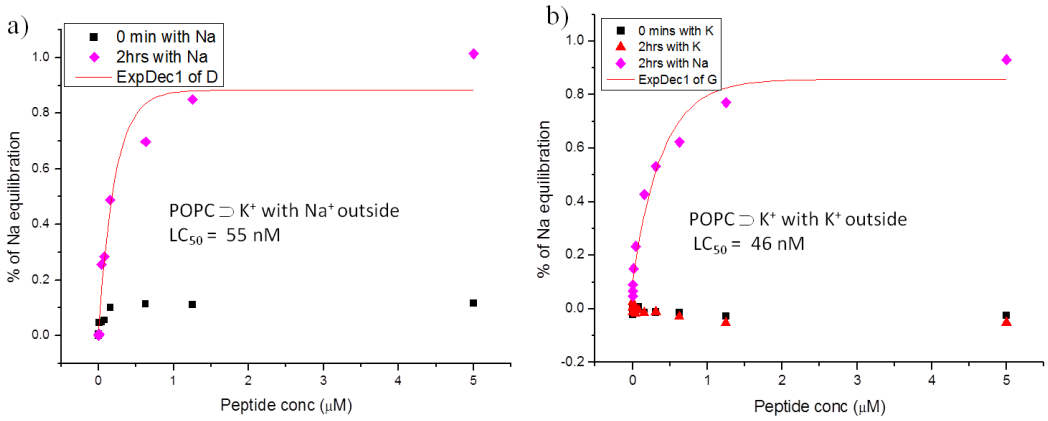

Figure 1-9. Relationship between peptide concentration (**gA-WT**) and the percentage of Na^+ ion equilibration through the transmembrane gA channel. The Na^+ ion leakage was determined in a) system I, in which Na^+ ion gradient exists before peptide addition or b) system II, in which a Na^+ ion gradient is generated 2 hours after peptide addition. LC_{50} values were obtained by fitting the concentration profile into an exponential function.

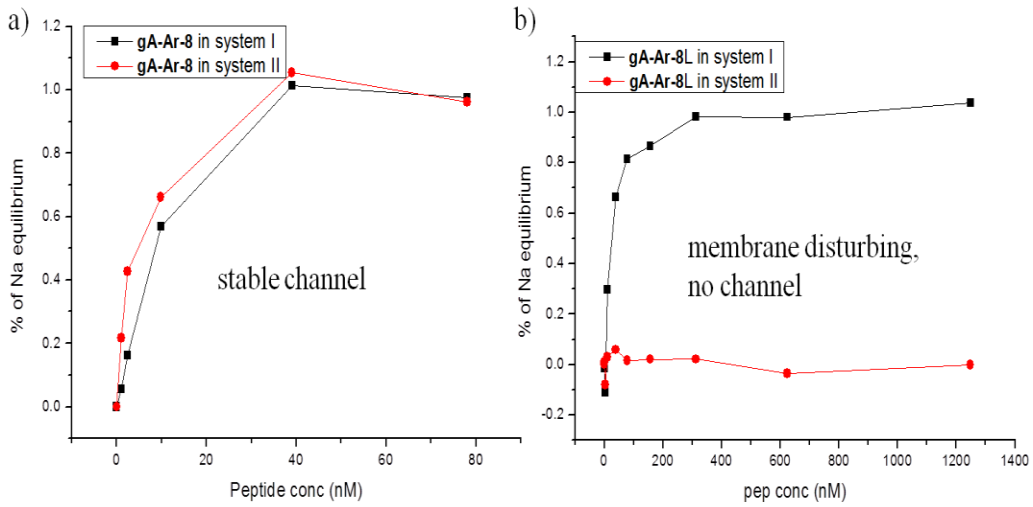

Figure 1-10. Relationship between peptide concentration and the percentage of Na^+ ion equilibration caused by **a)** a stable channel forming peptide **gA-Ar-8** and **b) gA-Ar-8**L that does not form stable β-helical channel.

The alternating D- and L- amino acids arrangement is considered to be important to gA channel formation.[4] We expect **gA-Ar-8**L (formyl-L-Val-Gly-L-Ala-D-Leu-L-Ala-D-Val-L-Val-D-Val-L-4Pal-**L-Leu**-L-4Pal-D-Leu-L-4Pal-D-Leu-L-Trp-ethanolamine) to be incapable of forming stable channels. Consistent with our expectation, no Na^+ ion equilibration is observed when **gA-Ar-8**L is added into system II. **gA-Ar-8**L only causes Na^+ ion leakage when it is added to system I, where the Na^+ ion gradient exists before the peptide addition. In contrast, similar concentration profiles were observed in both systems for **gA-Ar-8** (formyl-L-Val-Gly-L-Ala-D-Leu-L-Ala-D-Val-L-Val-D-Val-L-4Pal-**D-Leu**-L-4Pal-D-Leu-L-4Pal-D-Leu-L-Trp-ethanolamine). We concluded that Na^+ leakage caused by **gA-Ar-8**L in system I is caused by membrane disturbance due to peptide binding and/or translocation. The lack of **gA-Ar-8**L induced ion leakage in system II suggested that Na^+ ions cannot diffuse through the bilayer when no stable channel is formed, and peptide

folding and translocation are complete after 2 hours (Figure 1-10b). In summary, the leakage assay performed in system II is a reliable method to evaluate ion channel formation. It reflects the amount of stable channels formed on the vesicles instead of nonspecific membrane disturbance.

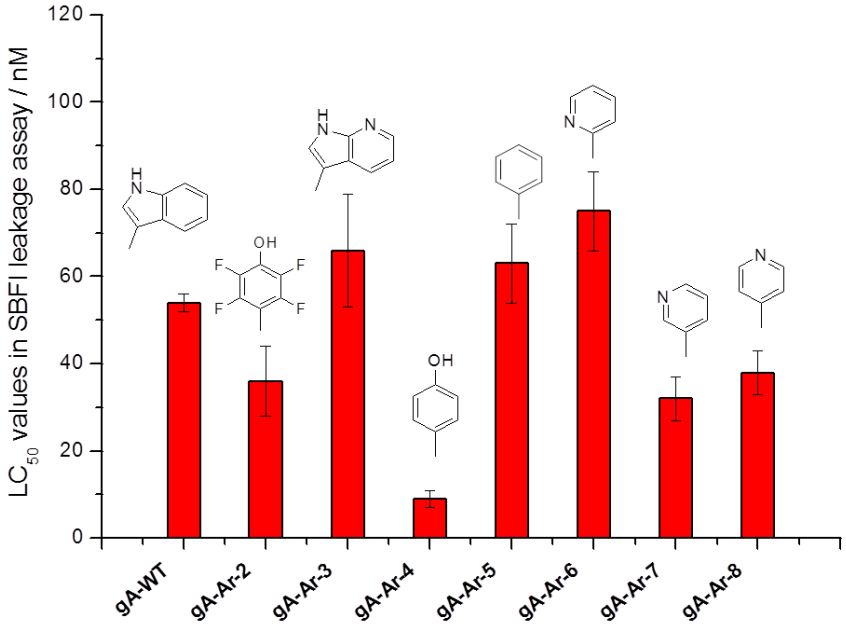

Figure 1-11. LC_{50} values of gA aromatic mutants in causing Na^+ ion equilibration across a POPC lipid bilayer. The values were obtained from fitting the concentration profile of the SBFI leakage assay with an exponential function in system I. The structures of the aromatic residues are labeled on top of each bar. Similar LC_{50} values were obtained in system II.

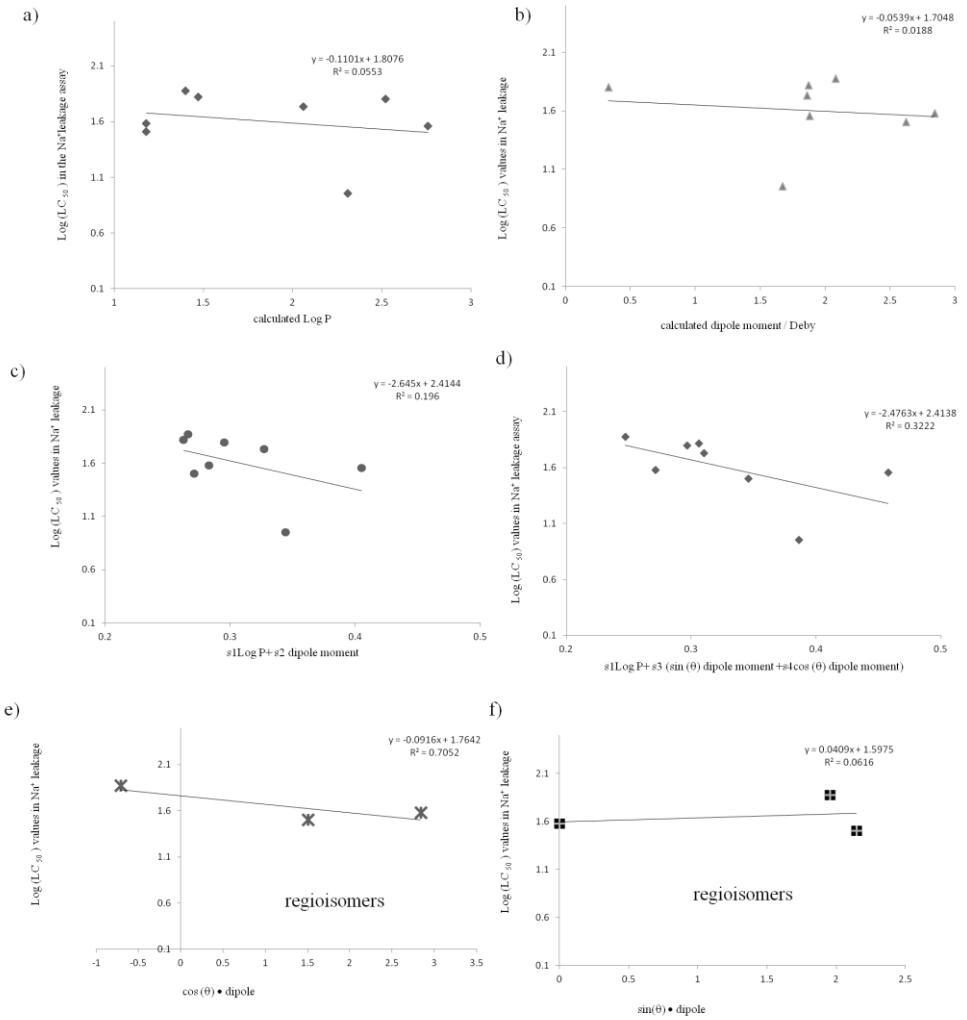

Figure 1-12. Correlation between the Log (LC_{50}) values and physical properties of corresponding aromatic amino acids. Plots are shown for the Log (LC_{50}) values of **gA-Ar-(WT-8)** vs (a) LogP, (b) magnitude of dipole moment, (c) the linear combination of dipole moment and LogP(s1• dipole + s2 Log P, in which s1 and s2 are the slope in a) and b) respectively, (d) the synthetic parameter (s1Log P + s3cos θ• dipole + s4sin θ •dipole), in which s3 and s4 are the slopes when Log (LC_{50}) values were plotted vs cos θ• dipole(0.0498) and sin θ •dipole (0.0657) respectively. Also plots for Log (LC_{50}) of **gA-Ar-(6-8)** vs (e) cos θ• dipole, (f) sin θ •dipole. θ is the angle between the calculated dipole moment and the C_β-C_γ carbon- carbon bond.

The channel formation efficiency of the gA mutants listed in Table 1-1 was evaluated by the leakage assay described above. Fitting the concentration profile into an exponential function yielded the LC_{50} values (Figure 1-11). Values of Log (LC_{50}) were plotted against the calculated physical properties of corresponding aromatic residues. Poor correlations between Log (LC_{50}) and Log P and dipole moment (Log P, Figure 1-12a, $R^2 = 0.055$; dipole moment, Figure 1-12b, $R^2 = 0.018$) suggested that no single factor is enough to determine the peptides' channel formation potency. Better correlation was observed when a linear combination of dipole moment and LogP was considered (Figure 1-12c, $R^2 = 0.20$). When the dipole moment direction was added to the combination, the correlation was further improved (Figure 1-12d, $R^2 = 0.32$). The directional dipole is quantified by the angle between the dipole and the C_β-C_γ bond. Components at directions along and perpendicular to the C_β-C_γ bond were considered separately (Table 1-1) in calculating the synthetic factor (Figure 1-12d). However, this correlation is still not good enough to reliably predict channel activity of a **gA-Ar** mutant from the dipole and LogP value of corresponding aromatic residues. When the **gA-Ar-(6-8)** are considered separately, a positive correlation was observed between the values of Log (LC_{50}) and the calculated cos θ• dipole but not sin θ• dipole (Figure 1-12e, Figure 1-12f). It suggests that the component of the dipole along the C_β-C_γ bond plays a significant role when regioisomers are considered. We were not able to evaluate the contribution from hydrogen bonding capability and amphiphilicity to channel activity as it is hard to quantify these two factors.

Additional interesting phenomena should be noticed. **gA-Ar-4** showed higher channel potency than the **gA-WT**, and **gA-Ar-5** showed comparable activity with **gA-WT**. These observations seem to be inconsistent with earlier reports that **gA-WT** shows the highest single channel conductance. [9,11] Substitution of Trp with Phe decreases the single channel conductance. However, in the voltage clamp assay, peptides were added from both sides of the planar bilayer to

close proximity of the membrane. The assay records the channel conductance of individual channels. Therefore, the results do not account for the amount of membrane bound peptides and peptide folding and translocation from the outer leaflet to the inner leaflet. We propose that the discrepancies might be attributed to the differences in peptide membrane binding affinities and/or the folding propensities of these mutants.

We then measured the dissociation constants of these peptides with POPC vesicles (K_d in lipid/peptide L/P ratio, Figure 1-13, Figure 1-14) through titration. Various amounts of lipids were titrated into a solution of 1μM gA mutant and the Trp fluorescence was monitored. Upon binding to a hydrophobic membrane, the emission of Trp fluorescence blue shifts (from 350 nm to 330 nm). This fluorescence shift has been widely used to monitoring peptide-membrane binding. Unfortunately, only two peptides (**gA-WT** and **gA-Ar-2**) have strong enough Trp fluorescence for reliable and conclusive recording. The quantum yield of 7-azatryptophan (7-AW) increases from 0.01 in aqueous solution (pH 7) to 0.25 in acetonitrile.[32] Therefore the fluorescence intensity at 380 nm (λ_{max} of 7-AW) instead of Trp fluorescence was used to report membrane binding of **gA-Ar-3** (Figure 1-13). None of the other five peptides showed reliable fluorescence at a concentration relevant to the leakage assay (3 μM was the highest used). There might be energy transfer between the closely positioned Trp and other aromatic residues, which quenches the Trp fluorescence. The **gA-Ar** mutants have similar hydrophobicities as their retention times on the C4 HPLC column are very similar. Importantly, the three mutants mentioned above showed K_d values smaller than 50 in L/P ratio (Figure 1-14). Because all leakage assays were performed at L/P ratio higher than 1,000, which is about 20 times higher than the K_d values, we believe that all peptides are bound onto the vesicles in the leakage assay. Therefore the differences in channel activity determined by Na^+ leakage assay are most likely not

due to membrane binding, but rather due to the folding propensity of **gA-Ar** mutants in membranes.

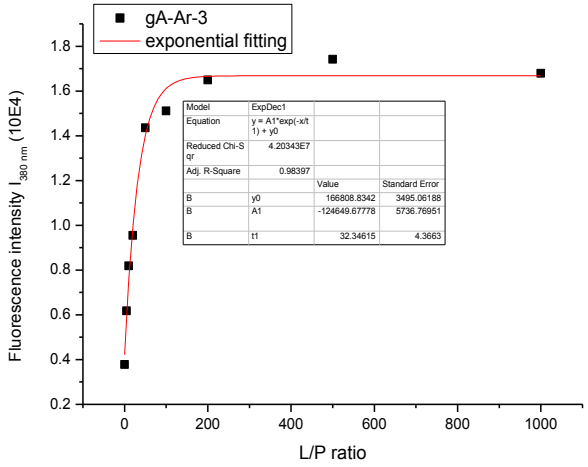

Figure 1-13. Binding curves of **gA-Ar-3**, plotting the fluorescence intensity at 380 nm over the L/P ratio (filled square). The apparent dissociation constant was obtained by fitting into an exponential function.

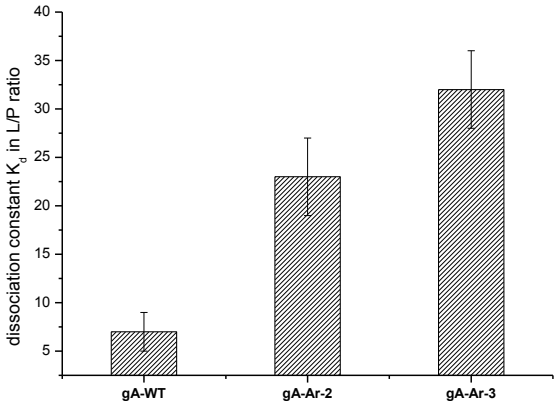

Figure 1-14. Dissociation constants of three **gA-Ar** mutants. The values of **gA-WT** and **gA-Ar-2** were obtained by fitting $I_{330\ nm}/I_{350\ nm}$ of Trp fluorescence against the L/P ratios into an exponential function and the value of **gA-Ar-3** is determined by 7-AW fluorescence at 380 nm.

Circular dichroism (CD) spectroscopy has been a widely used method in determining protein secondary structure. Unfortunately, the actual shape and magnitude of the CD signal can be significantly affected by the number and the type of aromatic amino acids present. The ellipticity that arises from aromatic amino acids are highly dependent on their mobility, the nature of their environment (hydrogen bonding, polar groups and polarizability) and their spatial disposition in the protein.[33,34] Therefore, structure charaterization of these gA mutants via CD has been difficult, due to the high abundance (4 out of 15 amino acids) of aromatic residues. This is also supported by the inconsistencies in the reported gA CD spectra,[11,17,35] as well as our own experience with poor reproducibility of CD data for the gA mutants (data not shown).

As an alternative, we applied an indirect method to probe the structures of these gA mutants. This was assessed by the ion selectivity of the gA mutants, which was measured with liposomes encapsulating K^+ or Tb^{3+} respectively. If the channel structure is similar to that of **gA-WT**, they should display ion specificity, allowing only small monovalent ions (e.g., Na^+) to pass through. The leakage of Tb^{3+} from liposome was monitored by the luminescence of Tb/DPA complex.[36] To be more specific, Tb^{3+} ions were encapsulated into LUVs. If Tb^{3+} ions diffuse to the exterior solution through the channel, the Tb^{3+} luminescence intensity at 490 nm increases upon binding to the membrane impermeable dipicolinic acid (DPA) in the external buffer. Under the same experimental conditions, all gA mutants show potent activity in Na^+ equilibration, yet no Tb^{3+} leakage is observed at concentrations that cause complete K^+ release (Figure 1-11, Figure 1-15). The selective transport of K^+ ions indicates that the active gA channels have wild type like structures. However, this assay fails to quantify the amount of active gA channels. Since all peptides are bound onto the membrane under experimental conditions, we hypothesize that it is the degree of peptide misfolding in membrane that accounts for the range of activities in the Na^+ ion leakage assay. Detailed structure analyses of these mutants need to be done to prove our hypothesis.

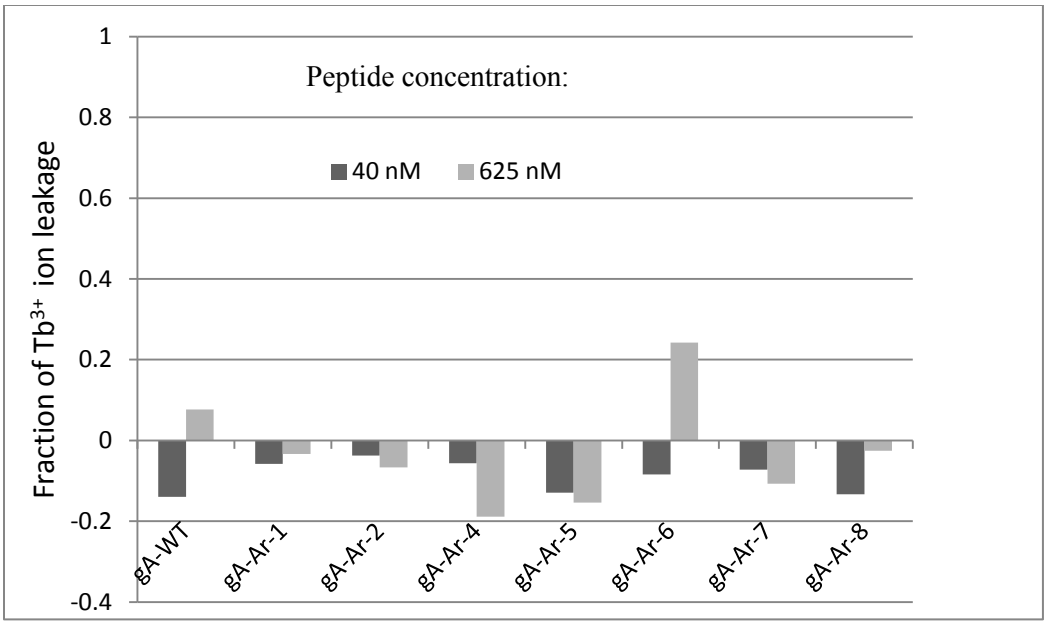

Figure 1-15. Fraction of Tb^{3+} leakage from liposomes induced by the **gA-Ar** mutants. The complete release of Tb^{3+} ions was triggered by 0.1% of TX-100, and the DMSO addition was considered as the negative control.

1.3 Summary

In summary, we have evaluated the ion channels formed by **gA-Ar** mutants with the Trp residues at positions 9, 11, 13 replaced by seven different aromatic amino acids. Compared to the previous work, the aromatic amino acids we selected are largely amphiphilic, and therefore better mimics of Trp than simple hydrophobic aromatic residues. The potential of these aromatic residues to mediate gA folding was analyzed and compared. We have successfully set up a liposome-based leakage assay to determine the channel induced Na^+ ion leakage, which reflects the channel formation efficiency of our designed gA mutants. As three of the aromatic residues cannot serve as hydrogen bond donors, which was believed to be crucial for Trp to interact with the phospholipids, we conclude that a hydrogen bond donor is not essential for aromatic amino

acid as a membrane anchor. The direction of the dipole moment for amphiphilic aromatic membrane anchors appears to be important for gA channel activities. Detailed structure analyses need to be performed to fully understand the structure activity relationship of these **gA-Ar** mutants.

1.4 Materials and methods

I. General materials and methods

Fmoc-Trp-Wang resin, Wang resin and all Fmoc-protected amino acids were purchased from either Advanced Chemtech (Louisville, KL) or Chem Impex Int. Inc (Wood Dale, IL). Unprotected valine, wild-type gA and other chemicals were obtained from Sigma-Aldrich or Acros Organics unless otherwise indicated. 1-Palmitoyl-2-oleoyl-sn-glycero-3-phosphocholine (POPC), was purchased from Avanti Polar Lipids (Alabaster, AL). SBFI tetraammonium salt was purchased from Invitrogen (Eugene, OR). Peptide synthesis was carried out on a Tribute peptide synthesizer (Protein Technologies, Tucson, AZ). ^{1}H-NMR data were collected on a Varian Gemini 500 MHz NMR spectrometer. LC/MS (ESI^{+}) data were generated by the Boston College mass-spectrometry facility(Waters MS system). The protein concentration of all samples used in this study was determined by measuring their absorbance at 280 nm on a Nanodrop 2000c UV/Vis spectrometer. The liposomes were prepared by using Liposofast Mini Extrusion system (Avanti Polar Lipids, Alabaster, AL) and following the procedure posted by Avanti Polar Lipids.

The physical properties (dipole moments, LogP, and surface areas)of the aromatic amino acids side chain was calculated with Spartan'10 (Wavefunction, Inc.) using the PM3 semi-empirical model and the results were listed in Table 1-1.

II. Peptide synthesis

1. Synthesis of formyl-L-valine

Acetic anhydride (4 mL, 0.04 mol) was added dropwise to a solution of L-valine (1 g, 8.35 mmol) in formic acid (12 mL, 0.32 mol) while stirring on ice. The mixture was then warmed up to RT and kept stirring for 24 hours before the solvent was removed by rotary evaporation under high vacuum. The formyl-valine was recrystallized from ethyl acetate and the desired

product was obtained as a white solid. Yield: 0.78 g (64%) ^{1}HNMR (500 MHz, [D6] Acetone, 25 °C, TMS): δ = 8.22 (s, 1H), 7.41(b, 1H), 4.50 (m, 1H), 2.22 (m, 1H), 0.98(m, 6H).

2. Synthesis of Fmoc-L-7-azatryptophan

The synthesis of L-7-azatryptophan (7-AW) was achieved through an enzymatic reaction.[37] Firstly, the tryptophan synthase was expressed in *Escherichia coli* (*E. coli*). A sample of *E. coli* pre-transformed with pSTB7 was received as a gift. This was plated onto solid LB supplemented with ampicillin (100 μg/ mL). Following incubation of the plate at 37 ^{o}C overnight, a single bacterial colony was picked up and used to inoculate sterile LB medium (10 mL) for 6 hours before pouring this pre-culture to 500 mL sterilized LB medium supplemented with ampicillin. Next, the culture was incubated on an orbital shaker with 200 rpm, at 37 ^{o}C. After 12 hours, the cultures were centrifuged (15,000 rpm, 4 ^{o}C, 20 mins). The cell pellet was re-suspended in a buffer (500 mM trishydrochloride, 5 mM EDTA, 10 mM mercaptomethanol, 1 mM PESF, 0.1 mM PLP, pH 7.8). The cells were lysed by sonication, centrifuged (10,000 rpm, 4 ^{o}C, 20 mins) to remove cell debris, and the crude supernatant (solution of tryptophan synthase) can be used in the catalytic reaction without further purification.

L-Serine (0.127 g, 1.21 mmol), 7-azaindole (1 eq, 143 mg, 1.21 mmol), and PLP (0.8 mg, 0.003 mmol) were mixed in 50 mL of buffer (0.1 M KH_2PO_4, pH 7.8). The solution was cooled to 5 ^{o}C, cell lysate (2 mL at 5 ^{o}C) was then added to the flask. Reactions were incubated at 37 ^{o}C for 24 hours. The reaction mixture was filtered and extracted with ethyl acetate (2 × 50 mL) to remove any un-reacted indole and recover the starting materials. The aqueous layer was subjected to RP-HPLC purification with a C18 column to obtain the purified 7-azatryptophan. 7-azatryptophan (100 mg, 0.48 mmol) dissolved in water was mixed with a solution of Fmoc-OSU (135 mg, 0.40 mmol) in acetonitrile. The reaction mixture was stirred at room temperature for 2

hours. The solution was acidified (pH ~ 2), and the Fmoc- protected 7-azatryptophan was extracted with ethyl acetate. The combined organic layer was dried with Na_2SO_4 . The final product was obtained by removing the solvent through rotary evaporation.

3. Loading Wang resin with Fmoc-D-Leu

Wang resin loaded with Fmoc-D-Leu was used to synthesize the N-fragment. In a 50 mL polypropylene centrifuge tube, 1 g (0.56 mmol) Wang resin is suspended in 15 mL of 9:1 (v/v) DCM/DMF mixture for 30 mins to swell. In a 20 mL glass vial, Fmoc-D-Leu (989.5 mg, 2.8 mmol, 5 eq. relative to the resin) was dissolved in a minimum amount of DMF. HOBt (378 mg, 2.8 mmol) was added and the mixture was stirred until HOBt is fully dissolved. Then, DIC (353 mg, 2.8 mmol) was added to the mixture, and stirred at 0 ^{o}C for 10 mins. The mixture was transferred to the swelled resin. In a separate flask, 0.1 equivalents of DMAP (342 mg, 0.056 mmol) was dissolved in a minimum amount of DMF (about 0.2 mL). The DMAP solution was added to the resin suspension. The mixture was shaken at room temperature for 3 hours. Then acetic anhydride (112 μL, 1.2 mmol, 2 eq.) and pyridine (90 μL, 1.2 mmol, 2 eq.) were added to the reaction mixture for an additional 30 mins to cap any remaining hydroxyl groups on the Wang resin. The resin was filterred through a medium fritted plastic funnel and washed with DMF, DCM and MeOH three times respectively. After the final wash, the resin was driedwith air flow and then high vacuo overnight.

The loading yield was determined by measuring the absorbance of DBU-released Fmoc at 305 nm. 20 mg of the prepared Fmoc-D-Leu-Wang resin and commercially available Fmoc-Gly-Wang resin (0.65 mmol/g) with known loading yield were weight into separate container. In the blank sample, no resin was added. Add 2 mL of 2% DBU in DMF to the resin. When the Fmoc protection group is released in DBU solution, a distinct species absorbing at 305 nm is

formed. After 30 minutes agitation, 1 mL of the solution was diluted until the absorbance of the solution falls into the range 0.2 – 1.0. The exact same dilution procedure was applied to the standard (Fmoc-Gly-Wang resin) and the blank (no resin). The loading yield can be calculated by $x/standard = (A_{sample}-A_0)/(A_{standard}-A_0) \times m_{standard}/m_{sample}$, in which, x and standard are the loading yield of the Fmoc-D-Leu-Wang resin prepared above and the purchased Fmoc- Gly-Wang resin in mmol/g; A_{sample}, $A_{standard}$, and A_0 are the absorbance of the sample, standard and blank at 305 nm; $m_{standard}$, m_{sample} are the mass of resin used. The samples were prepared as triplicates and the average is used as the final loading yield.

4. Peptide synthesis

All peptides were synthesized using the standard Fmoc/HBTU chemistry. In general, five equivalents of each amino acid and 4.5 equivalents of HBTU were used for each coupling reaction. The 7-azatryptophan mutant was synthesized through linear synthesis. All other mutants were made through fragment condensation (Scheme 1-1). The first 9 amino acids (from formyl-Val1 to Ar9, in which Ar is the chosen aromatic residue in a gA mutant) were coupled onto the Fmoc-D-Leu loaded Wang resin to make N-fragment. Then the resin was stirred in reagent K (80% TFA, 5% H_2O, 2.5% EDT, 5% thioanisole and 7.5% phenol) for 2 hours at RT to cleave the N-fragment. The C-fragment was synthesized by coupling four amino acids (from Ar11 to D-Leu14) onto the Fmoc-Trp-Wang resin. Then the C-fragment was cleaved off the resin with ethanolamine (40% (v/v) in degassed DMF, 55^{o}C, 5 hours). Next, the resin was filtered off through a medium fritted plastic funnel and rinsed three times with DCM and MeOH to release the peptide into the filtrate. The peptide containing filtrate was dried by rotary evaporation to a minimal volume. Water (6-7 times of filtrate volume) was added to precipitate both fragments from the cleavage cocktail. The precipitates were isolated by centrifugation (14,000 rpm, 1 hour) and the pellet was

dried on a lyophilizer to give two peptide fragments. The crude material was directly used in the following condensation reaction. The two peptide fragments (1:1 ratio) were dissolved in DCM/DMF (3: 1, v/v) to make a concentration about 0.05 M. HOAt (4 e.q.) and DIPEA (3 e.q.) were added to the solution and the reaction mixture was stirred at room temperature for 10 mins, at which point HATU (2.5 e.q.) was added. The mixture was stirred at room temperature for another 8-12 hours. The reaction was monitored by LC-MS until a complete conversion of starting material was achieved. The reaction mixture was dried by rotary evaporation to a minimal volume. The final product was again precipitated by deionized water and separated from the supernatant by centrifugation. The pellet was then re-dissolved in MeOH and purified by preparative scale RP-HPLC (Waters Prep LC, Jupiter 10 μm C4 300A Column). The identity and purity of each peptide was confirmed by analytical RP-HPLC-MS (Waters e2695, Phenomenex, Jupiter 5μm C4 300R, ESI^+) as $[M]^+$. All peptides were confirmed to have purity of 90% or higher.

The peptide **gA-Ar-8**L was also synthesized through fragment condensation. Fmoc-L-Leu-Wang resin was used to make its N-fragment of **gA-Ar-8**L, while the C-fragment was identical. The two full-length peptides (**gA-Ar-8** and **gA-Ar-8**L) were subjected to analytical HPLC (Waters e2695, Phenomenex, Jupiter 5μm C4 300R) analysis and the results are presented in Figure 1-5.

Table 1-3. sequences and MS of the gA-Ar mutants discussed in chapter 1

Name	Sequence	Calculated mass	Idendified
gA-Ar-2	formyl-V-G-A-*d*L-A-*d*V-V-*d*V-**f4Y**-*d*L-**f4Y**-*d*L-**f4Y**-*d*L-W-ethanolamine	2031	1016 $[M+H]^{2+}$
gA-Ar-3	formyl-V-G-A-*d*L-A-*d*V-V-*d*V-**AW**-*d*L-**AW**-*d*L-**AW**-*d*L-W-ethanolamine	1890	1891
gA-Ar-4	formyl-V-G-A-*d*L-A-*d*V-V-*d*V-**Y**-*d*L-**Y**-*d*L-**Y**-*d*L-W-ethanolamine	1815	1816
gA-Ar-5	formyl-V-G-A-*d*L-A-*d*V-V-*d*V-**F**-*d*L-**F**-*d*L-**F**-*d*L-W-ethanolamine	1767	1767
gA-Ar-6	formyl-V-G-A-*d*L-A-*d*V-V-*d*V-**2Pal**-*d*L-**2Pal**-*d*L-**2Pal**-*d*L-W-ethanolamine	1768	1768
gA-Ar-7	formyl-V-G-A-*d*L-A-*d*V-V-*d*V-**3Pal**-*d*L-**3Pal**-*d*L-**3Pal**-*d*L-W-ethanolamine	1768	1768
gA-Ar-8	formyl-V-G-A-*d*L-A-*d*V-V-*d*V-**4Pal**-*d*L-**4Pal**-*d*L-**4Pal**-*d*L-W-ethanolamine	1768	1768
gA-Ar-8L	formyl-V-G-A-*d*L-A-*d*V-V-*d*V-**4Pal**-L-**4Pal**-*d*L-**4Pal**-*d*L-W-ethanolamine	1768	1768

single letter codes, the D- amino acids were labelled by the italic "***d***", and mutation sites are highlighted in bold

III. Preparation of peptide stock solutions

Each peptide stock solution was prepared in DMSO. The concentration was determined by monitoring the Trp absorbance at 280 nm. The absorbance contributed by Phe, 2Pal, 3Pal, 4Pal, f4Y at 280 nm was negligible. Therefore, the following extinction coefficient were used in concentration calibration: **gA-WT** is 22760 $cm^{-1}\bullet M^{-1}$ (W 5690 $cm^{-1}\bullet M^{-1} \times 4$); **gA-Ar-3** is 20930 $cm^{-1}\bullet M^{-1}$ (W 5690 $cm^{-1}\bullet M^{-1}$ + AW 5080 $cm^{-1}\bullet M^{-1} \times 3$); **gA-Ar-4** is 9530 $cm^{-1}\bullet M^{-1}$ (W 5690 $cm^{-1}\bullet M^{-1}$ + Y 1280$cm^{-1}\bullet M^{-1} \times 3$); all other five mutants (**gA-Ar-2 and gA-Ar-(5-8)**) are 5690 $cm^{-1}\bullet M^{-1}$ (W 5690 $cm^{-1}\bullet M^{-1}$). Then solutions with a series of dilution (2×) in DMSO were made. Final DMSO concentration was controlled at 1% for all samples prepared for the binding and leakage assay.

IV. Size exclusion chromatography

Peptide conformers (monomers and ds-dimers) of gA of the different mutants were separated and quantified by analytical HPLC through a size-exclusion column from Waters (Milford, MA, Ultrastyragel 1000 Å column eluted with pure THF). [17] Briefly, 10 μL of a peptide solution dissolved in DMSO (50 μM) is injected directly onto the column, releasing the polypeptide conformational isomers to the eluent stream. In THF, the ds-dimer and β-helical monomer exchange extremely slowly, therefore, the results reflect the peptide conformational isomers in the DMSO stock solution. The flow rate was 1.0 mL/min, and the eluting peptides were detected with a dual-wavelength detector (280 nm and 254nm). Previous studies showed that **gA-WT** incubated in THF exists as a mixture of monomers and ds-dimer. Therefore, a solution of **gA-WT** in THF was used as a standard to determine the retention times of the monomers and ds-dimer under our experimental condition. The relative amount of the conformational isomers is determined by the integration.

V. Na^+ ion leakage assay

1. Determination of SBFI-Na^+ binding constant in solution

For the determination of SBFI-Na^+ binding constant in the absence of interfering ions, two solutions of 5 μM SBFI dissolved in **A** (10 mM MOPS, pH 7.0) or **B (**10 mM MOPS, 135 mM NaCl, pH 7.0) were mixed in different ratios so that the mixture would have constant SBFI concentration and various amount of Na^+. For the SBFI-Na^+ binding in the presence of K^+ ions, two solutions of 5 μM SBFI dissolved in **C** (10 mM MOPS,135 mM KCl, pH 7.0) and **B** were mixed in different ratio to have a solution with constant SBFI (5 μM) , various amount of Na^+, but constant total ion concentration (135 mM Na^+ and K^+ together). Then the excitation spectra

of these mixtures were recorded by monitoring emission at 505 nm. The intensity ratio at 340 nm over 380 nm was plotted against the Na^+ concentration and the apparent dissociation constant was obtained by fitting the plot into an exponential function.

2. Liposome preparation and the leakage assay

A chloroform solution containing 76 mg POPC (POPC LUVs) was dried under reduced pressure to form a thin film, which was then hydrated with 2 mL aqueous buffer (10 mM MOPS, 135 mM KCl, 20 μM SBFI pH 7.0). After 20 cycles of freezing and thawing, the liposome suspension was extruded 21 times through a 100 nm polycarbonate membrane (Liposofast Mini Extrusion system, Avanti Polar Lipids; Whatman Nuclepore Track-Etch Membrane) at RT. Free K^+ and SBFI were removed by gel filtration (ÄKTA FPLC with HiPrepTM 16/60 Sephacryl TM-S-500HR column) using solution **B** for system I and solution **C** for system II as the eluent. The lipid concentration was determined by Stewart assay following the reported protocal[38] . This colorimetric method is based on the complex formation between phospholipids and ammonium ferrothiocyanate. Briefly, 2 mL of phospholipid solution in chloroform with 2 mL of 0.1M $NH_4Fe(SCN)_4$ in aqueous solution was mixed and shaked for 2min.The mixture was then centrifuged for 5 min at 2000 rpm. The UV absorption of the chloroformsolution of the lipids was measured at 465 nm. The concentrations of the lipids were calculatedwith the reported extinction coefficient of PC 7960 $M^{-1}cm^{-1}$. Size distribution of liposomes was confirmed by Dynamic Light Scattering (DLS, DynaPro nanostar, Wyatt, Santa Barbara, CA). The instrument setup used the standard PBS parameters: refractive index @589 nm & 20°C is 1.333, viscosity is 1.019 cp, Cauchy coefficient is 3119 nm^2. Data were acquired in auto-attenuation mode, and processed with DYNAMIC V6TM software. The diameters of all liposomes were found to fall into the narrow range of 100~150 nm with a polydispersity lower than 30% (Figure 1-16).

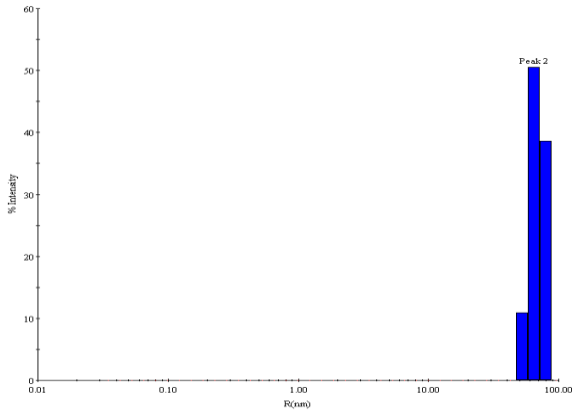

Figure 1-16. Size distribution of LUVs made of POPC determined by DLS

The leakage assay with system I was performed as described below. Various amount of peptide (concentration varies from 1 nM to 5 μM) were mixed with POPC LUVs (500 μM, LUVs ⊃ 20 μM SBFI, 10 mM MOPS, 135 mM KCl, pH 7.0) suspended in solution **B**. The excitation spectra of these mixtures were recorded by emission at 505 nm at 0 mins, 30 mins, 90 mins and 2 hours for the first trial. The results suggested that the ion exchange reaches equilibration around 2 hours (Figure 1-17). There are minimal changes from 90 mins and 2 hours at all concentrations tested. When the experiments were repeated, the mixture was incubated at room temperature for 2 hours before the first excitation spectrum was recorded at 505 nm. The $I_{340nm}/I_{380\ nm}$ of each sample was plotted against the peptide concentration. The activity was presented as LC_{50} values (the peptide concentration required to cause about 50% of Na^+ ion leakage). The values were obtained by fitting the concentration profile to an exponential function. The complete ion equilibration was achieved by lysing the liposome with 0.1% TritonX-100 (w/v) at the end of each titration experiment and 1% (v/v) DMSO addition was used as negative control. The $I_{340nm}/I_{380\ nm}$ values were normalized against both values to give the % of Na^+ equilibration.

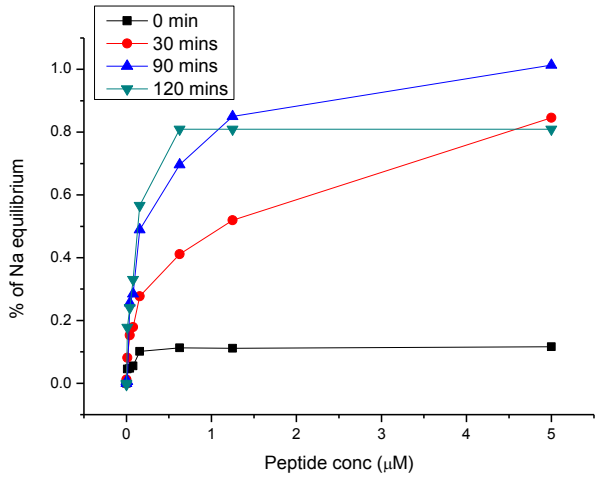

Figure 1-17. Kinetic profiles of **gA-WT** induced Na^+ ion leakage. The graph shows relationship between peptide concentration and the percentage of Na^+ ion leakage at 0 mins, 30 mins, 90 mins and 2 hours.

The leakage assay with system II was performed in a similar fashion. POPC LUVs (500 μM POPC ⊃ 20 μM SBFI, 10 mM MOPS, 135 mM KCl, pH 7.0) was suspended in solution **C** , which has no Na^+ ions. 2 hours after peptide addition, the excitation spectra were recorded. No excitation wavelength shift was observed. Then 135 mM NaCl was titrated into the mixture to generate a Na^+ ion gradient across the lipids bilayer. The systems were equilibrated for an additional 2 hours before the second excitation spectrums was recorded. Similarly, the $I_{340nm}/I_{380\ nm}$ of each sample was normalized and plotted against the peptide concentration. The activity was again presented as LC_{50} values. The values were obtained by fitting the concentration profile to an exponential function. The complete ion equilibration was achieved by lysing the liposomes with 0.1% TritonX-100 (w/v) at the end of each titration.

Channel formation of all aromatic residue modified gA mutants was tested in both system I and system II. Similar LC_{50} values were obtained. Figure 1-11 shows the values obtained in

system I. For reasons unknown, the absolute fluorescence intensity in system II decreases when peptide concentration is higher than 250 nM after 4 hours of incubation. Similar LC_{50} values in system II were obtained when data from the low peptide concentration were fitted.

VI. The determination of peptide binding

20 mg of POPC was dissolved in 2 mL of chloroform and dried under high vacuum to form a thin layer. Then the lipids were hydrated with 5 mL of buffer solution **B** (10 mM MOPS, 135 mM NaCl, pH 7.0) by ultrasonication as described in the Avanti Polar Lipids protocol. Small unilamellar vesicles (SUVs) form during the process. After the solution becomes transparent (normally takes about 20 mins), it was filtered through 0.2 μm syringe filter to remove possible aggregates and a small amount of metal tip leaked from the ultrasonication probe. SUVs were chosen over LUVs to minimize the light scattering effect and presumably the error in the measurement. Similar K_d values but with much bigger error were obtained with both SUVs and LUVs for gA-Ar-2 (SUVs: 23±4, LUVs: 22±9).

Peptide binding was monitored by the fluorescence shift of the Trp emission maximum upon binding to hydrophobic liposomes or the fluorescence enhancement of 7-azatryptophan upon binding. The gA mutants (1 μM) were mixed with various amounts of SUVs in solution **B**. The mixture was agitated gently for 30 mins before the fluorescence spectra of Trp or 7-azatryptophan were scanned between 320 nm and 400 nm (λ_{ex} = 280 nm) on a SpectraMax M5 (Molecular Devices, Sunnyvale, CA). For **gA-Ar-3** the intensity at 380 nm was plotted against the L/P ratios. And for the rest of gA mutants, the ratio of fluorescence intensity at 330 nm and 350 nm (I_{330nm}/I_{350nm}) was calculated and plotted against the L/P ratios. Then binding curve was fitted into an exponential function to obtain an apparent dissociation constant (τ value, Figure 1-13).

VII. Tb^{3+} ion leakage assay

A chloroform solution containing 76 mg of POPC (POPC LUVs) was dried under reduced pressure to form a thin film, which was then hydrated with 2 mL aqueous buffer (10 mM TES, 100 mM sodium citrate, 50 mM $TbCl_3$, pH 7.0). After 20 cycles of freezing and thawing, the liposome suspension was extruded 21 times through a 100 nm polycarbonate membrane (Liposofast Mini Extrusion system, Avanti Polar Lipids; Whatman Nuclepore Track-Etch Membrane) at RT. The external solution was removed by gel filtration using 10 mM TES, 100 mM sodium citrate, pH 7.0 as eluent. The leakage of Tb^{3+} from liposomes was monitored by the luminescence of the Tb/DPA complex. To a mixture of LUVs (500 μM, POPC ⊃10 mM TES, 100 mM sodium citrate, 50 mM $TbCl_3$, pH 7.0) and DPA (50 μM) in buffer (10 mM TES, 100 mM sodium citrate, pH 7.0), peptide was added (the amount of DMSO was controlled to less than 1%). The peptide liposome mixture was incubated at RT for 30 mins before the fluorescence intensity of the Tb/DPA complex (λ_{ex}=270nm, λ_{em}=490 nm) was recorded (I_c) in a quartz cuvette on a MicroMax 384 fluorescence spectrometer (Jobin Yvon, Horiba Scientific).[39] Complete Tb^{3+} leakage was assessed by TritonX-100 lysing of liposomes (I_f). A sample with pure DMSO addition was used as blank (I_0) and the fraction of Tb^{3+} leakage was calculated as fraction = $(I_c-I_0)/(I_f-I_0)$.

References:

(1) Venter, J. C.; Adams, M. D.; Myers, E. W.; Li, P. W.; Mural, R. J.; Sutton, G. G.; Smith, H. O.; Yandell, M.; Evans, C. A.; Holt, R. A.; Gocayne, J. D.; Amanatides, P.; Ballew, R. M.; Huson, D. H.; Wortman, J. R.; Zhang, Q.; Kodira, C. D.; Zheng, X. H.; Chen, L.; Skupski, M.; Subramanian, G.; Thomas, P. D.; Zhang, J.; Gabor Miklos, G. L.; Nelson, C.; Broder, S.; Clark, A. G.; Nadeau, J.; McKusick, V. A.; Zinder, N.; Levine, A. J.; Roberts, R. J.; Simon, M.; Slayman, C.; Hunkapiller, M.; Bolanos, R.; Delcher, A.; Dew, I.; Fasulo, D.; Flanigan, M.; Florea, L.; Halpern, A.; Hannenhalli, S.; Kravitz, S.; Levy, S.; Mobarry, C.; Reinert, K.; Remington, K.; Abu-Threideh, J.; Beasley, E.; Biddick, K.; Bonazzi, V.; Brandon, R.; Cargill, M.; Chandramouliswaran, I.; Charlab, R.; Chaturvedi, K.; Deng, Z.; Francesco, V. D.; Dunn, P.; Eilbeck, K.; Evangelista, C.; Gabrielian, A. E.; Gan, W.; Ge, W.; Gong, F.; Gu, Z.; Guan, P.; Heiman, T. J.; Higgins, M. E.; Ji, R.-R.; Ke, Z.; Ketchum, K. A.; Lai, Z.; Lei, Y.; Li, Z.; Li, J.; Liang, Y.; Lin, X.; Lu, F.; Merkulov, G. V.; Milshina, N.; Moore, H. M.; Naik, A. K.; Narayan, V. A.; Neelam, B.; Nusskern, D.; Rusch, D. B.; Salzberg, S.; Shao, W.; Shue, B.; Sun, J.; Wang, Z. Y.; Wang, A.; Wang, X.; Wang, J.; Wei, M.-H.; Wides, R.; Xiao, C.; Yan, C. *Science* **2001**, *291*, 1304.

(2) Hübner, C. A.; Jentsch, T. J. *Human Molecular Genetics* **2002**, *11*, 2435.

(3) Zaydman, M. A.; Silva, J. R.; Cui, J. *Chemical Reviews* **2012**.

(4) Kelkar, D.; Chattopadhyay, A. *Journal of Biosciences* **2006**, *31*, 297.

(5) Kelkar, D. A.; Chattopadhyay, A. *Biochemical and Biophysical Research Communications* **2006**, *343*, 483.

(6) Valley, C. C.; Cembran, A.; Perlmutter, J. D.; Lewis, A. K.; Labello, N. P.; Gao, J.; Sachs, J. N. *Journal of Biological Chemistry* **2012**, *287*, 34979.

(7) Fink, A.; Sal-Man, N.; Gerber, D.; Shai, Y. *Biochimica Et Biophysica Acta-Biomembranes* **2012**, *1818*, 974.

(8) R.J. Dubos, C. C. *The Joural Experimental Medicine* **1939**, *70*, 249.

(9) Kelkar, D. A.; Chattopadhyay, A. *Biochimica Et Biophysica Acta-Biomembranes* **2007**, *1768*, 2011.

(10) Mo, Y.; Cross, T. A.; Nerdal, W. *Biophysical Journal* **2004**, *86*, 2837.

(11) Denise V. Greathouse, R. E. K. I. *Methods in Enzymology* **1999**, *294*, 525.

(12) Pankiewicz, R.; Wojciechowski, G.; Schroeder, G.; Brzezinski, B.; Bartl, F.; Zundel, G. *Journal of Molecular Structure* **2001**, *565*, 213.

(13) Kubota, S.; Ozaki, S.; Onishi, J.; Kano, K.; Shirai, O. *Analytical Sciences* **2009**, *25*, 189.

(14) Ketchem, R. R.; Lee, K. C.; Huo, S.; Cross, T. A. *Journal of Biomolecular NMR* **1996**, *8*, 1.

(15) ila- omeu, . ieto-Su r e , . ynarowic - a tka, P. *The Journal of Physical Chemistry B* **2005**, *109*, 14965.

(16) Chattopadhyay, A. R., SatinderS *J Chem Sci* **2007**, *119*, 135.

(17) Salom, D.; Perez-Paya, E.; Pascal, J.; Abad, C. *Biochemistry* **1998**, *37*, 14279.

(18) Durrant, J. D.; Caywood, D.; Busath, D. D. *Biophysical Journal* **2006**, *91*, 3230.

(19) Svensson, F. R.; Lincoln, P.; Norden, B.; Esbjoerner, E. K. *Biochimica Et Biophysica Acta-Biomembranes* **2011**, *1808*, 219.

(20) Sidorov, V.; Kotch, F. W.; Abdrakhmanova, G.; Mizani, R.; Fettinger, J. C.; Davis, J. T. *Journal of the American Chemical Society* **2002**, *124*, 2267.

(21) Fyles, T. M. *Chemical Society Reviews* **2007**, *36*, 335.

(22) Marsh, D. *Biophysical Journal* **2012**, *102*, 1079.

(23) Szoka, F.; Papahadjopoulos, D. *Annual Review of Biophysics and Bioengineering* **1980**, *9*, 467.

(24) Butterfield, S. M.; Hennig, A.; Matile, S. *Organic & Biomolecular Chemistry* **2009**, *7*, 1784.

(25) Hakonen, A.; Hulth, S. *Analytica Chimica Acta* **2008**, *606*, 63.

(26) Tsubokawa, H.; Miura, M.; Kano, M. *The Journal of Physiology* **1999**, *517*, 135.

(27) Minta, A.; Tsien, R. Y. *Journal of Biological Chemistry* **1989**, *264*, 19449.

(28) Gokel, G. W.; Mukhopadhyay, A. *Chemical Society Reviews* **2001**, *30*, 274.

(29) Jordan, J. B.; Easton, P. L.; Hinton, J. F. *Biophysical Journal* **2005**, *88*, 224.

(30) Chattopadhyay, A.; Rawat, S. S.; Greathouse, D. V.; Kelkar, D. A.; Koeppe, R. E. *Biophysical Journal* **2008**, *95*, 166.

(31) Harootunian, A. T.; Kao, J. P.; Eckert, B. K.; Tsien, R. Y. *Journal of Biological Chemistry* **1989**, *264*, 19458.

(32) De Filippis, V.; De Boni, S.; De Dea, E.; Dalzoppo, D.; Grandi, C.; Fontana, A. *Protein Science* **2004**, *13*, 1489.

(33) EH, S. *Critical Review in Biochemistry* **1974**, *2*, 113.

(34) Kelly, S. M.; Jess, T. J.; Price, N. C. *Biochimica et Biophysica Acta - Proteins and Proteomics* **2005**, *1751*, 119.

(35) Hicks, M. R.; Damianoglou, A.; Rodger, A.; Dafforn, T. R. *Journal of Molecular Biology* **2008**, *383*, 358.

(36) Rathinakumar, R.; Wimley, W. C. *Journal of the American Chemical Society* **2008**, *130*, 9849.

(37) Goss, R. J. M.; Newill, P. L. A. *Chemical Communications* **2006**, 4924.

(38) Stewart, J. C. M. *Analytical Biochemistry* **1980**, *104*, 10.

(39) Rathinakumar, R.; Walkenhorst, W. F.; Wimley, W. C. *Journal of the American Chemical Society* **2009**, *131*, 7609.

Chapter 2. Towards Bacterium Specific Ion Channels: Solublized Gramicidin A as Potential Systemic Antibiotics

2.1 Introduction

2.1.1 Antibiotic resistance

Bacterial infections cause a high morbidity and mortality and serious problems in public health. Since the introduction of the first effective antibiotics, namely the sulfonamide-based antibiotics, followed by the golden age of antibiotic development (1950-1980), antibiotics were considered as a panacea to cure infections (Figure 2-1).[1] Unfortunately, the success of new antibiotics was later found to be compromised by the fast development of resistance. Antibiotic resistance was identified since the 1960s (Figure 2-1). While the number of resistant bacterial strains continues to increase at an alarming rate, new antibiotic production is actually slowing down (Figure 2-2).[2,3] Traditional antibiotics bind to specific receptors and inhibit crucial processes such as cell wall synthesis, protein synthesis, and DNA replication. It is surprisingly easy for bacteria to generate resistance through a variety of mechanisms (Table 2-1).[1,4] An ever evolving pipeline of antibiotics is required for modern medicine to remain one step ahead of pathogens. The main challenge of developing a new antibiotic is the identification of new targets as well as molecules that inhibit that target. Because targeting certain receptors or enzymes likely leads to resistance development in a short period of time, antibiotics that function through a different mechanism are desirable. Membrane targeting peptides are considered as new and attractive candidates of antibiotics in the future.[5] In recent years, a significant amount of effort has been put into developing membrane-active peptides and their functional analogous as novel antibiotics.[6,7]

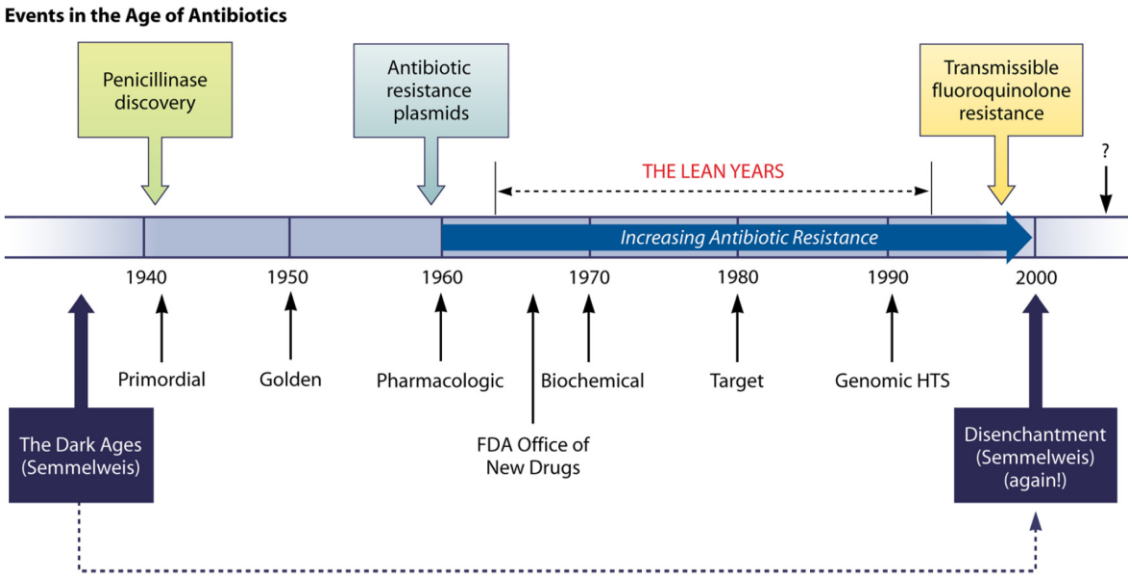

Figure 2-1. History of antibiotic discovery and concomitant development of antibiotic resistance. Graph is reconstructed from reference 1.

Table 2-1. Modes of action and resistance mechanisms of commonly used antibiotics

Antibiotic class	Example(s)	Target	Mode(s) of resistance
β-Lactams	Penicillins (ampicillin)	Peptidoglycan biosynthesis	Hydrolysis,efflux, altered target
Aminoglycosides	Gentamicin,streptomycin, spectinomycin	Translation	Phosphorylation, acetylation, nucleotidylation,efflux, altered target
Glycopeptides	Vancomycin, teicoplanin	Peptidoglycan biosynthesis	Reprogramming peptidoglycan biosynthesis
Tetracyclines	Minocycline, tigecycline	Translation	Monooxygenation, efflux, altered target
Sulfonamides	Sulfamethoxazole	C1 metabolism	Efflux, altered target
Quinolones	Ciprofloxacin	DNA replication	Acetylation, efflux, altered target
Streptogramins	Synercid	Translation	C-O lyase (type B streptogramins), acetylation (type A streptogramins), efflux, altered target
Macrolides	Erythromycin, azithromicin	Translation	Hydrolysis, glycosylation, phosphorylation, efflux, altered target

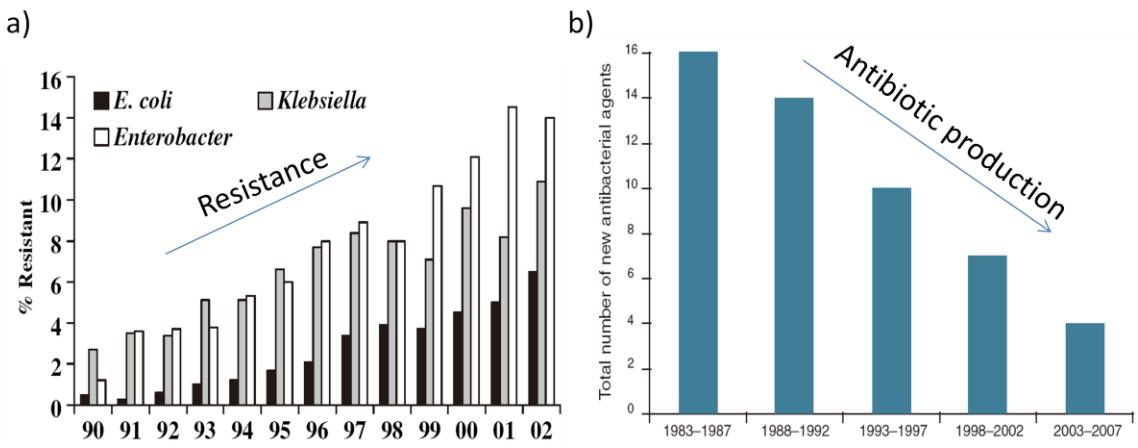

Figure 2-2: a) Trends of antibiotic resistance, y-axis represents the growing proportions of ciprofloxacin resistance b) Trends of new antibiotic production in the past two decades. The x-axis represents the time. Graphs are reconstructed from references 4 and 5.

2.1.2 Antimicrobial peptides

Antimicrobial peptides (AMPs) are a family of short peptides (12-80 amino acids) that function as broad-spectrum antimicrobial agents and serve as the frontline to combat bacteria, protozoa and other microbial agents.[8,9] As a class, AMPs are loosely defined. The only shared property is their prototypical function in killing bacteria. AMPs include a variety of primary and secondary structures.[10] Despite other mechanisms proposed recently, they are generally believed to work by directly perturbing the plasma membrane.[11,12,13] Multiple models have been proposed to explain AMPs mechanism of action. The three most prominent models are the carpet model, the barrel-stave model, and the toroidal pore model (Figure 2-3).[11] In the carpet model, the peptides disrupt the membrane by orienting parallel to the surface of the lipid bilayer and forming an extensive layer or carpet. In the barrel-stave model, the attached peptides aggregate and insert into the membrane bilayer so that the hydrophobic peptide regions align with the lipid core region

and the hydrophilic peptide regions form the interior region of the pore. In the toroidal model, the attached peptides aggregate and induce the lipid monolayers to bend continuously through the pore so that the water core is lined by both the inserted peptides and the lipid head groups. However the actual mechanism may follow a mix of these three and there are no selectivity on the leakage of internal contents.

To survive, a cell must have an intact plasma membrane that functions as a barrier to separate the interior contents from the outside environment, and controls the transport of polar molecules. Proper cell function and viability rely on membrane integrity and a normal ion gradient across the membrane. When AMPs disrupt the membrane integrity, cellular metabolism is interrupted and cells are killed.

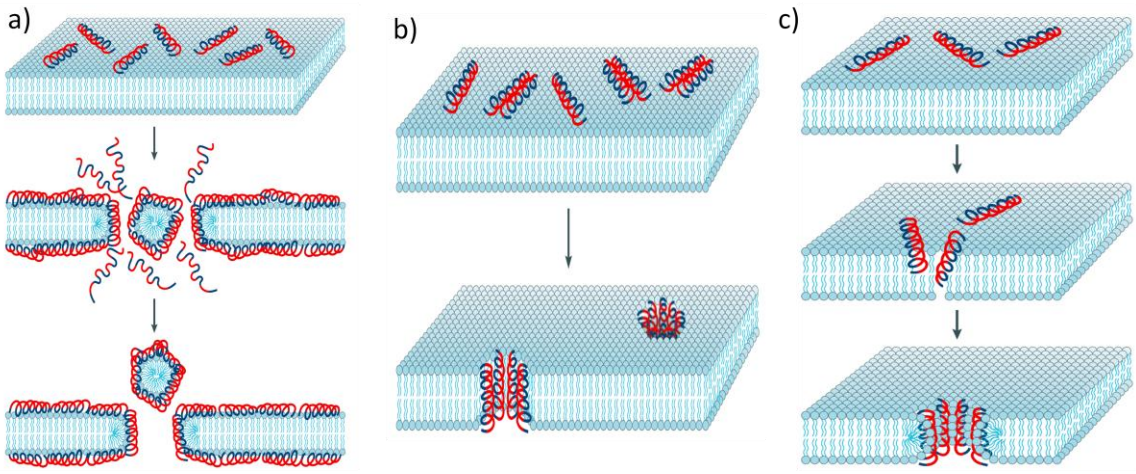

Figure 2-3. Proposed mechanisms of AMP induced killing. a) the carpet model; b) the barrel stave model; and c) the toroidal pore model. Graphs are reconstructed from reference 11.

Different cell types have distinct membrane composition.[7,14,15] The plasma membrane of mammalian cells consists of about 60% of phospholipids and 25% of cholesterol with an

asymmetric distribution of phospholipids between the outer and inner leaflets of the bilayer, exposing the zwitterionic phosphatidylcholine (PC) and sphingomyelin (SM) to the extracellular side.[15] In contrast, both Gram-positive and Gram-negative membranes consist of a large fraction of negatively charged lipids such as phosphatidylglycerol (PG) and diphosphatidylglycerol or cardiolipin (CL) and the zwitterionic phosphatidylethanolamine (PE). This is the primary reason that most AMPs have a net positive charge. Due to the charge-charge attraction, AMPs preferentially bind and disrupt the microbial (negatively charged) rather than the eukaryotic (neutral) membranes. The characteristic lipid composition described above for a given cell membrane results from millions of years of evolution. Modification of the lipid composition and distribution is considered to be highly costly for bacteria. Therefore, AMPs are expected to have a longer effective lifetime before the rise of resistance. However, rational improvement of naturally occurring AMPs or synthetic membrane toxins into systemic antibiotics has been difficult due to the lack of detailed mechanistic understandings.

2.1.3 Gramicidin A as an antibiotic

The structure and mechanism of gA as a transmembrane channel have been described in chapter 1.[16] gA is not only considered as a model membrane channel, but also has been used as an ingredient in the commercialized antibiotic ointment polysporin in Canada. As described, gA binds onto a membrane lipid bilayer and forms channels that allow monovalent ions to diffuse through. When gA forms a channel on the cell membrane, it disrupts the essential ion gradient and consequently causes cell death. In contrast to the majority of AMPs, gA has a clearly defined structure and mechanism of membrane lysis. Thus rational optimization of its properties is feasible. As one can tell from its primary sequence, gA is essentially insoluble in water (< 50 nM) and induces hemolysis under the concentrations required to cause bacterial cell death (*vide infra*). As a result, its therapeutic usage has been limited to topical applications. [17,18]

Herein, I will introduce my research on developing a solubilized gA that no longer suffers from the problems mentioned above but retains membrane channel activity, holding great promise as a systemic antibiotic. There are several reasons for us to choose gA as the starting point for further engineering and optimization. First, gA has been used as an antibiotic. Its efficacy as an antibiotic has been confirmed. Second, gA is composed of alternating D- and L-amino acids and is both N-terminal (formyl) and C-terminal (ethanolamine) protected. Therefore, the peptide is more resistant to protease degradation.[19] Third, gA has well defined structure and mechanism of action. Finally, gA functions as a monovalent ion channel. For mammalian cells, monovalent ion channels have been reported to play an important role in controlled cell death.[20] We hope that bacterium death caused by gA would go through a similar controlled cell death pathway. Thus it is less likely to trigger a serious immune response compared other AMPs, which release cytosolic material instantly through a detergent type mechanism. Our peptide design was inspired by natural cationic AMPs, and the experimental results have shown that gA mutants carrying multiple positive charges (e.g. D-Lys residues) are highly soluble in aqueous solution. These peptides are shown to inhibit bacterium growth at a concentration much lower than that needed to cause hemoglobin leakage from human red blood cells (hRBCs), yielding a greater therapeutic window. Furthermore, modification on the Lys side chains allows one to fine tune the antimicrobial activities of these gA mutants.

2.2 Design and characterization of solubilized gA

As mentioned above, bacterial cell membranes consist of a large fraction of negatively charged lipids, and therefore display a greater affinity for cationic peptides. Inspired by this, we hypothesize that strategic incorporation of cationic residues into gA will afford specific bacterial toxicity if the mutants retain the channel-forming structure and function. In addition, the charged residues will greatly improve the water solubility.

2.2.1 Synthesis and structure analysis of the gA mutants

The structure of gA in a lipid bilayer was determined by solid state NMR in 1996.[21] A close examination of the dimeric channel structure reveals that the D-Leu residues at positions 10, 12 and 14 are ideal for mutation because they are located at the membrane-water interface, where charged side chains can be best accommodated without altering the channel structure (Figure 2-4). More specifically, the distance between the α-carbon of the residues at position 10 to the tail of gA is about 15 Å, which is similar to the length of four carbon-carbon bonds. Among the twenty natural amino acids, both Lys and Arg have a proper side chain length that would allow the positive charge carried by these residues to locate at the aqueous environment without altering the channel structure. As the number of charged residues would affect water solubility and selective membrane association of gA mutants, we first varied the number and the position of the charged residues by replacing one or multiple D-Leu with D-Lys to achieve an optimized combination (Table 2-2). Given the high abundance of Arg residues in natural antimicrobial peptides, we would also tested gA muant with D-Arg residues in the best combination.

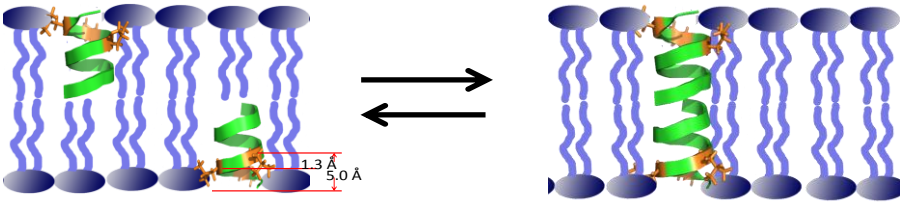

formyl-V-G-A-*d*L-A-*d*V-V-*d*V-W-*d*L-W-*d*L-W-*d*L-W-NHCH$_2$CH$_2$OH

Figure 2-4. Mechanism of gA channel formation in a lipid bilayer and a detailed structure analysis. The distance between the α-carbon at position 10 and the peptide tail, and the distance changes with positions 10 and 12 are labeled respectively. The D-Leu residues are highlighted in orange and the gA peptide sequences are shown in the bottom in which the D- amino acids are marked by italic "*d*".

All peptides were synthesized through solid phase peptide synthesis using the standard Fmoc/HBTU chemistry (see experimental procedures). The formyl-Val was incorporated into the peptide as a building block.[22] After peptide elongation on Wang resin, the gA mutants were cleaved off from the resin with 40% ethanolamine in DMF, and precipitated with water to give the gA mutants with Boc- protected D-Lys. Then the Boc- protecting groups were removed by TFA treatment. The final product was precipitated from the cleavage cocktail by diethyl ether and purified by preparative scale RP-HPLC. The incorporation of D-Lys into the gA sequence made the peptides much easier to synthesize and purify. All peptides were characterized by LC-MS for purity (> 95%) and integrity (Table 2-2 and Table 2-10).

Table 2-2. Sequences of the gA mutants used in this section

Peptide	Sequences[a]
gA-WT	formyl-V-G-A-*d*L-A-*d*V-V-*d*V-W-***d*L**-W-***d*L**-W-***d*L**-W-NHCH$_2$CH$_2$OH
gA-1	formyl-V-G-A-*d*L-A-*d*V-V-*d*V-W-***d*K**-W-***d*L**-W-***d*L**-W-NHCH$_2$CH$_2$OH
gA-2	formyl-V-G-A-*d*L-A-*d*V-V-*d*V-W-***d*L**-W-***d*L**-W-***d*K**-W-NHCH$_2$CH$_2$OH
gA-3	formyl-V-G-A-*d*L-A-*d*V-V-*d*V-W-***d*K**-W-***d*L**-W-***d*K**-W-NHCH$_2$CH$_2$OH
gA-4	formyl-V-G-A-*d*L-A-*d*V-V-*d*V-W-***d*K**-W-***d*K**-W-***d*L**-W-NHCH$_2$CH$_2$OH
gA-5	formyl-V-G-A-*d*L-A-*d*V-V-*d*V-W-***d*K**-W-***d*K**-W-***d*K**-W-NHCH$_2$CH$_2$OH
gA-6	formyl-V-G-A-*d*L-A-*d*V-V-*d*V-W-***d*R**-W-***d*R**-W-***d*R**-W-NHCH$_2$CH$_2$OH

[a] single letter codes, the D- amino acids were labelled by the italic "***d***", and mutation sites are highlighted in bold

2.2.2 *In vitro* characterization of the solubilized gA

To test our hypothesis, we first determined the peptides' solubility in aqueous buffer (10 mM HEPES, pH 7.0 with 1% of DMSO). As expected, the D-Lys incorporation dramatically improves the water solubility of gA mutants. Under our experiment conditions, **gA-WT** is not

detectable by Trp absorption. In contrast, our gA mutants carrying various numbers of charges display the characteristic Trp absorption in aqueous solution with no indication of aggregation (Figure 2-5). Peptide solubility increases with the number of D-Lys residues and does not depend on their positions. The triple D-Lys peptide (**gA-5**) is readily soluble at concentrations close to 100 μM. The solubility is better than that of the wild type by three orders of magnitude.

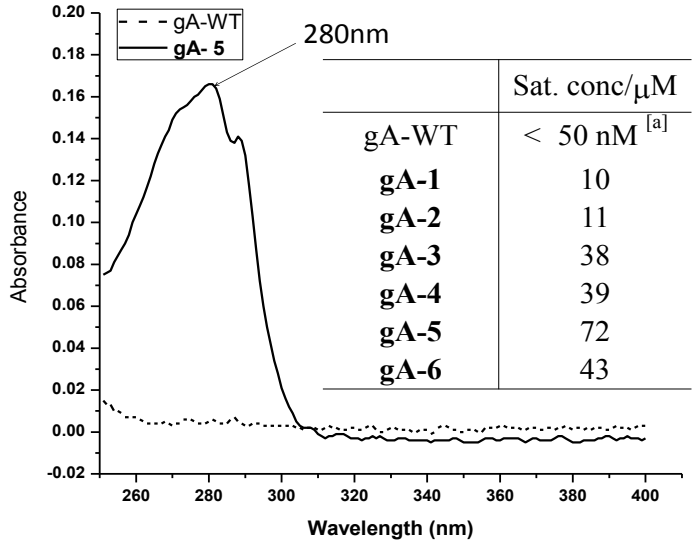

	Sat. conc/μM
gA-WT	< 50 nM [a]
gA-1	10
gA-2	11
gA-3	38
gA-4	39
gA-5	72
gA-6	43

Figure 2-5. Water solubility of the gA variants is determined by Trp absorbance at 280 nm. Representative Trp absorption spectra of **gA-WT** and **gA-5** and solubility of gA mutants are listed in the table. [a] The solubility of **gA-WT** was obtained from reference 22.

To further understand the distribution of these D-Lys containing gA mutants in a cell suspension solution, we measured the binding affinities of the gA mutants to membranes of different compositions. LUVs (~100 nm in diameter) made of POPC were used as a mimic of mammalian cells, while vesicles composed of POPC/POPG (1:1; 1-palmitoyl-2-oleoyl-sn-glycero-3-phosphocholine/1-palmitoyl-2-oleoyl-sn-glycero-3-phosphoglycerol) were prepared to represent bacterial membranes. The peptide-vesicle association was evaluated via a titration

experiment, in which LUVs were titrated into peptide solutions, and the spectral shift of Trp fluorescence was recorded. Fitting the titration curves yielded the apparent dissociation constants (K_d) that are presented in lipid/peptide ratios (Figure 2-6, Figure 2-28). The single D-Lys mutants, **gA-1** and **gA-2** display no discrimination against neutral and negative membranes, yielding apparent K_d values close to that of the **gA-WT**. In contrast, the double D-Lys variants **gA-3** and **gA-4** exhibit a much reduced affinity (by ~ 70 fold) to POPC vesicles, while their affinity to POPC/POPG vesicles remains comparable to that of **gA-WT**. Therefore, these two gA mutants display a minor selectivity on the lipid composition of vesicles. Under the same experimental conditions, the triple D-Lys mutant **gA-5** shows no detectable binding to the neutral POPC vesicles (up to L/P = 2,000), while its K_d value toward the negatively charged membrane dropped by a marginal four folds compared to the wild-type. The membrane selectivity of the triple D-Arg mutant gA-6, however, is minor. It binds much tighter with the neutral vesicles compared to **gA-5**. In general, the cationic **gA-x** mutants are less hydrophobic, and therefore less likely to binds with neutral POPC liposomes. Peptide associations with negative POPC/POPG vesicles were promoted by the Coulombic attraction. As a result, gA mutants with cationic residues show membrane selective association. Their promise as novel systemic antibiotics ultimately relies on their ability to cause ion gradient equilibration by forming effective channels in the lipid bilayer.

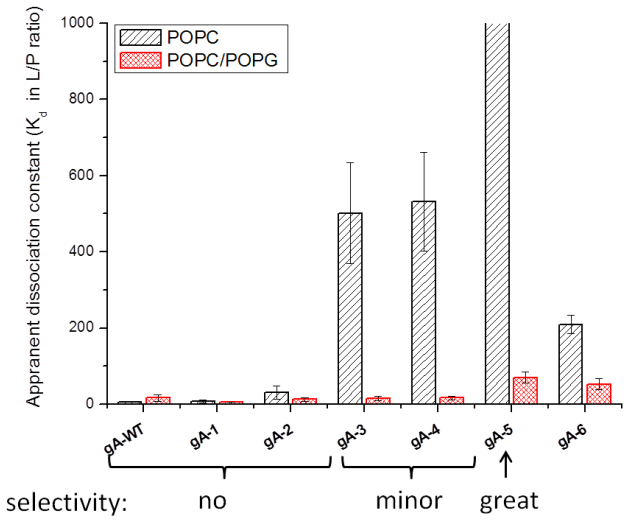

Figure 2-6. Apparent dissociation constants (K_d) of the gA mutants presented as lipid/peptide (L/P) ratios.

We then tested the channel activities of these gA mutants by a K^+ ion leakage assay. K^+ ions were encapsulated in neutral (POPC only) or negatively charged (POPC/POPG = 1:1) vesicles with the same amount of Na^+ ions in the outside buffer to balance the osmotic pressure. Upon channel formation, driven by the ion gradient, K^+ ions diffuse out across the lipid bilayer through the channel and are detected by a potassium ion selective electrode (K-ISE). DMSO addition was used as negative control, while 10 μM **gA-WT** was added to achieve 100% ion equilibration. Similar to the binding results, we observed a selective activity on the negative charged vesicles by the cationic gA mutant but not the **gA-WT**(Figure 2-7). gA mutants carrying multiple D-Lys residues readily induce K^+ ion leakage from the negatively POPC/POPG LUVS, which contrast sharply to the neutral liposomes (POPC LUVs).

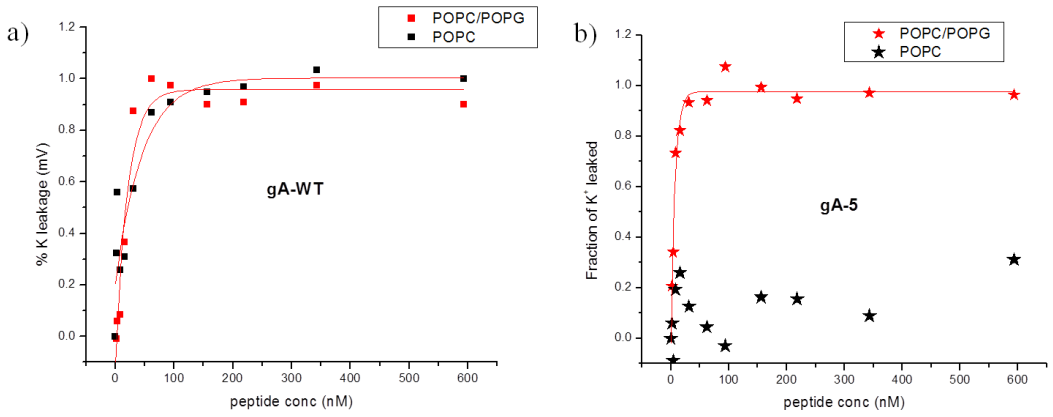

Figure 2-7. Ion leakage profile of gA mutants a) The concentration profile of **gA-WT** induced K^+ leakage from the negative (POPC/PCPG) and neutral (POPC) vesicles. b) The concentration profile of **gA-5** induced K^+ leakage from the negative (POPC/PCPG) and neutral (POPC) vesicles. K^+ ion concentrations were detected by voltage changes of K-ISE.

With the D-Lys residues incorporated towards the C-terminus, the gA mutants described above display amphipathic sequences. Since many amphipathic peptides are known to cause membrane damage through a detergent-like mechanism,[23] we further examined whether it is the case with the gA mutants studied here. As described earlier, while the K^+ ions are small enough, Tb^{3+} ions are too big to diffuse through if the gA mutants form a similar channel as the **gA-WT**. (Figure 2-8). Otherwise, a similar leakage profile would be observed for both ions. Toward this end, we assessed the mutants' conformation with an ion selectivity assay by comparing the efficacy of gA mutants in inducing ion leakage from liposomes encapsulating K^+ and Tb^{3+} respectively.

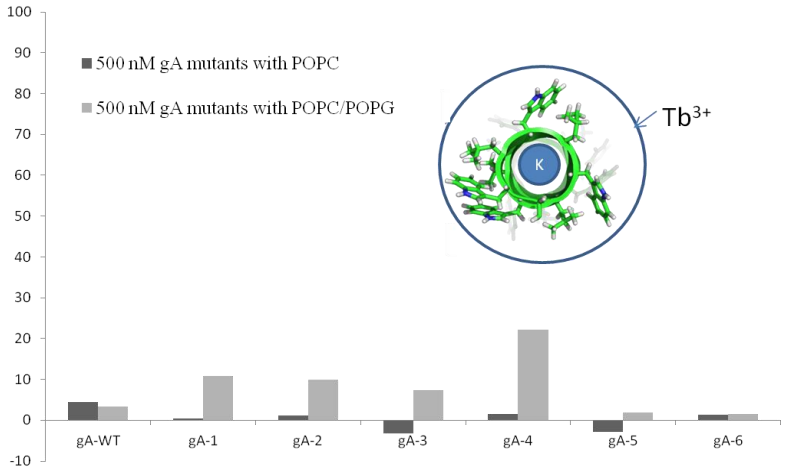

Figure 2-8. gA mutants (500 nM) induced Tb^{3+} ion leakage from LUVs (500 μM, POPC or POPC/POPG) determined by luminescence spectra of the Tb^{3+}/DPA complex. DMSO addition was used as negative control and complete ion release is induced by 0.1% TritonX-100. The insert graph: a schematic representation of the relative size of K^+ ion, gA channel and Tb^{3+} ion.

For all gA mutants, essentially no Tb^{3+} leakage was observed at a peptide concentration five times of that required for complete K^+ ion release from the LUVs (Figure 2-7, Figure 2-8). This indicates that these gA mutants fold into the wild type like structures, which selectively transport monovalent cations. The wild type like channel structure of the D-Lys mutants is further supported by the fact that **gA-5** and **gA-WT** share similar signatures in their circular dichroism spectra (CD spectra, Figure 2-9). This exclusive leakage of monovalent cations is supportive to our hypothesis that cationic residues incorporated at the C-terminus can be well accommodated without altering the channel structure.

Indeed, the results of *in vitro* characterization are consistent with our hypothesis about the designed gA mutants. Their potential as systemic antibiotics was tested with cell based assays.

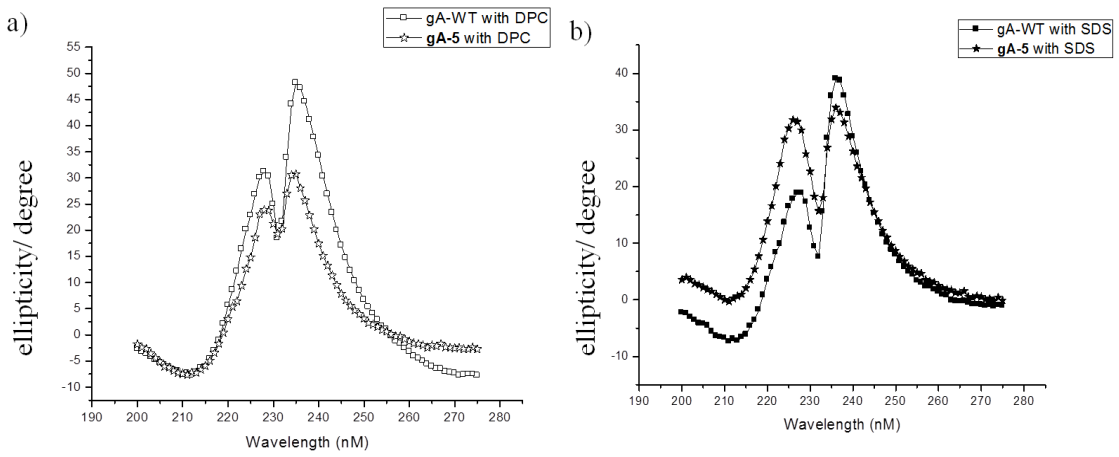

Figure 2-9. CD spectra of **gA-WT** and **gA-5** in (A) DPC or (B) SDS micelles at 1: 50 gA: lipid ratio. (The spectra shown are the averaged signal of three scans after subtracting the DPC or SDS micelle signal).

2.2.3 Cell based antimicrobial activity and toxicity evaluation

The antimicrobial activity of the gA mutants was evaluated on four bacterial strains and the results were compared to the wild type gA (**Table 2-3**). The bacterial strains tested included the Gram-negative *E. coli* (BL 21), and Gram-positive *B. subtilis* (ATCC 663), *S. aureus* (ATCC 6538) and *S. pyogenes* (ATCC 19615). The minimum inhibitory concentration (MIC) was determined by a standard microdilution procedure.[24] Consistent with the previous reports, none of the peptides, including **gA-WT**, effectively kills the Gram-negative *E. coli*.[25,26] In sharp contrast, potent antimicrobial activity was observed against all three strains of Gram-positive bacteria, with MIC values ranging from high nM to low μM. To kill a bacterium, gA peptides need to form channels on bacterial cytoplasmic membrane. The peptides could be trapped into the outer membrane of Gram-negative *E. coli*, on which channel formation does not affect the membrane potential of the bacterium. For Gram-positive bacteria, the peptides can directly function on cytoplamic membrane. Interestingly, all gA mutants except **gA-5** display MIC values essentially

identical to that of **gA-WT**, indicating the charged residues do not compromise the channel forming potential of gA in bacterial membranes. A reduced potency against *S. aureus* was observed for the triple D-Lys mutant **gA-5**, with a MIC value greater than 10 μM. However, it remains highly potent against *B. subtilis* and *S. pyogenes*. The antimicrobial potency of the gA mutants parallels the best antimicrobial peptides reported to date (low μM).[27,28]

As a preliminary evaluation of the peptides' toxicities, we measured their membrane activity against hRBCs (Table 2-3) through two complementary approaches. The typical hemolytic assay[29] monitors leakage of hemoglobin as a consequence of peptide-induced membrane damage. In addition, we also specifically evaluated peptide-induced K^+ leakage from the red blood cells by using atomic emission spectroscopy (AES)[30], in which K^+ concentration released can be assessed by its characteristic emission at 766.5 nm. The results show that **gA-WT** is highly efficient in inserting into hRBC membranes to give transmembrane channels. 50% of intracellular K^+ ion leakage was observed at a peptide concentration of only 140 pM (KC_{50}, 140 pM). **gA-WT** causes hemoglobin release from hRBCs at a concentration similar to that of MIC (MIC, 2.5 μM and HC_{50}, 5 μM), consistent with the known fact that **gA-WT** lacks membrane selectivity and is therefore highly toxic. Importantly, there is a concentration gap for the gA-triggered K^+ leakage and hemoglobin release, indicating that **gA-WT** predominantly forms K^+ specific channels at low concentrations (< 5 μM).

Table 2-3. Antibacterial activity and preliminary toxicity against hRBCS of **gA-x**.

	MICs [a][b] / μM				
	B. subtilis	*S. aureus*	*S. pyogenes*	HC_{50} [c]	KC_{50} [d]
gA-WT	2.5	2.5	0.16	5	1.40E-4
gA-1	5	2.5	0.16	5 ~ 10	0.01
gA-2	5	2.5	0.16	5 ~ 10	0.01
gA-3	5	5	0.32	> 70	5 ~ 10
gA-4	2.5	5	0.32	> 100	5 ~ 10
gA-5	5	>10[e]	0.16	> 100	> 100
gA-6	2.5 ~5	>10[e]	0.62	20	0.16

[a] MIC is the minimum inhibition concentration determined by a standard micro-dilution procedure.[24] [b] None of the peptides tested was active against *E. coli* at a concentration up to 100 μM. [c] HC_{50} is the peptide concentration required to cause 50% of the haemoglobin leakage relative to cell lysis by 1% TritonX-100. For **gA-3/4** the highest concentration tested are not enough to cause 50% haemoglobin leakage. And for **gA-5** there is no noticeable haemoglobin leakage at 100 μM. [d] KC_{50} is the peptide concentration required to cause 50% K^+ Ion leakage relative to the cell lysis by 1% TritonX-100; **gA-5** does not cause noticeable K^+ ion leakage from the hRBCs at the highest concentration tested 100 μM. *nd* stands for not determined [e] **gA-5/6** do not show complete inhibition of *S. aureus* growth at the concentration range tested, and the IC_{50} for both peptides against *S. aureus* are 2.5 -5 μM.

As we anticipated, D-Lys incorporation reduces the membrane lytic potency of gA towards hRBCs. The KC_{50} values correlate well with the number of Lys residues incorporated:

the single Lys mutants display KC_{50} values higher by ~ 100 folds than that of **gA-WT**. Again the channel-forming potential appears to be independent of the position of the D-Lys residue. Addition of the second D-Lys residue reduces the peptides' ability to induce K^+ leakage by another three orders of magnitude to give KC_{50} values of ~ 10 μM. For the triple D-Lys mutant **gA-5**, no K^+ leakage is observed even at concentrations as high as 100 μM. Similarly, the peptide-induced hemoglobin release requires gA mutants at higher concentrations as well. While the single D-Lys mutants display hemolytic potency comparable to **gA-WT**, the double mutants afford significantly higher HC_{50} values (>70 μM). Again the triple D-Lys **gA-5** induces no detectable hemoglobin release at the concentrations tested. These results demonstrate that introducing D-Lys residues effectively eliminates gA toxicity towards hRBCs.

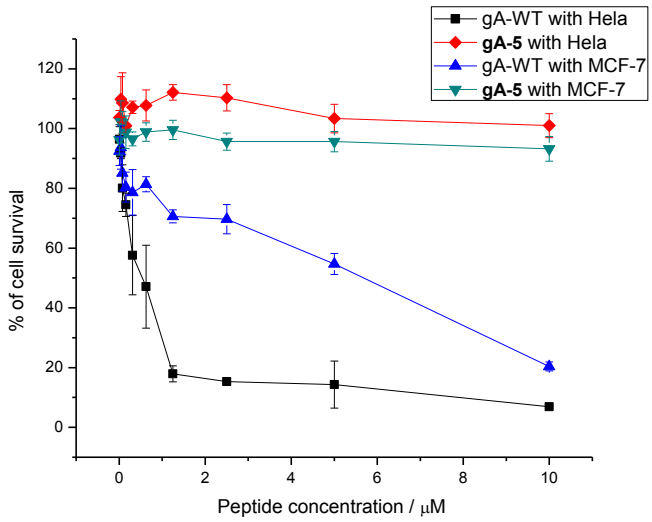

Figure 2-10. Distinct toxicity profiles of **gA-WT** and **gA-5** against two human cancer cell lines (HeLa and MCF-7), demonstrating D-Lys incorporation abolishes gA's toxicity against mammalian cells.

We further examined the toxicity of the gA mutants against two commonly used human cancer cell lines (HeLa and MCF-7). Specifically we measured the percentages of cell survival

under varied peptide concentrations through the MTT assay.[31] Similar to the results for hRBCs, **gA-WT** effectively kills both types of cells with low μM potency. In sharp contrast, cell growth is essentially unaffected by the triple D-Lys mutant **gA-5** (Figure 2-10). Comparison of the bacterial and mammalian cell toxicity data reveals a remarkable therapeutic window (at least three orders of magnitude in concentration) for **gA-5**, which parallels the best amphipathic antimicrobial peptides reported to date.[27,28]

A full characterization of D-Lys modified gA mutants suggested the triple modification had the most optimized properties. We then prepared and evaluated the gA mutant (**gA-6)** substituting the three D-Lys in **gA-5** with three D-Arg residues. Compared to **gA-WT**, **gA-6** also has increased water solubility (Figure 2-5) and membrane selectivity (Figure 2-6). It also forms an ion specific channel on liposomes. While **gA-6** keeps low μM potency against bacterial cells, it displays hemolytic activity with an HC_{50} value of 20 μM, which is less favourable than the gA mutants with two or three D-Lys residues (Table 2-3). The higher hemolytic activity is presumably because arginine, in comparison to Lys, better facilitates the peptide partitioning into mammalian cell membranes.[32,33]

2.2.4 Summary

In summary, we have successfully converted the nonselective channel-forming toxin gA into a bacterium-specific ion channel. Our best candidate **gA-5** is highly potent against Gram-positive bacteria, yet nontoxic toward at least three mammalian cell lines (hRBCs, HeLa and MCF-7). Our design strategy introduces cationic residues into the gA sequence in order to increase the aqueous solubility and to target the negatively charged membranes of bacteria. Based on the detailed structure and mechanism analysis, the charged residues are strategically placed towards the C-terminus of gA, where they appear to be easily accommodated without

compromising gA channel formation. The gA mutants discussed above are novel because they form well-defined channels only permeable to water and monovalent cations, while most of amphipathic AMPs cause nonspecific membrane damage whose mechanism remains largely unknown. The well defined mechanism of action, in addition to the remarkable bacteria-selectivity, makes these gA mutants highly promising as the novel systemic antibiotics. And this strategy has potential to be expanded through engineering of other peptides.

2.3 Lys side chain modifications of the solubilized gA

2.3.1 Hydrophobicity and antimicrobial peptides

The structure and activity relationship of cationic AMPs has been heavily studied in the past decade. AMPs are believed to function by disrupting the plasma membrane of bacterial cells.[11,12,13] From a therapeutic point of view, the ideal antimicrobial peptide should rupture the bacterial membrane without disturbing the mammalian cell membrane. From a mechanistic point of view, high membrane absorption is prerequisite for potent membrane disruption. In addition to the net positive charges that drive the bacterial membrane association through charge-charge attraction. The hydrophobicity also plays an important role in peptide-membrane interactions. In general, increased hydrophobicity promotes the membrane association and boosts the antimicrobial activity. [34,35] Accordingly, we hypothesized that increasing the hydrophobicity of the Lys containing gA mutants while keeping the positive charges would selectively increase the antibacterial activity but not mammalian cell toxicity.

Lys N^{ε}-methylation recently received attention for its role in regulating the transcriptional status of chromatin through the histone proteins.[36,37] In contrast, few references are available about the effect of Lys methylation in the AMP field. It is well known that Lys N^{ε}-trimethylation increases the hydrophobicity while keeping the same net charge as Lys at physiological pH. A simple Spartan calculation showed consistent results. The desolvation energy of tetramethylammonium is 100kJ/mol less than that of methylammonium (CH_3CH_2-$N(CH_3)_3^+$: -200.09 kJ/mol and CH_3CH_2-NH_3^+: -313.52 kJ/mol). Therefore, lysine N^{ε}-trimethylation could be a useful way to adjust the hydrophobicity of gA mutants and to keep the positive charge, consequently, tuning the antimicrobial activity of gA mutants. In this section, I will discuss the effect of Lys N^{ε}-trimethylation on gA Lys containing mutants.

2.3.2 Synthesis and characterization of gA mutants with Lys N^{ε}-trimethylation

Synthesis and characterization of gA mutants with Lys N^{ε}-trimethylation was easily achieved in high yield and purity (Table 2-10) by mixing the lysine containing gA mutants (Table 2-2) with methyl iodide in large excess at high temperature. The peptide was named accordingly (Table 2-4, in the following contents, the gA mutants with Lys are named as **gA-x**, and the gA mutants with N^{ε}-trimethylation Lys are named as **gA-xM**, in which x is the number of each gA mutant).

Table 2-4. Sequences of the Lys N^{ε}-trimethylated gA mutants

Peptide	Sequences[a]
gA-WT	formyl-V-G-A-*d*L-A-*d*V-V-*d*V-W-***d*L**-W-***d*L**-W-***d*L**-W-$NHCH_2CH_2OH$
gA-1M	formyl-V-G-A-*d*L-A-*d*V-V-*d*V-W-***d*Me$_3$K**-W-***d*L**-W-***d*L**-W-$NHCH_2CH_2OH$
gA-2M	formyl-V-G-A-*d*L-A-*d*V-V-*d*V-W-***d*L**-W-***d*L**-W- ***d*Me$_3$K** -W-$NHCH_2CH_2OH$
gA-3M	formyl-V-G-A-*d*L-A-*d*V-V-*d*V-W- ***d*Me$_3$K** -W-***d*L**-W- ***d*Me$_3$K** -W-$NHCH_2CH_2OH$
gA-4M	formyl-V-G-A-*d*L-A-*d*V-V-*d*V-W- ***d*Me$_3$K** -W- ***d*Me$_3$K** -W-***d*L**-W-$NHCH_2CH_2OH$
gA-5M	formyl-V-G-A-*d*L-A-*d*V-V-*d*V-W- ***d*Me$_3$K** -W- ***d*Me$_3$K** -W- ***d*Me$_3$K** -W-$NHCH_2CH_2OH$
[a] single letter codes, the D- amino acids are labelled by the italic "***d***", and mutation sites are highlighted in bold.	

To evaluate the relative hydrophobicity, the gA mutants were subjected to RP-HPLC analysis, in which the retention time reflects peptide hydrophobicity. On a reverse phase column, the longer the retention time is, the more hydrophobic the peptide.[38 ,39] Unfortunately, the

retention time differences before and after N^{ε}-trimethylation were too small to gain insight into the hydrophobicity of gA mutants (Table 2-5). When peptides solubility were evaluated, **gA-xM** mutants showed decreased solubility compared to the corresponding **gA-x** mutants, suggesting that Lys N^{ε}-trimethylation indeed increases the peptide hydrophobicity(Table 2-5).

Table 2-5. Hydrophobicity and solubility comparison of gA mutants containing N^{ε}-trimethylated Lys and Lys

Peptide	C4 column retention time/min [a]	Solubility/ μM [b]
gA-1M	26.8	4.3
gA-1	27.0	10
gA-2M	26.5	3.6
gA-2	26.4	11
gA-3M	24.9	30
gA-3	24.9	38
gA-4M	24.9	27
gA-4	24. 8	39
gA-5M	22.9	55
gA-5	22.9	72

A peptide solution in DMSO was injected on C4 RP-HPLC column and eluted with linear gradient (5 % -95% buffer B over 20 min, in which buffer A is 5% CH_3CN, 95% water and 0.1% TFA; buffer B is 95% CH_3CN, 5% water and 0.1% TFA

The antimicrobial activities were first tested using the same micro-dilution procedures (section 2.2) against four bacterial strains: the Gram-negative *E. coli* (BL 21), and Gram-positives *B. subtilis* (ATCC 663), *S. aureus* (ATCC 6538) and *S. pyogenes* (ATCC 19615). Consistent with other gA mutants, none of the peptides show activity against the Gram-negative *E. coli* (data not shown). However, most mutants showed decreased antimicrobial activity against the Gram-positive strains compared to the Lys version (Table 2-3, Table2-6, Figure 2-11, Figure 2-12). Despite the fact that Lys N^{ε}-trimethylation increased peptide hydrophobicity; it failed to boost its antibacterial activity as we had proposed. Especially, the **gA-5M** fails to kill bacteria at concentration up to 80 μM; it lost its antibacterial activity against the three Gram-positive bacterial strains we tested. The **gA-4M** mutant lost its activity against two of the three Gram-positive strains tested (Table 2-6).

Similarly, the toxicities were evaluated on human red blood cells through two complementary assays: (1) the typical hemolytic assay monitors leakage of haemoglobin as a consequence of peptide-induced membrane damage; (2) the peptide-induced K^+ leakage assay monitors the ion channel formation on hRBCs membrane under identical conditions (Table 2-6). The results combined together suggested that **gA-(1-2)M** reduced toxicities to a larger extent than antibiotic activities (Table 2-6). The peptides containing more than one N^{ε}-trimethylated Lys (**gA-(3-5) M**) showed little hemolytic activity against hRBCs at the concentrations tested. We were only able to comparatively quantify this change in activities and the toxicities of the single modified mutants (**gA-1M, gA-2M**), as the HC_{50} values **gA-(3-5)M** are out of tested range**.** A moderate gain (2-7 folds, Table 2-7) in therapeutic index[40] was observed. In general, Lys N^{ε}-trimethylation decreases the activities of gA mutants in a membrane dependent manner. And to our benefit as potential systemic antibiotics, the loss of activity against the neutral mammalian cell is more important.

Table 2-6. Antimicrobial activities and toxicities against hRBCs of the **gA-xM** mutants

Peptide	Minimum Inhibition Concentration (MIC) / μM[a]			Toxicity/ μM	
	B. subtilis	*S. aureus*	*S. pyogenes*	HC_{50}[c]	KC_{50}[d]
gA-WT	2.5	2.5	0.16	5	0.00014
gA-1M	2.5	2.5	0.15	19	0.04
gA-2M	2.5	1.25-2.5	0.078	24	0.015
gA-3M	2.5	15	1.25	>24	20
gA-4M	*na* (15)[b]	*na* (15)	15	>10	>10
gA-5M	>80 (80% killing)[e]	*na* (80)	> 80 (90% killing)	>95	>95

[a] The minimum inhibition concentration is determined by the standard micro-dilution methods, all tests were repeated at least three times to confirm the reproducibility. None of the peptides tested was active against the Gram-negative *E. coli* (data not shown). [b] *na* (concentration) means that no noticeable bacteria growth inhibition were observed up the concentration labelled in the parentheses. [c] HC_{50} is the peptide concentration required to cause 50% of haemoglobin leakage from human red blood cells (hRBCs) compared to the complete lysis of same amount cells by 1% TritonX-100. [d] KC_{50} is the peptide concentration required to cause 50% K^+ ion leakage from human red blood cells relative to the cell lysis by 1% TritonX-100. The K^+ release is monitored with atomic emission spectroscopy. [e] > 80 (% killing) as percentage of bacteria killing at the highest concentration tested shown before the parentheses

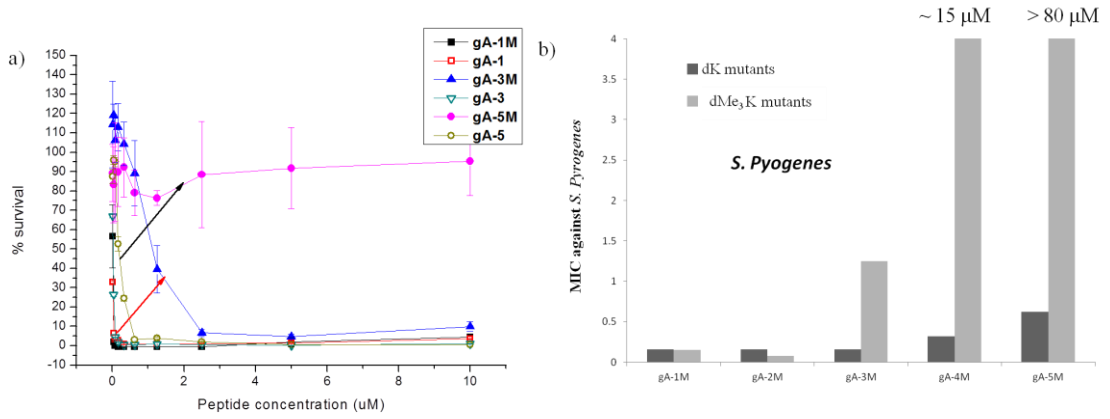

Figure 2-11. Effects of Lys N^{ε}-methylation on antimicrobial activities of gA mutants. a) Representative concentration profile of antibacterial activities against *S. Pyogenes*. The arrow marked the change upon Lys N^{ε}-trimethylation on two series of gA mutants (**gA-x** with open symbol and **gA-xM** with filled symbol). b) comparisons of MIC values of gA mutants against *S. pyogenes* before and after Lys N^{ε}-trimethylation.

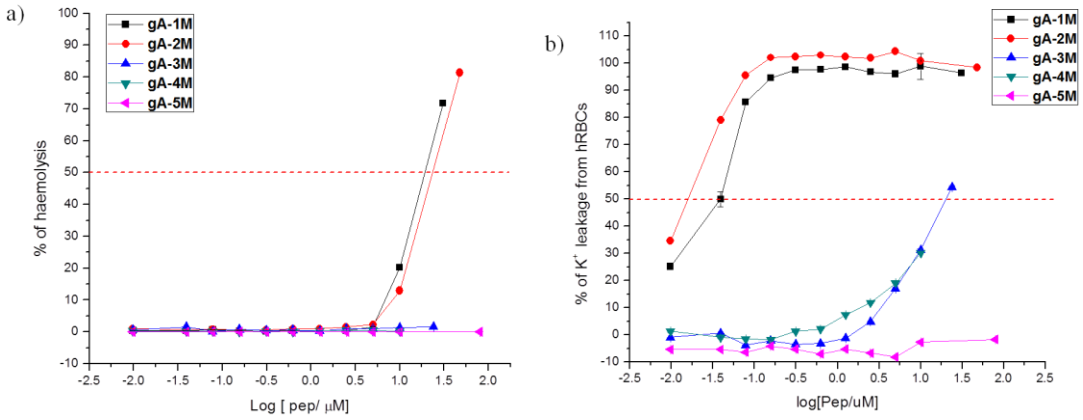

Figure 2-12. Cellular toxicities of N^{ε}-trimethylated Lys containing **gA-xM** mutants. Concentration profiles of a) hemoglobin leakage; b) K^+ leakage from hRBCs. The HC_{50} and KC_{50} values listed in Table 2-6 were obtained from graphs above.

Table 2-7. Therapeutic indices comparison of gA-x and gA-xM mutants against the three Gram-positive strains tested

Bacterial strains	Therapeutic index		Folds increases	Therapeutic index		Folds increases
	gA-1	**gA-1M**		**gA-2**	**gA-2M**	
B. subtilis	1.5	7.6	*5.0*	1.5	4.8	*3.2*
S. aureus	3	7.6	*2.5*	3	9.6	*3.2*
S. pyogenes	47	126	*2.7*	47	308	*6.6*

therapeutic index was calculated as HC_{50}/ MIC,[40] and the folds of changes upon Lys N^{ε}-methylation were calculated as the therapeutic index of **gA-xM** divided by that of **gA-x**, in which is the peptide number as labeled

To better understand our observation that the less soluble gA mutants (**gA-xM**) showed less potent membrane activities, a series of mechanistic studies in model liposomal systems were carried out. Two types of liposomes were used in all characterizations. LUVs, (~100 nm in diameter) made of POPC were used as a mimic of hRBCs, while liposomes composed of POPC/POPG (1:1) were prepared to represent bacterial membranes. All experiments were performed under identical conditions as the studies of the **gA-x** mutants.

Firstly, we determined membrane association through titration. Various amounts of LUVs were titrated into a solution of peptide (500 nM) and the apparent dissociation constants (K_d) of all gA mutants were determined by monitoring Trp fluorescence as described above. Surprisingly, all **gA-xM** mutants exhibited decreased binding affinities with both negatively charged (POPC/POPG) and neutral liposomes (POPC only) compared to the **gA-x** mutants

(Figure 2-13, Table 2-8). The decreased membrane association could be responsible for the decreased membrane activities. Lys N^{ε}-trimethylation does not affect the charges carried by the peptide in neutral aqueous solution. Therefore, the charge-charge attraction between gA mutants and vesicles are not affected. The decreased binding affinity is also contradictory to the increased hydrophobicity upon Lys N^{ε}-trimethylation. We concluded that membrane association of gA mutants is not only driven by the electrostatic attractions and hydrophobicity, but also other factors. It is likely that hydrogen bonding between lysine sidechains and phospholipid headgroups stabilizes the bound form. Replacements of hydrogen with three methyl groups remove the hydrogen bond potential from the peptides, consequently, destabilizing the bound form. Especially, **gA-5M,** carrying three N^{ε}-trimethylated Lys showed no binding to either type of the vesicles, which might account for the loss of activities against cells.

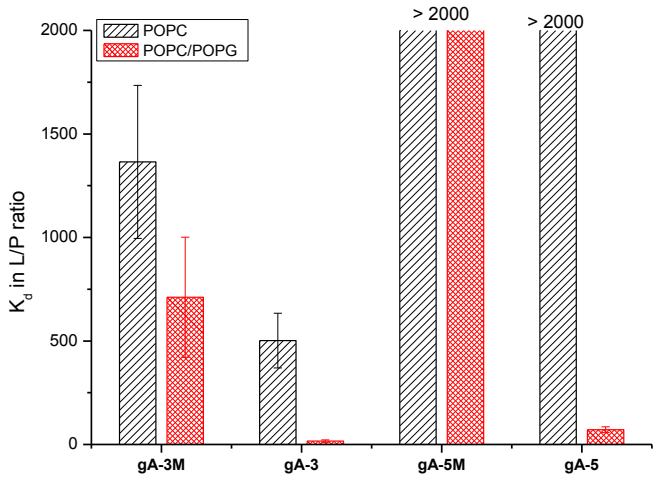

Figure 2-13. Comparison of the apparent dissociation constants (K_d) before and after peptides Lys N^{ε}-trimethylation. y-axis represents apparent dissociation constant (K_d) yielded by fitting the plot of Trp fluorescence signal ($I_{330}/ _{350\ nm}$) vs L/P ratio into an exponential function. Two sets of peptides were shown as examples in the graph.

Table 2-8. Apparent dissociation constant (K_d in L/P ratio) of **gA-x** and **gA-xM** mutants

Peptide	*POPC*[a]	*POPC/POPG*	*Peptide*[b]	*POPC*	*POPC/POPG*
gA-1M	9 ± 2	10 ± 3	**gA-1**	8 ± 4	5 ± 2
gA-2M	119 ± 36	28 ± 7	**gA-2**	31 ± 17	13 ± 5
gA-3M	1365±370	711±290	**gA-3**	502±132	16±6
gA-4M	797 ± 202	168 ± 27	**gA-4**	532 ± 130	17 ± 5
gA-5M	>2000	>2000	**gA-5**	>2000	71±14

The channel structures of these **gA-xM** mutants were indirectly probed by the ion selective leakage assay (Figure 2-8). We measured the potency of the **gA-xM** mutants in causing K^+ and Tb^{3+} ion leakage from LUVs respectively (Figure 2-14). **gA-5M** does not form a channel effectively on either vesicle, especially neutral ones. As expected, K^+ ions readily diffuse out from the interior of vesicles through the channels formed by **gA-(1-4)M** mutants. Complete K^+ ions release was achieved at a concentration of 100 nM, while less than 1% of Tb^{3+} leakage was observed at a much higher concentration (500 nM). These results suggested that, **gA-xM** mutants form channels having **gA-WT** channel structure, which allows only small monovalent ions to pass through. In K^+ leakage assay, all peptides bound on membrane (L/P ratio ~ 5,000, much higher than the determined K_d values). Consistent with the specific toxicity against bacteria, the **gA-xM** mutants shows slightly better channel activities on the negatively charged vesicles (POPC/POPG) than on the neutral ones (POPC only) (Figure 2-14a). Lys N^{ε}-trimethylation changes both the binding affinity and the channel formation potency of the Lys containing mutants. However, the binding selectivity actually gets worse with Lys N^{ε}-trimethylation of gA mutants. Binding cannot explain the observed increase therapeutic indices. Further investigation in the future needs to be done to address this issue and understand the conformational change of gA mutants upon Lys N^{ε}-trimethylation.

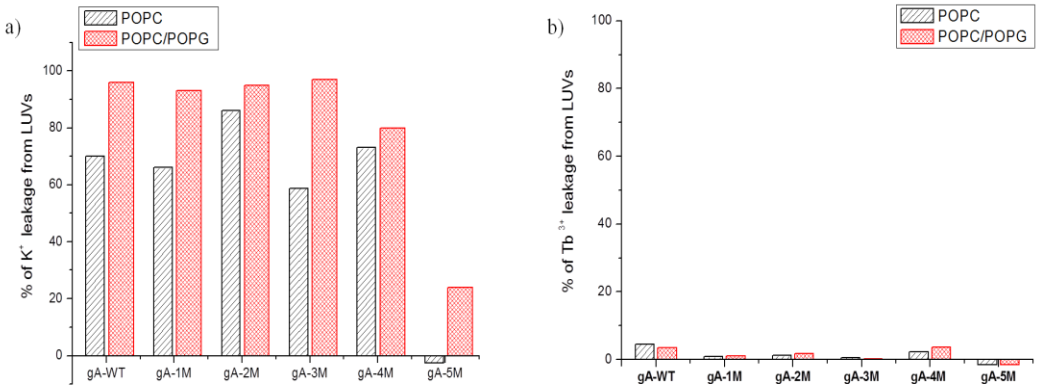

Figure 2-14. Ion selectivity of **gA-xM** mutants. a) **gA-xM** mutants (95 nM) induced K^+ leakage from LUVs (500 μM, lipids ⊃ 10 mM HEPES, 150 mM KCl, pH 7.0) detected by potassium ion selective electrode. b) **gA-xM** mutants (500 nM) induced Tb^{3+} leakage from LUVs (500 μM, lipids ⊃ 10 mM TES, 100 mM sodium citrate, 50 mM $TbCl_3$) detected by the luminescence of Tb/DPA complex. The negative % in the figure could be experimental error.

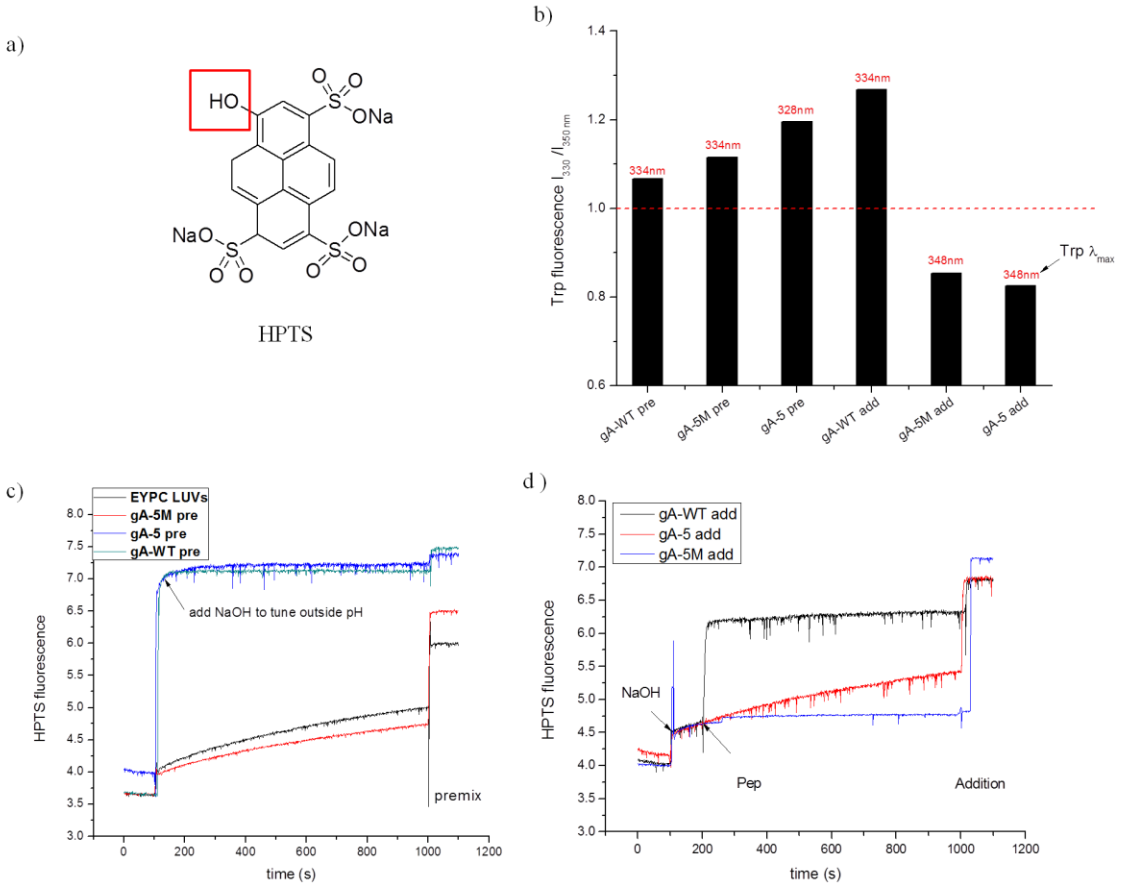

Figure 2-15. a) HPTS structure, with the pH sensitive 8-hydroxyl group highlighted; b) the peptide local environment in EYPC LUVs solutions determined by Trp fluorescence. The y-axis represents Trp fluorescence intensity ratio at 330 nm over 350 nm, and the maximum λ_{em} was labeled on top. The premixed samples labeled as "pre" and samples with peptide added into LUVs solution labeled as "add"; c) the kinetic profile of proton diffusion in the premixed peptides-lipids system. NaOH solution was added at 100s to generate the transmembrane pH gradient; d). the kinetic profile of proton leakage from EYPC LUVs, The exterior bulk solution was tuned from pH =7.0 to 7.6 by adding NaOH solution at 100 s before the peptides addition at 200 s.

Another interesting observation was that **gA-5M** lost channel activity in both model systems and cellular experiments, changing from the best antibiotic candidate **gA-5** (section 2.2) to a nonfunctional molecule upon Lys N^{ε}-trimethylation. We decided to perform more structure activity relationship studies with these two peptides. To evaluate the effect of membrane association, we premixed **gA-5M** and lipids in MeOH/$CHCl_3$ and dried the mixture before hydration in liposomes preparation. We hypothesized that peptides would be kinetically trapped into the vesicle bound state. If a channel formed on the lipid bilayer, encapsulated K^+ ions would leak out spontaneously before the measurements. Therefore, an alternative assay was applied to monitor the channel activity. HPTS is a membrane impermeable pH sensitive fluorophore (Figure 2-25a). Its fluorescence intensity strongly depends on ionization state of the 8-hydroxylgroup (pKa = 7.3). Upon deprotonation, HPTS fluorescence at 460 nm is dramatically enhanced.[41,42,43] Anionic lipids like POPG could cause spontaneous proton transport through lipid flip flop.[44,45] To monitor the proton diffusion, HPTS (10 μM) was encapsulated into the neutral egg yolk phosphatidylcholine (EYPC) LUVs. These lipid bilayers are more tightly packed and able to effectively maintain a pH gradient (black trace in Figure 2-15c). NaOH was added to the exterior buffer to generate a pH gradient. Upon channel formation, protons diffuse out through the channel and encapsulated HPTS is deprotonated, and a fluorescence enhancement can be observed (Figure1-3b). The local environment of the peptides was determined by monitoring Trp fluorescence (Figure 2-15b).[46] When **gA-5** and **gA-5M** were added to neutral EYPC vesicles, neither of the two peptides bind onto membranes (**gA-5M** add and **gA-5** add bars in Figure 2-15b). However, the two peptides are indeed trapped into the membrane bound states in the premixed samples (**gA-5M** pre and **gA-5** pre bars in Figure 2-15b). Then the channel activities were determined. Consistent with the lack of membrane association, no channel activities were observed when **gA-5** or **gA-5M** was added into the EYPC LUVs (red and blue traces in Figure 2-

15d). However, even if gA-5M was trapped in lipid membranes, it did not cause proton leakage (red trace in Figure 2-15c). In sharp contrast, **gA-5** causes proton leakage from EYPC LUVs when the peptides were trapped in lipid bilayer (blue trace in Figure 2-15c). These data together suggested that Lys N^{ε}-trimethylation not only changed the binding profile but also disturbed the structure of the **gA-5** mutant. When stuck in lipid membrane as described above, gA-5M may adopt a different structure which does not form ion channel. This is supported by secondary structure analysis. The CD spectrum of **gA-5M** showed a different signature from that of **gA-WT** and **gA-5** (Figure 2-16). The structure alteration might also happen in other gA mutants upon Lys N^{ε}-trimethylation. Further analysis is required to understand the detailed structural changes.

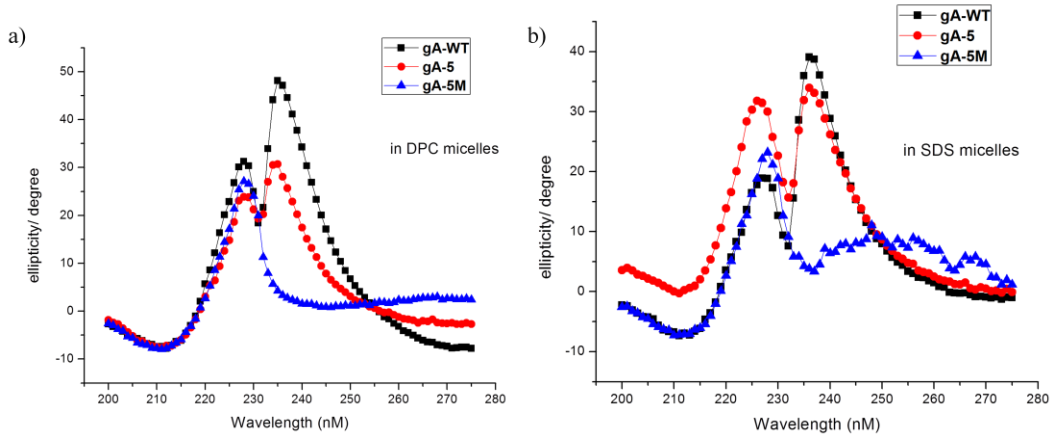

Figure 2-16. CD spectra of **gA-WT**, **gA-5M** and **gA-5** in a) DPC or b) SDS micelles at 1: 50 gA: lipids ratio. (The spectra shown are the averaged signal of three scans after subtracting the background DPC or SDS micelle signal).

2.3.3 Synthesis and characterization of gA mutants with Lys N^{ε}-dimethylation and D-Lys homologs

Lys-N^{ε}-trimethylation not only increases the peptide hydrophobicity, but also removes the hydrogen bonding capability. We hypothesize that the hydrogen bonding capability of the Lys side chain could be very important for membrane association and channel activity. Instead of Lys-N^{ε}-$(Me)_3$. We then incorporated Lys-N^{ε}-$(Me)_2$, which keeps the hydrogen bonding capability of Lys side chain, at positions 10, 12, 14. In addition, we synthesized a series of gA mutants with different Lys homologs incorporated at positions 10, 12, 14. These homologs have free amine groups but different carbon chain length, and varied hydrophobicity (Figure 2-17, Table 2-10). Combined together, we would be able to address the contribution of hydrophobicity and hydrogen bonds to the antimicrobial activity of gA mutants.

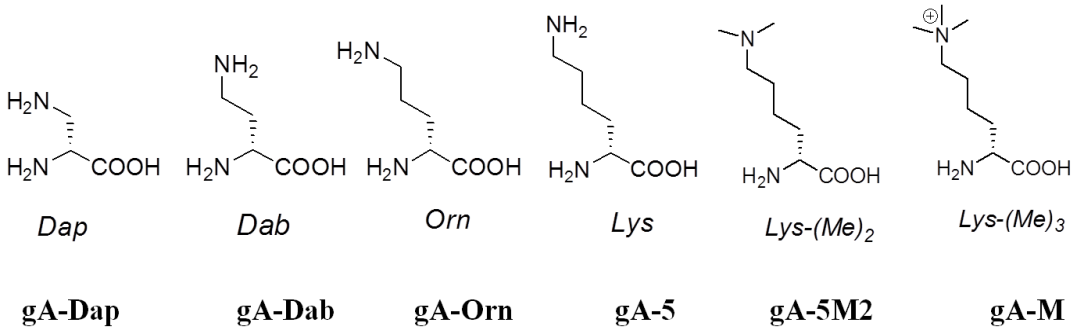

Figure 2-17. Structures of D-Lys homologs incorporated into gA mutants. The names of gA mutants with each D-Lys homolog substitution the D-Leu at positions 10, 12, 14 (highlighted in bold, formyl-V-G-A-*d*L-A-*d*V-V-*d*V-W-***d*L**-W-***d*L**-W-***d*L**-W-$NHCH_2CH_2OH$) were labeled at the bottom .

The antimicrobial activities and toxicity of these gA mutants were tested first (Table 2-9). No toxicities against hRBCs were observed with any of the gA mutants at the concentrations tested (up to 10 μM). Unfortunately, none of the gA mutants showed in Figure 2-17 showed higher antimicrobial activities than the **gA-5** (Table 2-9, Figure 2-18).

Table 2-9. Antimicrobial activities of gA mutants with Lys homologs

Peptide	Minimum Inhibition Concentration (MIC) / μM[a]		
	B. subtilis	*S. aureus*	*S. pyogenes*
gA-WT	2.5	2.5	0.16
gA-5	5	> 10 (80% killing)[c]	0.62
gA-5M	>80 (80% killing)	*na*(80) [b]	> 80 (90% killing)
gA-5M2	20	*na*(20)	20
gA-Orn	10	>10 (50 % killing)	0.625
gA-Dab	>10 (50 % killing)	> 10 (30 % killing)	5
gA-Dap	> 10 (80% killing)	> 10 (30% killing)	5

[a] The minimum inhibition concentration is determined by the standard micro-dilution methods, all tests were repeated at least three times to confirm the reproducibility. None of the peptides tested was active against the Gram-negative *E. coli* (data not shown). [b] *na* (concentration) as no noticeable bacteria growth inhibition were observed up the concentration labelled in the parentheses. [c] > 80 (% killing) as percentage of bacteria killing at the highest concentration tested shown before the parentheses

Apparent dissociation constants of these gA mutants listed above were determined by monitoring the Trp fluorescence following the same procedure. All gA mutants listed above (Figure 2-17) preferentially bind to negatively charged vesicles. However, the trend of membrane association does not reflect the antimicrobial activities of these gA mutants (Figure 2-18). The **gA-Dap** tends to aggregate in low L/P ratios, suggested by the blue shifted Trp fluorescence spectra. This self-association could affect its channel formation potency and its antibiotic activity. However, these preliminary results are not enough to make a conclusion yet. Further investigation needs to be done to understand the relationship between gA primary structure and activities.

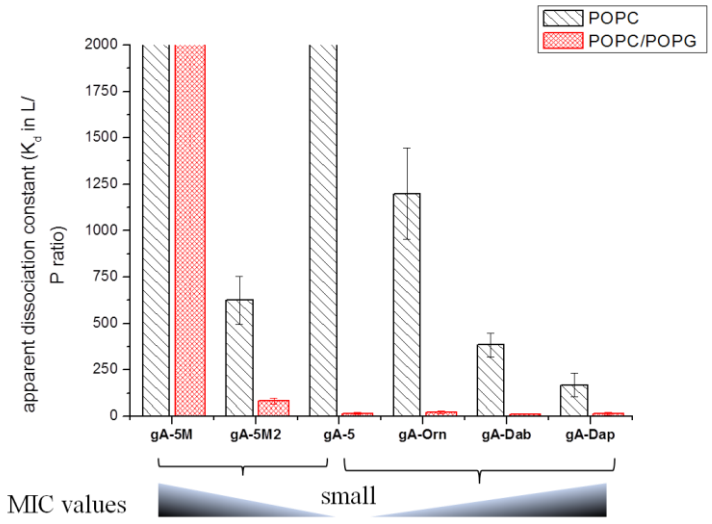

Figure 2-18. Apparent dissociation constants of gA mutants with Lys homologs and N^{ε}-methylated Lys. The antimicrobial activities presented as MIC values are indicated below.

2.3.4 Summary

In summary, the potential of solubilized gA as antibiotics can be fine tuned by Lys N^{ε}-trimethylation. Upon Lys N^{ε}-trimethylation, antibacterial activities of the **gA-(1-3)M** mutants were mildly affected, while their toxicities against hRBCs are significantly decreased. As a result, we gained 2-7 fold increases in therapeutic indices. Studies in model liposomal systems suggested that, Lys N^{ε}-trimethylation affects both the binding affinity between peptides and vesicles, and peptides' structural preference in membranes. For the inactive **gA-5M**, more detailed analyses were performed. Lys N^{ε}-trimethylation on the **gA-5** not only changes the membrane association, but also affects the structure of **gA-5M**. **gA-5M** did not form channel when the peptide is trapped into membranes while **gA-5** did. Further investigation of the conformation/structure changes and activities needs to be done to fully understand the effect Lys N^{ε}- trimethylation on these antimicrobial peptides. Following our investigation into the gA mutants, we further adjusted the properties of cationic gA mutants by incorporating Lys homologs or Lys-N^{ε}-$(Me)_2$ at positions 10, 12, and 14. The preliminary results suggest that these modifications fail to make the gA mutants better antibiotics than **gA-5**. More studies of the structure activity relationship should be performed to understand the chemical basis of the low antimicrobial activity of these cationic gA mutants.

2.4 Using boronic acid to target bacterial membranes

In previous sections, I have introduced our efforts in converting the nonspecific channel forming toxin gA into potential bacterium specific antibiotics. It was achieved by targeting the anionic charges displayed by bacterial cells through electrostatic attraction with the cationic residues incorporated into gA mutants. By tuning the number of cationic residues, hydrogen bonding ability and hydrophobicity, we were able to further adjust the properties of these gA mutants. Our results suggested that purely relying on the Coulombic interaction is not enough to obtain high specific antibiotics. Novel strategies are needed to specifically target the bacterial cell membrane.

2.4.1 Targeting PG headgroup with boronic acid

As described in section 2.2, the plasma membrane of mammalian cells is largely composed of cholesterol and zwitterionic lipids mainly including PC, and SM (Figure 2-19a). In contrast, the plasma membranes of both Gram-positive and Gram-negative bacteria consist of 30-50 % negatively charged lipids mainly including PG and CL, in addition to the zwitterionic PE (Figure 2-19b).[14,15] Bacterium specific membrane toxins reported to date predominantly rely on charge-charge attraction as a driving force for the preferential activity against bacterial cells. However, such peptides often lose their antimicrobial potency when put into physiologic media, presumably because the high salt concentration significantly dampens the Coulombic interactions between the cationic peptides and the anionic membranes[47,48] . Our observed discrimination between the channel activity determined in model membranes and the antimicrobial activity against bacteria could potentially be attributed to this reason. Therefore, novel strategies and/or synergistic strategies are needed to achieve potent and exquisite recognition of bacterial membranes. A close examination of the PG headgroup suggests that besides its global anionic charge, the unique 1,2-diol substructure can be considered as a secondary target (Figure 2-19b).

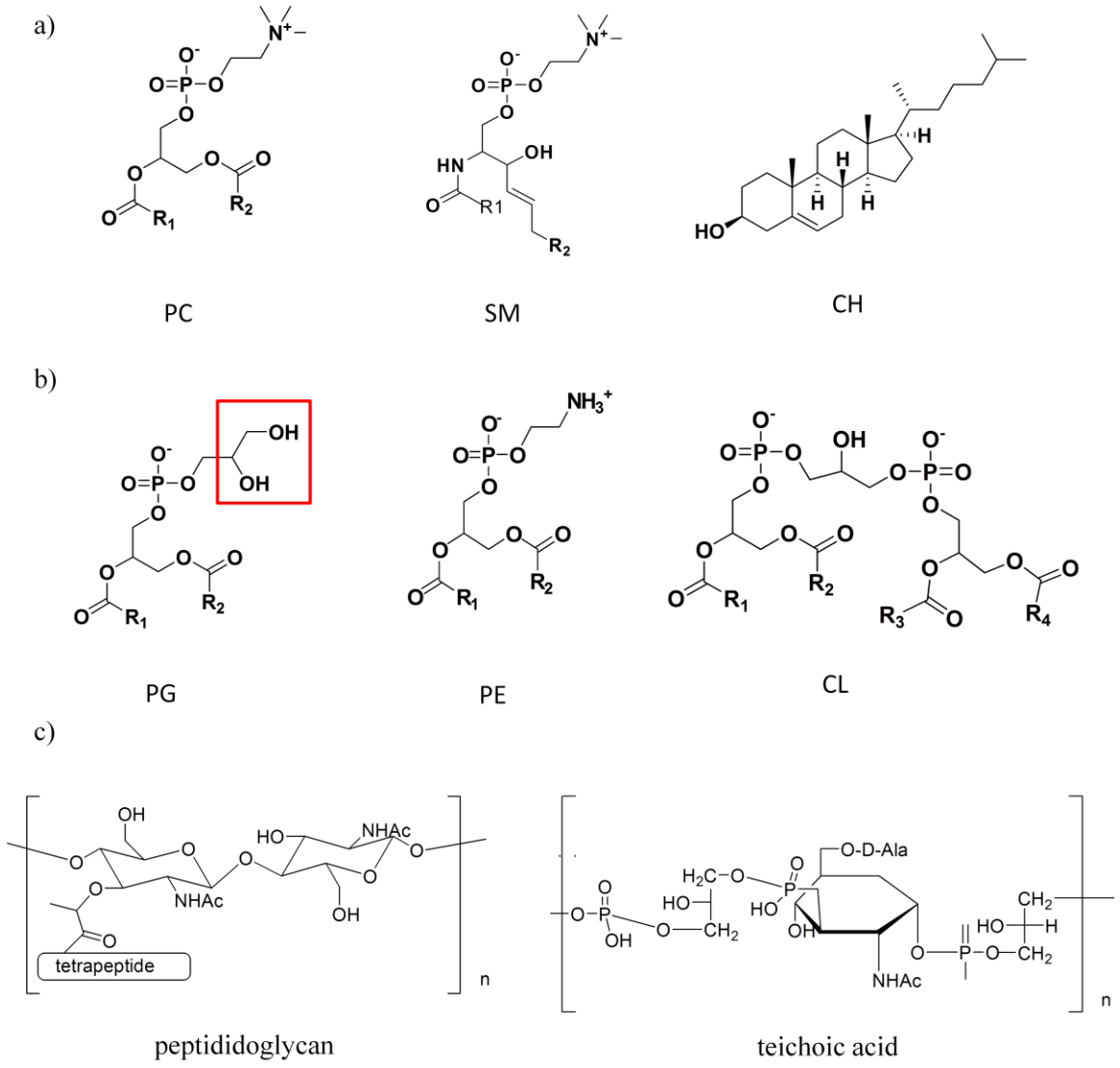

Figure 2-19. Structures of major lipid components in a mammallian cell membrane (a), and a bacterial plasma membrane (b), and important bacterial cell wall carbohydrates (c). The 1,2-diol substructure on the PG headgroup is highlighted with a red square. The carbohydrates in the bacterial cell wall lack the 1,2-diol in the *syn* conformation for boronic acid binding.

In supramolecular chemistry, a boronic acid is often used as a synthon to covalently target 1,2-diol structures (Figure 2-20a).[49] Optimized binding pairs have been used to promote drug delivery and to develop tools in glycoprotein detection.[50,51] The binding affinity between a boronic acid and a 1,2-diol varies depending on the structures of each component[52,53]. In general, boronic acids bind tighter to restrained 1,2-*syn*-diols. We hypothesize that a peptide displaying boronic acids will preferentially bind to PG headgroup, and thus able to specifically attack bacterial cells (Figure 2-20). Although boronic acids display a modest affinity to glycerol in aqueous solutions, we envision that the high density of PG headgroups displayed on the bacterial membrane would increase the local concentration dramatically and favor peptide binding,

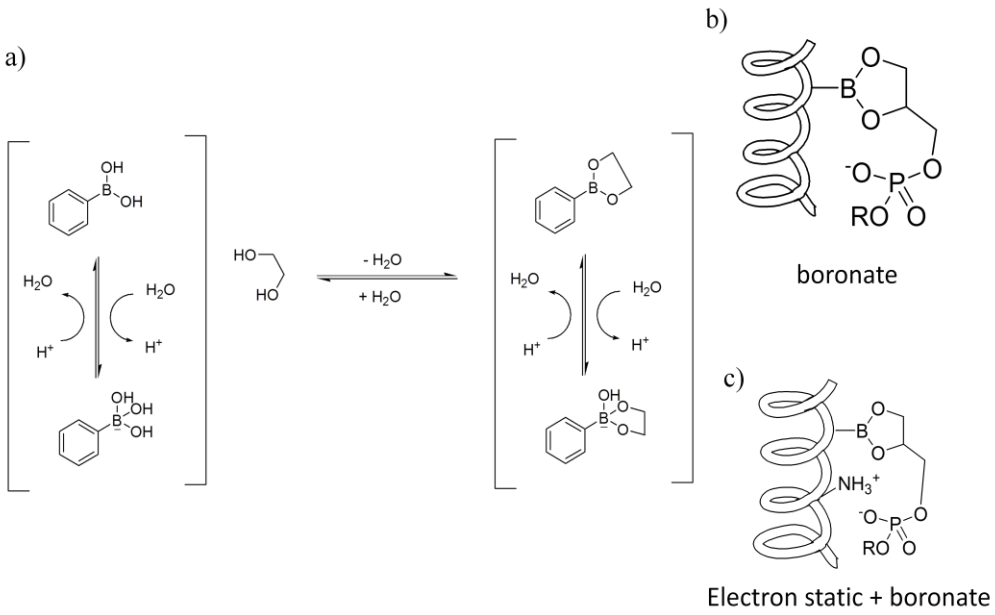

Figure 2-20. Targeting the PG headgroup with boronic acid containing peptides a) binding equilibrium between boronic acid and 1,2-diol in aqueous solution; b) boronic ester formation between boronic acid containing peptide and PG headgroup ; c) synergized charge-charge interaction and boronic ester formation between the PG headgroup and the cationic peptide carrying boronic acid

especially when the peptides carry multiple boronic acids. A polyvalent display of boronic acid has been proven to promote binding between the carrier protein and sugars.[54] In our system, potential competition could come from various carbohydrates. However, they are unlikely to be a strong trap of boronic acid-containing peptides because monosaccharides only display modest affinities to boronic acids while sugar polymers, such as peptidoglycan and teichoic acid do not have 1,2-diols in the *syn* conformation required for boronic acid binding (Figure 2-19c). We believe, well organized peptide structures carrying multiple boronic acid moieties would match the high density of 1,2-diols and consequently favor bacterial membrane binding. If these boronic acids are introduced into cationic peptides, they will be able to synergize charge-charge interaction and boronic ester formation to preferentially target PG over other lipids and carbohydrate molecules (Figure 2-20c). Here I will introduce my project using boronic acid to target the 1,2-diol substructure in PG headgroup and present some preliminary results I obtained on this project.

2.4.2 Detection of boronic acid and 1,2-diol binding

The binding affinities between boronic acids and representative 1,2-diols were determined by a competitive assay. Alizarin Red S (ARS) is a small molecule with a restricted 1,2-diol substructure. It has been widely used to probe boronic acids and 1,2-diol binding.[52,55] An excited state proton transfer from the phenol hydroxyl group of ARS (Figure 2-21a) to the ketone oxygen results in the fluorescence quenching of free ARS. Upon boronate ester formation the quenching is eliminated, therefore, the fluorescence increases (Figure 2-21b). By taking advantage of such features, a three-component competitive ARS binding assay has been designed to determine the binding affinity of a boronic acid and a variety of diols. In the system, there are two competitive equilibria. The first equilibrium, between ARS and boronic acid, phenylboronic acid (PBA) to be specific, can be directly measured. The PBA/ARS binding affinity can be

determined by fitting the concentration profile into an exponential function (Figure 2-21c). The addition of other 1,2-diol molecules sets up the second equilibrium and perturbs the ARS/PBA equilibrium. To be more specific, the additional 1,2-diol forms a complex with PBA and then release ARS from the original ARS/PBA complex; consequently the fluorescence of the solution decreases as more and more competitive 1,2-diols are added to the solution (Figure 2-22). Based on the fluorescence intensity at 582 nm, the inhibitory concentration can be obtained, which reflects the binding affinity of 1,2-diol of interests and PBA. The smaller the value the tighter they bind.

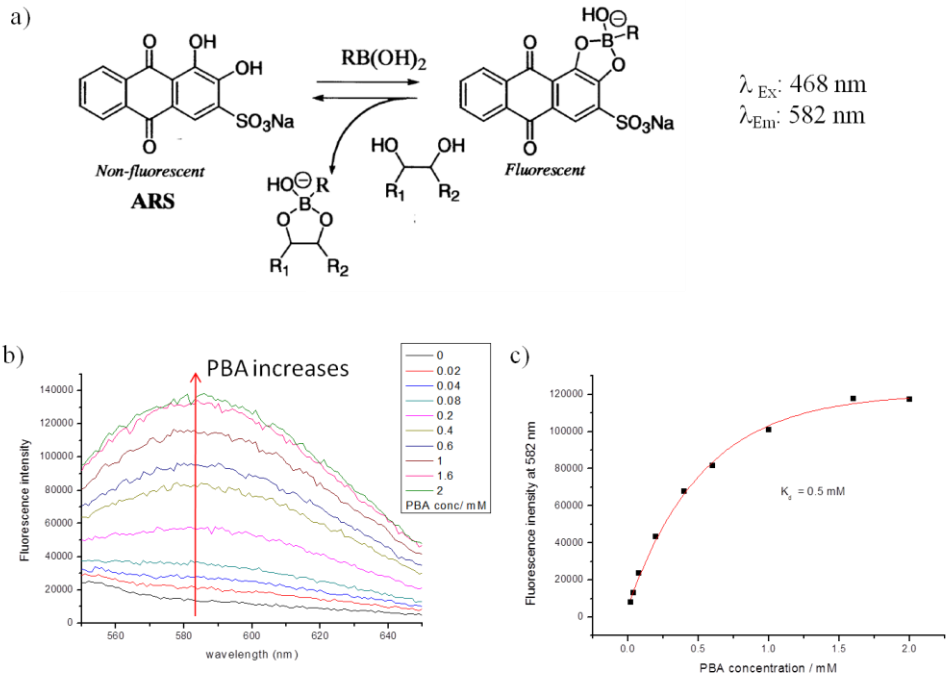

Figure 2-21. Competitive binding assay for determination of boronic acid and 1,2-diol complex formation. a) The two competitive equilibria in the ARS binding assay; b) the florescence spectra of ARS with various amounts of PBA in aqueous solution, (10 μM ARS, 0.1 M PBS, pH 7.0, λ_{ex} = 468 nm), the fluorescence intensity at 582 nm increases as the amount of PBA increases; c) the concentration profile $I_{582\ nm}$ and PBA concentration fitted into an exponential function.

Using fructose, glucose and glycerol as model diol molecules and PBA as the model boronic acid partner, we determined the respective dissociation constants with this ARS binding assay. Consistent with earlier reports, boronic acids bind better with constrained 1,2-*syn*-diols. The fructose inhibits the ARS-PBA fluorescence complex formation at a concentration of 14 mM, which is 32 times smaller than that of glucose. The difference in affinity is due to the favored 1,2-*syn*-diol in the most stable fructose conformation. No obvious PBA binding was observed with up to 1.5 M of glycerol added to the system. The loose binding between glycerol and boronic acid could be due to the rotation freedom. High entropy cost is expected when adjacent hydroxyl groups in glycerol are locked into the five-membered ring of boronic ester. Enhanced binding was indeed observed when 1,2- diol is displayed by the terminal in organized PG containing vesicles. It could be attributed to the increased local concentration (polyvalent display of diol structures).

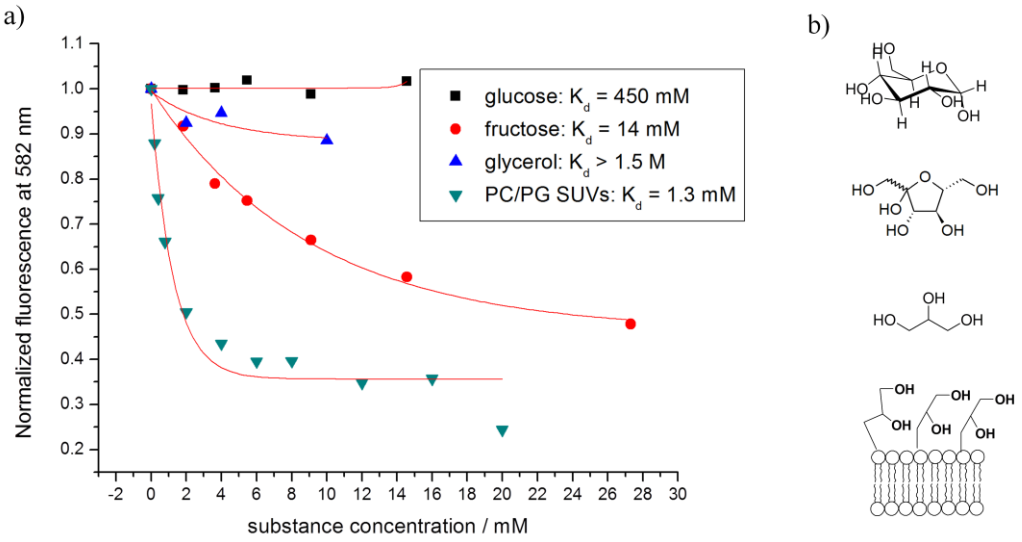

Figure 2-22. Inhibition of the ARS-PBA complex formation by different diols. a) Plots of the normalized fluorescence intensity at 582 nm against substance concentrations, in which total lipids concentration was used for PC/PG SUVs; b) the structure of substance tested.

On the other hand, a polyvalent display of boronic acids on a peptide also showed enhanced binding with diols. The incorporation of the PBA moiety was achieved by using the amino acid Fmoc- protected boronophenylalanine (Fmoc-Bpa(pin)-OH, Figure 2-23). The amino acid was synthesized by Dr. Qin in our group (Figure 2-23, top panel). Specifically, the synthesis starts from Boc- protected iodophenylalanine. The Boc-Bpa(pin)-OH was obtained through $PdCl_2$(dppf) catalyzed Miyaura borylation reaction with K_2CO_3 as the base in DMF. Then the Boc- group was cleaved by neat HCl in acetonitrile to achieve the unprotected H-Bpa(pin)-OH. The Fmoc-protection was carried out in DCM with Fmoc-Cl. The overall yield for the Fmoc-protected amino acids was 62% over three steps. Then the amino acid can be directly used in peptide synthesis. It is compatible with Fmoc/HBTU chemistry.[56]

The polyvalent display of boronic acids was tested with the peptide LP3B (lipid binding peptide with 3 PBA moieties, CBKBKBKWG, in which B stands for boronophenylalanine(Bpa)). The peptide sequence was designed according to the following reasons. 1) Tryptophan was chosen as a probe for concentration calibration or peptide binding with the membrane. 2) The terminal cysteine will conjugate with long wavelength fluorophore in future experiments, which could be potentially useful in bacterial imaging and flow cytometry analysis. 3) The cationic lysine residues were chosen to have Coulombic attraction with the anionic charges, resulting in potential synergistic effects. The peptide was synthesized by standard SPPS applying the Fmoc/HBTU chemistry. Standard TFA cleavage after the peptide synthesis failed to remove pinacol(pin) protecting groups completely (Figure 2-24a). The product is a mixture of four peptides carrying zero to three pinacol protecting groups. Therefore, we applied a boronic ester exchange step with a high concentration of free PBA solution in

DMF (1.6 M, overnight) before the TFA treatment to obtain the fully deprotected peptide in high purity and high yield (Figure 2-24b)[56,57].

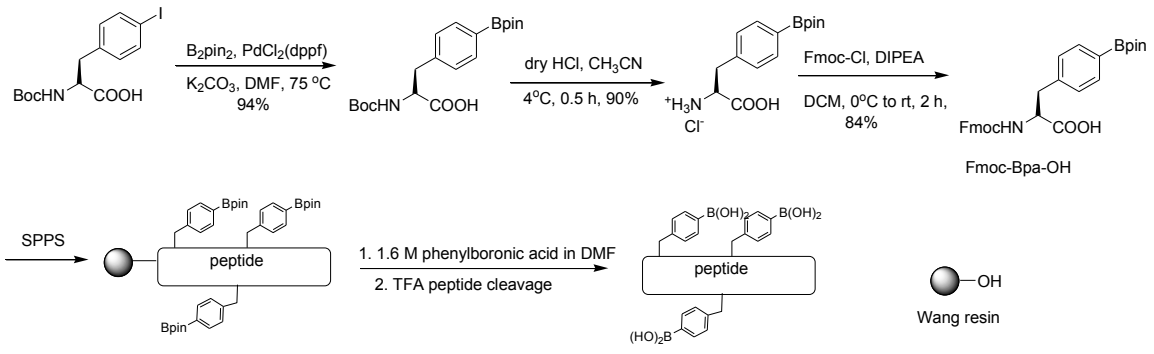

Figure 2-23. Synthesis of boronopeptides using standard solid phase peptide synthesis with Fmoc/HBTU chemistry. Through a three step procedure, we prepared the pinacol protected Bpa, also abbreviated as B in peptide sequence) in Gram quantities (prepared by Dr. Qin). Then the amino acid was incorporated into the peptide as a building block.

Interaction between the LP3B and the 1,2-diol was also determined by the ARS binding assay. Firstly, the fluorescence probe ARS was used as a model 1,2-diol. Compared to the PBA, the peptide gives an enhanced affinity for ARS binding (Figure 2-25) . We envision that even tighter binding can be achieved by matching the polyvalency of boronic acids on a peptide and the high density PG terminal diols on a membrane. Unfortunately, the peptide LP3B suffers from poor water solubility, which prohibits its evaluation against lipid vesicles in aqueous solution (peptide binding with ARS was evaluated in a 1:1 mixture of methanol/ water (v/v).

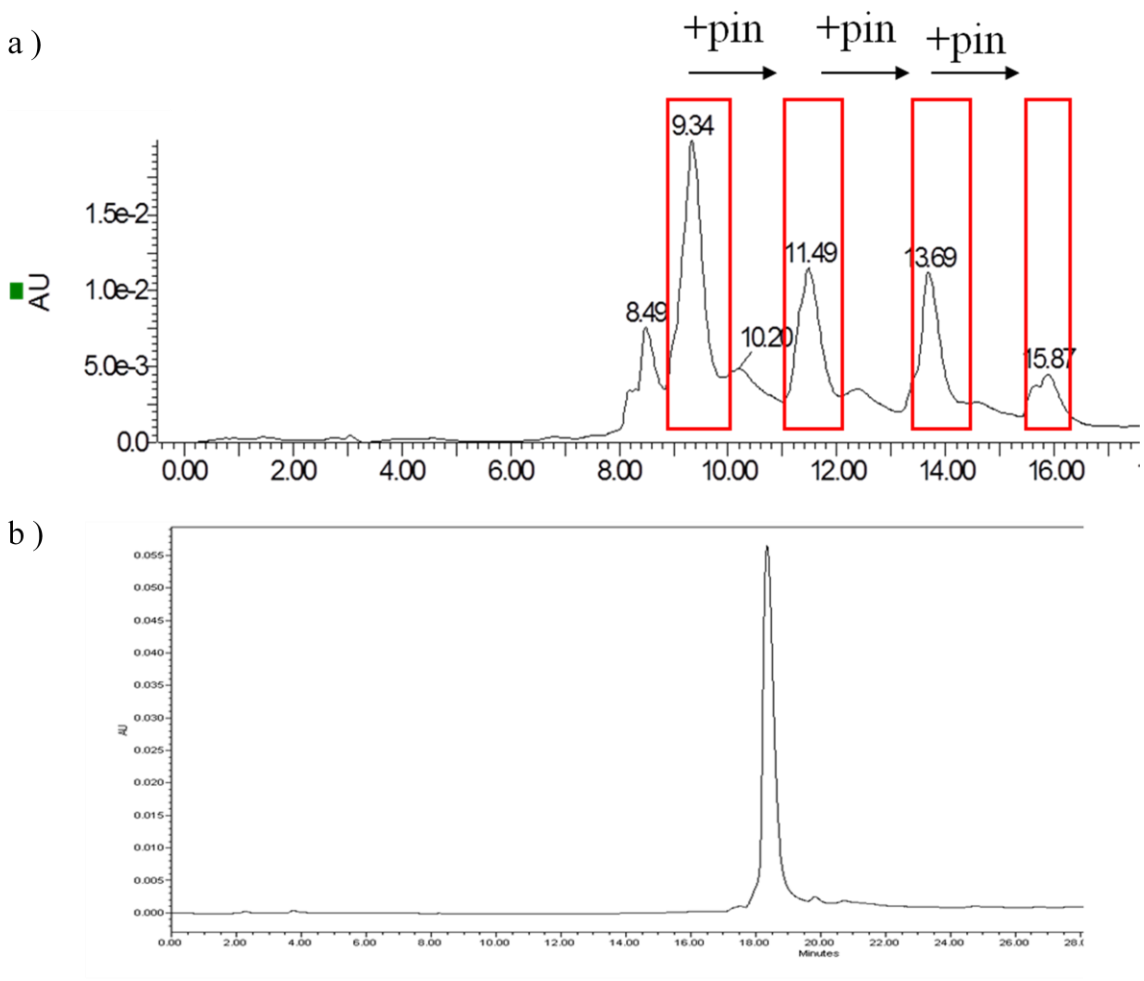

Figure 2-24. Illustration of LP3B peptide synthesis. a) analytical HPLC traces of LP3B peptide cleaved off the wang resin with reagent K; b) analytical HPLC trace of LP3B peptide cleaved off the resin with reagent K after boronic ester exchange reaction. Identity of each peak is determined by MS (ESI^+-TOF). Larger retention time in the bottom trace is because a slower gradient was used in the confirmation of the final product.

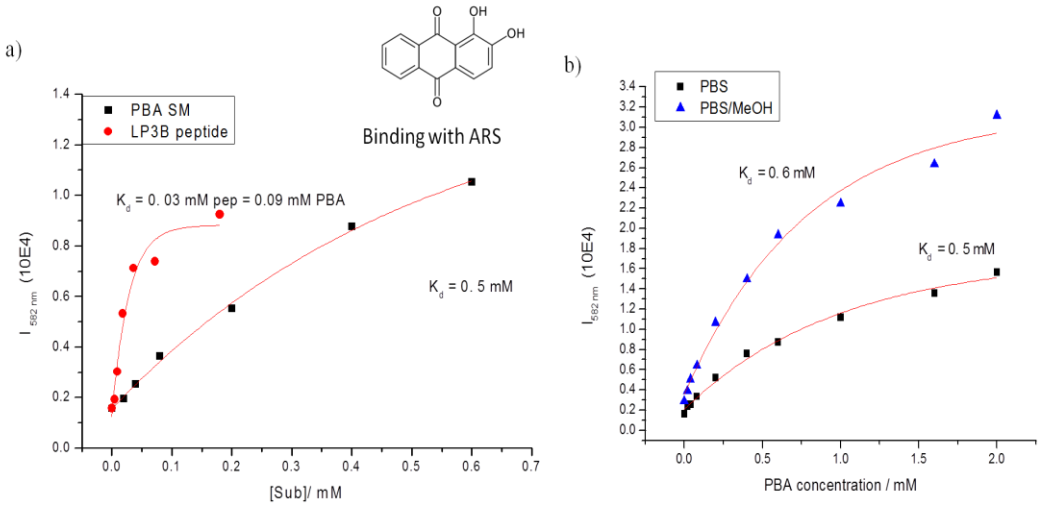

Figure 2-25. a) comparison of monomeric and polymomeric PBA binding with ARS. b) Effect of MeOH addition on PBA-ARS complex formation (0.1 M PBS, pH 7.0 only or a mixture of 0.1 M PBS/MeOH (v/v =1/1) pH 7.0) and the $I_{582\ nm}$ was plotted against the PBA concentration and fitted into an exponential function.

Collectively, these preliminary results suggest that the organized and high density display of the 1,2- diol on the PG containing membranes and polyvalent boronic acids both enhance the formation of the PBA-diol complex. Due to the poor water solubility of the LP3B peptide, I was not able to test the binding between the polyvalent boronic acids and polyvalent 1,2-diols nor the peptides' ability in differentiating PC only SUVs from PG containing SUVs . We suspect that the poor water solubility originates from the lack of net charge as the cationic Lys and anionic Bpa may form ion pairs with each other. To circumvent this problem, we will put in extra positive charges into the peptides in the future.

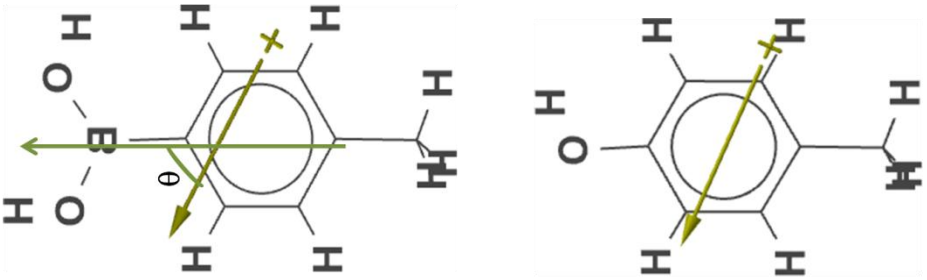

Figure 2-26. Structures and electronic properties of PBA and Tyr calculated in Spartan using the PM model as neutral molecules.

We will further elucidate the potential of boronopeptides in targeting bacterial cells by incorporating Bpa residues into gA. Similar to the D-Lys residues (Section 2.2), the PBA moiety should be accommodated toward the C-terminus of gA, which is expected to be better accommodated without disturbing the channel structure. The electronic properties of the PBA moiety were calculated in Spartan (Figure 2-26). These properties are very similar to tryrosine, which made the most active channel (Figure 1-11). Therefore, we would expect a mutant with relatively high channel potency when Bpa is used to replace the Trp residues. Given its low hemolytic activity, the triple D-Lys mutant **gA-5** (Table 2-2) will be used as a starting point to incorporate a varied number of Bpa residues. If our hypothesis is correct, there will be an borono-Lys-gA with optimized number of Bpa and Lys showing good water solubility, lower MIC values against bacteria while showing negaligible hemolytic activity.

2.4.3 Summary

In summary, our approach in targeting PG containing bacterial membrane jumps out of the canonical wisdom of exploiting the negative charge of bacterial membranes. Instead of the charge-charge attraction, we seek to develop covalent chemistry to target the PG head group. Success of this research will provide a different view in designing novel antibiotics and even bacterial imaging agents.

2.5 Materials and methods

I. General methods

Wang resin, all Fmoc-protected amino acids and Boc-protected amino acid were purchased from either Advanced Chemtech (Louisville, KL) or Chem Impex Int. Inc (Wood Dale, IL). Unprotected valine and other chemicals were obtained from Sigma-Aldrich unless otherwise indicated. 1-palmitoyl-2-oleoyl-sn-glycero-3-phosphocholine (POPC) and 1-palmitoyl-2-oleoyl-sn-glycero-3-phospho-(1'-rac-glycerol) sodium salt (POPG) were purchased from Avanti Polar Lipids (Alabaster, AL). Peptide synthesis was carried out on a Tribute peptide synthesizer (Protein Technologies, Tucson, AZ). PBS buffer, DMEM/High glucose media, Pen/Strep were purchased from Thermo Scientific (Amarillo, TX). Fatty acid-free bovine serum albumin (BSA), 0.25% Trypsin-EDTA solution, MTT cell proliferation Assay Kit were purchased from Invitrogen (Carlsbad, CA).^{1}HNMR data were collected on a Varian Gemini 500 MHz NMR spectrometer. LC/MS (ESI^{+}) data were generated by the Boston College Mass-Spectrometry facility. The protein concentration of all samples used in this study was determined by measuring their absorbance at 280 nm on a Nanodrop 2000c UV/Vis spectrometer. The liposomes were prepared by using Liposofast Mini Extrusion system (Avanti Polar Lipids, Alabaster, AL). All three Gram-positive negative bacteria (*B. subtilis* (ATCC 663), *S. aureus* (ATCC 6538) and *S. pyogenes* (ATCC 19615)) used in antibiotic activity tests were purchased from Microbiologics (Cloud, MN) as lyophilized cell pellet. *E. coli* (BL21) was a gift from the lab of Professor Mary. F. Roberts at Boston College.

II. Peptide synthesis and characterization

1. Synthesis of formyl-L-valine

Acetic anhydride (4 mL, 0.04 mol) was added dropwise to a solution of L-Valine (1 g, 8.35 mmol) in formic acid (12 mL, 0.32 mol) while stirring on ice. The mixture was then warmed up to RT and kept stirring for 24 hours before the solvent was removed by rotary evaporation under high vacuum. The formyl-valine was recrystallized from ethyl acetate and the desired product was obtained as a white solid. Yield: 0.78 g (64%) ^{1}HNMR (500 MHz, [d_5] Acetone, 25 °C, TMS): δ = 8.22 (s, 1H), 7.41(b, 1H), 4.50 (m, 1H), 2.22 (m, 1H), 0.98(m, 6H).

2. Synthesis of Fmoc-D-Lys-N^{ε}-$(Me)_2$-OH[58]

Fmoc-N^{ε}-Boc-D-Lys-OH (1.4 g, 3 mmol) was dissolved in formic acid (20 mL) and stirred at room temperature for 3 hours. The solvent was then removed by rotary evaporation. Trituration in diethyl ether yielded Fmoc-D-Lys-OH formate salt as a white solid (1.2 g, 98% yield, confirmed by LC/MS in high purity, calculated $(M)^+$: 368.43. found $(M+H)^+$: 369.25). To a stirred solution of the salt (600 mg, 1.4 mmol) in MeOH, 37% of aqueous formaldehyde (607 μL, 8.1 mmol) was added. After stirring for 20 min, the reaction mixture was cooled to 0 ^oC in an ice bath. $NaCNBH_3$ (180 mg, 2.8 mmol) dissolved in MeOH (2 mL) was added dropwise to the reaction. After warming to room temperature, the mixture was then stirred for 2 hours. The solvent was removed by rotary evaporation and the product was redissolved in acetone. Insoluble solid was removed by filtration. The filtrate was dried in vacuo to yield the product as a white solid (526 mg, 95% yield). The product is confirmed by LC/MS in high purity (calculated M^+: 396.2. Found $(M+H)^+$: 370.15) and ^{1}H-NMR(DMSO-d_6): d 7.26–7.92(8H, m), 7.1(1H, d), 4.3(3H, m), 3.75–3.77(1H, m), 2.27–2.36(2H, t), 2.2(6H, s), 1.22–1.37(4H, m), 1.49–1.69(2H, m)

3. Synthesis of gA mutants

Peptides, except the Lys N^{ε}-trimethylated gA mutants, were synthesized directly on Fmoc-Trp-Wang resin (64 mg, 0.79 mmol/g, 0.05 mmol) using standard Fmoc/HBTU chemistry. Five equivalents of each amino acid were used for the coupling reaction. The peptides were cleaved from the resin by treating the resin with ethanolamine (40% (v/v) in degassed DMF, 55^{o}C, 5 hours).[22] Then the resin was filtered through a medium fritted plastic funnel and rinsed three times with DCM and methanol to release the peptide efficiently into solvent. The filtrate containing peptide was dried by rotary evaporation to a minimal volume. Then six to seven times in volume of water was added to precipitate the peptide and the precipitation was separated out by centrifugation (14,000 rpm, 1 hour). The pellet was dried on lyophilizer to yield the side-chain protected peptide. The Boc protecting group on d-Lys was removed by treating the pellet with a mixture of 95% TFA, 2.5% TIS and 2.5% H_2O at RT for 2 hours. The Pbf protecting group on arginine was removed by reagent K (80% TFA, 5% H_2O, 2.5% EDT, 5% Thioanisole and 7.5% Phenol, 2 hours at RT). Once the reaction is finished, cold diethyl ether was added to give the crude peptide as white precipitate. The precipitate was again pelleted by centrifugation. The crude material was purified by RP-HPLC (Waters Prep LC, Jupiter 10 μm C4 300A Column). The identity and purity of each peptide was confirmed by analytical RP-HPLC-MS (ESI^{+}) (Waters e2695, Phenomenex, Jupiter 5μm C4 300R). All peptides were confirmed to have purity of 95% or higher.

The Lys N^{ε}-trimethylated gA mutants (**gA-xM**) were synthesized from the Lys containing mutants (**gA-x**). **gA-x** mutants were dissolved in acetonitrile. To the stirred solution, methyl iodide (20 eq) and DIPEA (30 eq) were added. The mixture was stirred at 80 °C for 24 hours in a pressure vessel. After cooling down, solvents and excess methyl iodide were removed by rotary evaporation. The residues were dissolved in acetonitrile/water mixture and peptides

were isolated by RP-HPLC. All peptides were confirmed by analytical RP-HPLC-MS (ESI^+) (Waters e2695, Phenomenex, Jupiter 5μm C4 300R) to have purity of 95% or higher. The MS results were listed in Table 2-10.

Table 2-10. LC-MS results of gA mutants

Peptides	*m/z* calculated	*m/z* found
gA-1	1899$[M]^+$	949.8/950.2 $[M+2H]^{2+}$
gA-2	1899 $[M]^+$	1900 $[M+H]^+$, 948.8/950.2$[M+2H]^{2+}$
gA-3	1913 $[M]^+$	957.3/957.8 $[M+2H]^{2+}$
gA-4	1913 $[M]^+$	957.8/958.3 $[M+2H]^{2+}$
gA-5	1927 $[M]^+$	964.7 $[M+2H]^{2+}$
gA-6	2012$[M]^+$	671.4/671.8/672.1$[M+3H]^{3+}$,1006.9/1007.4/1007.9 $[M+2H]^{2+}$
gA-1M	1941$[M]^+$	1942.0 $[M+H]^+$, 971.2/971.8/982.3 $[M+2H]^{2+}$
gA-2M	1941 $[M]^+$	1942.0 $[M+H]^+$, 971.2/971.8/982.3 $[M+2H]^{2+}$
gA-3M	1997 $[M]^+$	999.9/1000.4/1000.9 $[M+2H]^{2+}$
gA-4M	1997 $[M]^+$	999.9/1000.4/1000.9 $[M+2H]^{2+}$
gA-5M	2053 $[M]^+$	685.1/685.4/685.7 $[M+3H]^{3+}$
gA-5M2	2011$[M]^+$	670.7/671.0/671.3$[M+3H]^{3+}$, 1006.2 $[M+2H]^{2+}$
gA-Orn	1885$[M]^+$	630.7/631.0 $[M+3H]^{3+}$, 944.5 $[M+2H]^{2+}$
gA-Dab	1444$[M]^+$	615.7/616.1 $[M+3H]^{3+}$, 922.3/922.8/923.3 $[M+2H]^{2+}$, 1845.0
gA-Dap	1402$[M]^+$	467.3/467.7/468.1$[M+3H]^{3+}$

4. Synthesis of boronopeptide

Boronopeptide (LP3B) was synthesized using the same SPPS procedures described above. The PBA moiety was incorporated by the Fmoc-boronophenylalanine-OH (Fmoc-Bpa-OH). The Fmoc-Bpa-OH was synthesized with a three step reaction developed by Dr. Qin (Figure 2-23). After peptide elongation, the pinacol protecting groups were removed by a boronate ester exchange reaction on resin. Specifically, the resin loaded with LP3B peptide was incubated in 1.6 M of PBA in DMF overnight. Next, the resin was washed with DMF, MeOH and DCM three times respectively. Finally, the peptide was cleaved off the resin with reagent K (80% TFA, 5% H_2O, 2.5% EDT, 5% Thioanisole and 7.5% Phenol, 2 hours at RT). Once the reaction is finished, cold diethyl ether was added to give the crude peptide as white precipitate. The precipitate was separated by centrifugation. Crude material was purified by RP-HPLC (Waters Prep LC, Jupiter 10 μm C18 300A Column). The identity and purity of each peptide was confirmed by analytical RP-HPLC-MS (ESI^+) (Waters e2695, Phenomenex, Jupiter 5μm C18 300R, Figure 2-24b), calculated $[M]^+$ 1323, identified $[M+3H]^{3+}$ 442.

III. Peptide Solubility test

Peptide solubility in 10 mM HEPES buffer with 1% DMSO was measured by monitoring Trp absorbance at 280 nm. A concentrated (6.0 – 8.0 mM) peptide stock solution in DMSO was diluted 100 times (5 μL of the stock into 500 μl of 10 mM HEPES buffer, pH 7.0). The mixture was sonicated for 30 min and then subject to centrifugation (14,000 rpm, 10 min) to remove possible precipitate. The supernatant (400 μL) was transferred to a quartz cuvette (1 cm path length) and the peptide concentration was calculated according to Beer's law. Representative UV/Vis spectra of the supernatant are shown in Figure 2-5.

IV. Model membrane studies

Buffer A: 10 mM HEPES, 150 mM NaCl, pH 7.0

Buffer B: 10 mM TES, 150 mM sodium citrate, pH 7.0

1. Liposome preparation

A chloroform solution containing 76 mg of POPC (for POPC LUVs preparation) or a chloroform/methanol (1/1) containing 38 mg of POPC and 38.5 mg POPG sodium salt (for POPC/POPG LUVs preparation, POPC：POPG=1：1) was dried under reduced pressure to receive a thin film which was then hydrated with 2 mL aqueous buffer: (1) 10 mM HEPES, 150 mM KCl, pH 7.0 for K^+ leakage assay; (2) 10 mM TES, 100 mM sodium citrate, 50 mM $TbCl_3$, pH 7.0 for Tb^{3+} leakage assay; (3) 10 mM HEPES, 150 mM NaCl, pH 7.0 for peptide binding assay. After 20 cycles of freezing and thawing, the liposome suspension was extruded 21 times through a 100 nm polycarbonate membrane (Liposofast Mini Extrusion system, Avanti Polar Lipids; Whatman Nuclepore Track-Etch Membrane) at RT. Free K^+ or Tb^{3+} were removed by gel filtration (ÄKTA FPLC with HiPrepTM 16/60 Sephacryl TM-S-500HR column) using **Buffer A** for (1) and (3) or **Buffer B** for (2) as the eluent. The lipid concentration was determined by Stewart assay[6] and the size of liposome was confirmed by Dynamic Light Scattering (DLS, DynaPro nanostar, Wyatt, Santa Barbara, CA). The instrument setup used the standard PBS parameters: refractive index @589 nm & 20°C is 1.333, viscosity is 1.019 cp, Cauchy coefficient is 3119 nm^2. Data were acquired in auto-attenuation mode, and processed with DYNAMIC V6TM software. The diameters of all liposomes were found to fall into the narrow range of 100~150 nm with a polydispersity lower than 30%. After gel filtration the polydispersity of all liposome preparation is below 20%. The total lipids concentration in POPC/POPG LUVs was

calculated by doubling the measured POPC concentration, as the Stewart assay does not report the amount of POPG.

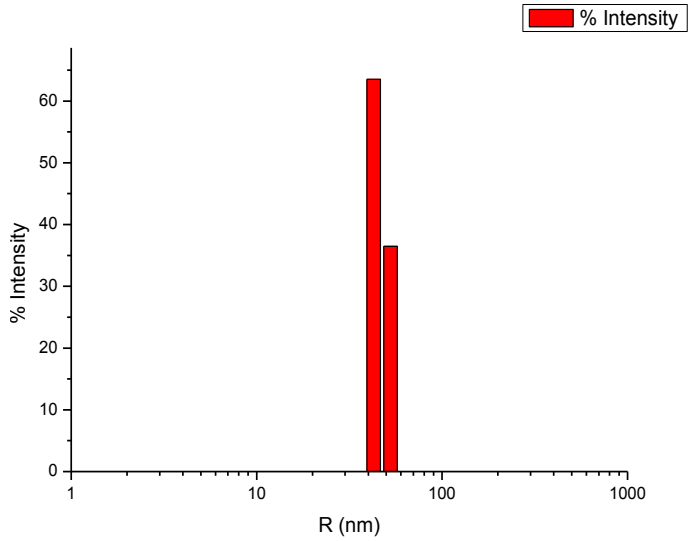

Figure 2-27. An representative bar graph of liposome size distribution determined by dynamic light scattering (POPC/POPG 1:1 LUVs).

2. K^+ leakage assay

The K^+ leakage from liposomes was determined by a potassium ion selective electrode (K-ISE) (Cole-Parmer, Vernon Hills, Il). The electrode was calibrated each day before experiments. A liposome solution in **Buffer A** (2 mL, 500 μM POPC or POPC/POPG ⊃ 10 mM HEPES, 150 mM KCl, pH 7.0) was stirred at constant speed and peptide at various concentration (1 μL in DMSO) was added accumulatively. Three minutes after each peptide addition, the K^+ concentration was measured and reported as potential. At the end, WT gA stock (1 μL, 1 mM) was added to induce 100% K^+ leakage. The potential reported by the K-ISE was plotted against peptide concentration after the background signal (caused by DMSO addition) was subtracted and normalized to 0 – 100%.

3. Peptide binding onto membranes

Peptide partitioning into lipid bilayers was monitored by fluorescence enhancement of tryptophan upon binding to hydrophobic liposomes. gA mutants (500 nM) were mixed with various amounts of liposome in **Buffer A** (POPC ⊃ 10 mM HEPES, 150 mM NaCl, pH 7.0 or POPC/POPG ⊃ 10 mM HEPES, 150 mM NaCl, pH 7.0). The mixture was agitated gently for 30 min before the tryptophan fluorescence spectra were scanned between 320 nm and 360 nm on a SpectraMax M5 (Molecular Devices, Sunnyvale, CA). For each peptide, the ratio of fluorescence intensity at 330 nm and 350 nm (I_{330nm}/I_{350nm}) was calculated and plotted against the Lipid/Peptide ratio (L/P ratio). The curve was fitted into an exponential function to give an apparent binding constant. Figure 2-28 shows some representative binding curves acquired.

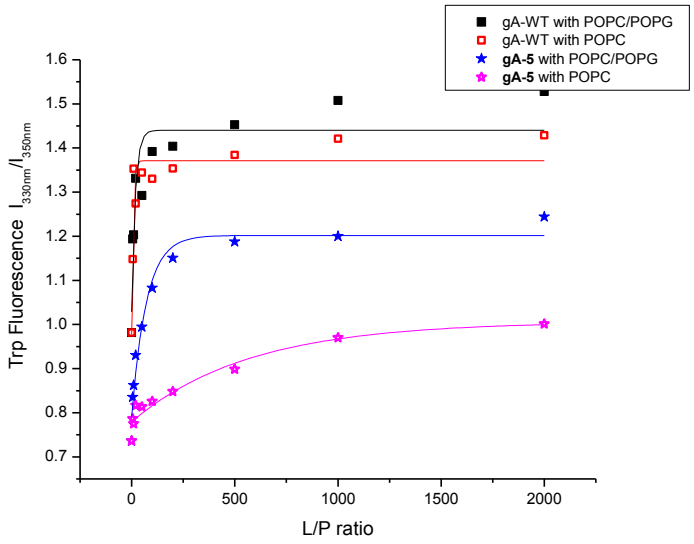

Figure 2-28. Representative binding curves of gA peptides, fitted with exponential function.

4. Tb^{3+} leakage assay

The leakage of Tb^{3+} from liposome was monitored by the fluorescence of Tb/DPA complex[7]. To a mixture of vesicles (500 μM, POPC or POPC/POPG ⊃ 10 mM TES, 100 mM sodium citrate, 50 mM $TbCl_3$) and DPA (50 μM) in **Buffer B**, peptide was added (0.5 μM, 2 μL of 250 μM stock in DMSO; 5μM, 5 μL of 1 mM stock in DMSO). The peptide liposome mixture was incubated at RT for 30 min before the fluorescence intensity of Tb/DPA complex (λ_{ex}=270nm, λ_{em}=490 nm) was recorded (I_c) in a quartz cuvette on a MicroMax 384 fluorescence spectrometer (Jobin Yvon, Horiba Scientific). Complete Tb^{3+} leakage was assessed by Triton X-100 lysis of liposomes (I_f). A sample with pure DMSO added was used as a blank (I_0) and the fraction of Tb^{3+} leakage was calculated as fraction = $(I_c-I_0)/(I_f-I_0)$.

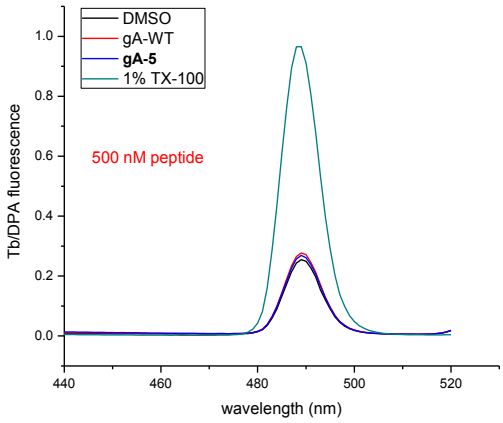

Figure 2-29. Representative luminescence spectra of the Tb^{3+}/DPA complex leakage assay upon peptide (500 nM) addition to POPC/POPG LUVs (there is no noticeable difference in the spectra of **gA-WT**, **gA-5** and DMSO addition).

5. Peptide secondary structure by Circular Dichroism (CD) spectrum

gA analogues (0.2 μmol) dissolved in DMSO were mixed with Fos-phosphatidylcholine-C_{12} (DPC, 10 μmol) or sodium dodecyl sulfate (SDS, 10 μmol) in methanol (L/P ratio 50). Then the mixture was dried by rotary evaporation and lyophilized overnight to remove all possible solvent. Next, dry Gramicidin/DPC or SDS films were resuspended in N_2-flushed H_2O (2 mL) before the incubation (55^{o}C, 15 min) and ultrasonication (RT, 1 min) cycles (three times) were performed[8]. The micelles containing peptides were centrifuged at 12,500 rpm for 5 min to remove possible aggregation and other residues generated in ultrasonication. The supernatant was transferred into a quartz cuvette and CD spectra were recorded (RT, 1 cm path length, scan 200-275 nm, integration time 3s) on AVIV Model 420 Circular Dichroism Spectrometer (Biomedical Inc, Lakewood, NJ).

V. Antimicrobial activity

1. Minimal Inhibitory Concentration measurements

Minimal Inhibitory Concentrations (MICs) were measured against Gram-negative E. *coli* (BL21) and Gram-positive *B. subtilis* (ATCC 663), *S. aureus* (ATCC 6538), *S. pyogenes* (ATCC19615) using the broth microdilution method.[2] Specifically, bacteria from a single colony were grown overnight in LB broth at 37^{o}C with agitation. An aliquot was taken and diluted (1: 50 for *E. coli*, 1:20 for *B. subtilis*, 1:200 for *S. aureus*, 1: 10 *for S. pyogenes*) in fresh broth and cultured for another ~ 3 hours until the cells reach mid-logarithmic phase (OD_{590} ~ 0.6). The cells were diluted to a concentration of ~ 5×10^5 Colony Forming Units/ml (CFU/ml) and the bacteria suspension (200 μL) was added to each well of a sterile 96-well plate. Serial diluted (2-fold) peptides in DMSO (2 μL) were added in triplicates. The plates were shaken for 30 seconds to mix the peptide solution well with the broth, and then incubated at 37^{o}C overnight before the

optical density at 590 nm was monitored using a microtiter plate reader (SpectraMax M5, Molecular Devices, Sunnyvale, CA). The viability of the bacterial was normalized as % survival = $(OD_{pep,bac} - OD_{broth\ only})/ (OD_{DMSO,\ bac} - OD_{broth\ only}) \times 100\%$. The effect of 1% DMSO is negligible as the bacterial cell density with DMSO addition is comparable with that of bacterial suspension in LB Broth. The MIC was recorded as the peptide concentration required for complete inhibition of cell growth (no change in absorbance). Representative curves plotting the cell viability against the peptide concentration are shown in **Figure 2-30**.

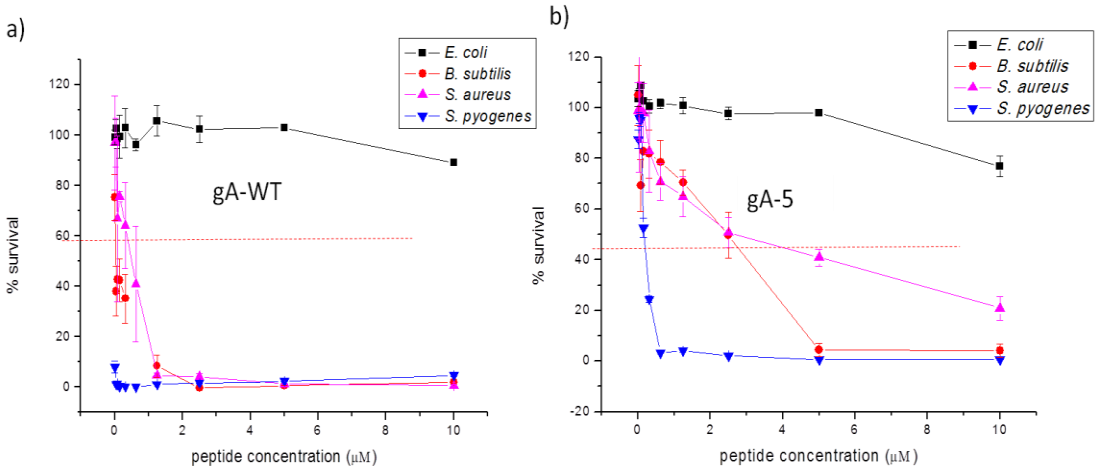

Figure 2-30. Antibiotic activity profiles for (a) **gA-WT** and (b) **gA-5** against bacteria strains tested

VI. Toxicity against mammalian cells

1. Hemoglobin release from hRBCs

Fresh hRBCs were centrifuged at 3500 rpm and washed with PBS buffer until the supernatant was clear. The hRBCs were then resuspended and diluted to a final concentration of 1% (v/v) in PBS and used immediately. 15 μL of serial dilution (2-fold) of peptides in DMSO or DMSO alone as negative control was added to 1.5 mL of hRBCs in PBS. The resulting mixture was gently shaken to mix well and incubated at 37°C for 1 h, followed by centrifugation at 3500 rpm for 10 min using tabletop centrifuge. Aliquot (50 μL) of supernatant (in triplicates) was transferred into a sterile 96-well plate containing 50 μL of H_2O in each well. Release of hemoglobin was monitored at 415 nm using a microtiter plate reader. Percentage hemolysis was calculated using percentage hemolysis = $100 \cdot (A_{415,\ peptide} - A_{415,\ DMSO}) / (A_{415,\ complete\ hemolysis} - A_{415,\ DMSO})$, where complete hemolysis is achieved by mixing hRBCs with 1% TritonX-100. The peptide concentration required to cause 50% hemoglobin leakage was read out from the graph and listed in **Table 2** as HC_{50}.

2. K^+ leakage from hRBCs

The rest of supernatant (1.2 mL) from each sample prepared as described in the hemoglobin leakage assay was transferred into a new sterile eppendorf tube and subject to the K^+ concentration measurement using a flame-atomic emission spectrometer (λ_{em}= 766.5 nm) (Perkin Elmer Atomic absorption Spectrometer 3100, acetylene/air flame). Three readings were taken for each sample and averaged as final results. The fraction of K^+ leakage from hRBCs was calculated as percentage K^+ leaked = $100 \cdot (I_{776.5,\ peptide} - I_{776.5,\ DMSO}) / (I_{776.5,\ complete\ lysis} - I_{776.5,\ DMSO})$. The peptide concentration required to cause 50% K^+ leakage was read out from the graph and listed in **Table 2** as KC_{50}.

3. Toxicity against representative human cell lines

Toxicity of **gA-WT** and **gA-5** were tested against two human cancer cell lines, HeLa and MCF-7 (gifts from professor Eranthie Weerapana at Boston College) by using the MTT assay as described in the protocol provided by Invitrogen. [5] Hela cells (in DMEM high glucose media with 10% FBS, 1% Pen/Strep, 37 ^{o}C, 5% CO_2) and MCF-7 cells (in RPMI media with 10% FBS and 1% Pen/Strep, 37 ^{o}C, 5% CO_2) were grown to about 80% confluence before being removed from the surface of 20 cm petri-dish with 25% trypsin with EDTA (3-5 minutes, 37 ^{o}C, 5% CO_2). Cells were pelleted (3,500 rpm, 5 minutes at 4 °C), and plated at 15,000 cells per well (100 μL per well) in a 96-well plate, then incubated for 48 h before peptide addition.

gA stock solutions in DMSO with varied concentration were prepared so that for each peptide concentration the total volume of DMSO addition was kept constant at 1 μL (1% total volume). For each concentration, samples were set up as four replicates. Control wells were loaded with 1 μL of DMSO. After overnight incubation, cells were washed once with PBS before being incubated for 4 h with 110 μL of 12 mM 3-(4,5-Dimethylthiazol-2-yl)-2,5-diphenyltetrazolium bromide (MTT) dissolved in RPMI midia. The MTT assay was quenched with 100 μL of 10% SDS in 0.01 M HCl and allowed to incubate overnight before absorbance at 570 nm was recorded. Wells were averaged and standard deviations determined for each peptide concentration. Data was normalized to the DMSO control to give % cell survival (Figure2- 3).

VII. ARS competitive binding assay:

First, the association constant for the ARS-PBA complex was determined. This was accomplished by mixing the following two solutions in various ratios: solution A, 10 μM ARS in 0.1 M PBS buffer pH 7.0; solution B, 10 μM ARS and 2 mM PBA in 0.1 M PBS buffer pH 7.0. In the mixture, the ARS concentration is kept constant while the amount of PBA increases as the

amount of solution B increases. Each mixture was agitated gently for 10 minutes before the fluorescence spectrum was recorded (λ_{ex} = 468 nm) in a quartz cuvette on a MicroMax 384 fluorescence spectrometer (Jobin Yvon, Horiba Scientifics). The fluorescence intensity at 582 nm was then plotted against the PBA concentrations. The data was then fitted into an exponential function to obtain the apparent binding constant (K_d).

To determine the binding affinities of the PBA and other 1,2-diol molecules, the competitive binding assay were applied. A third solution was prepared. For small molecules like sugars and glycerol, solution C contains 10 μM ARS and 2 mM PBA together with 1M of sugar or 1.5 M glycerol respectively in 0.1 M PBS buffer pH 7.0.

To test the PBA binding with 1,2-diol presented on the PG containing membrane, PC/PG (1:1) SUVs was used. 97 mg of POPG and 95 mg of POPC was dissolved in MeOH/$CHCl_3$ mixture, and the solution was dried under high vacuum to form a thin layer. The lipids were hydrated with 5 mL of solution B by ultrasonication until the solution becomes transparent (about 20 min). Small unilamellar vesicles (SUVs) formed during the process were filtered through 0.2 μm syringe filters to remove possible aggregates and small amounts of metal tips from the ultrasonication probe. A solution D containing 20 mM lipids (PC/PG 1:1), 10 μM ARS and 2 mM PBA in 0.1 M PBS buffer pH 7.0 was prepared. Solution B and solution C (for PBA-sugar binding) or solution B and solution D (for PBA-PG vesicles) were mixed in various ratios to obtain mixtures with constant amount of ARS, PBA but various amount of 1,2-diol molecules of interests. The mixtures were agitated at room temperature before the fluorescence spectra were recorded as described above.

The binding between the LP3B and 1,2-diols were determined with the same method. Due to the poor solubility of LP3B, a mixture of MeOH and 0.1 M PBS (1/1) pH 7.0 was used as solvent. The addition of MeOH does not affect the ARS-PBA binding, despite an increase in the

absolute fluorescence intensity of the mixture (Figure 2- 27). A solution of 0.5 mM peptide and 10 μM ARS was mixed with 10 μM ARS in various ratios, resulting in a series of solution with constant amount of ARS and various amount of peptide. Then the fluorescence spectra of the mixture were recorded and the data collected was analyzed as described above.

References

(1) Davies, J. D. a. D. *Microbiology and molecular biology reviews* **2010**, *74*, 417.

(2) Livermore, D. M. *Clinical Microbiology and Infection* **2004**, *10*, 1.

(3) Fox, J. L. *Nat Biotech* **2006**, *24*, 1521.

(4) Marc Torrent, D. P., Luis Rivas, David Andreu *Current Drug Targets* **2012**, *13*, 1138.

(5) Fischbach, M. A.; Walsh, C. T. *Science* **2009**, *325*, 1089.

(6) Porter, E. A.; Wang, X. F.; Lee, H. S.; Weisblum, B.; Gellman, S. H. *Nature* **2000**, *404*, 565.

(7) Srinivas, N.; Jetter, P.; Ueberbacher, B. J.; Werneburg, M.; Zerbe, K.; Steinmann, J.; Van der Meijden, B.; Bernardini, F.; Lederer, A.; Dias, R. L. A.; Misson, P. E.; Henze, H.; Zumbrunn, J.; Gombert, F. O.; Obrecht, D.; Hunziker, P.; Schauer, S.; Ziegler, U.; Kaech, A.; Eberl, L.; Riedel, K.; DeMarco, S. J.; Robinson, J. A. *Science* **2010**, *327*, 1010.

(8) Zasloff, M. *Nature* **2002**, *415*, 389.

(9) Shai, Y. *Current Pharmaceutical Design* **2002**, *8*, 715.

(10) Wimley, W. C. *Acs Chemical Biology* **2010**, *5*, 905.

(11) Brogden, K. A. *Nature Review Microbiology* **2005**, *3*, 238.

(12) Shai, Y. *Biochimica Et Biophysica Acta-Biomembranes* **1999**, *1462*, 55.

(13) Huang, H. W. *Biochemistry* **2000**, *39*, 8347.

(14) van Meer, G.; Voelker, D. R.; Feigenson, G. W. *Nat Rev Mol Cell Biol* **2008**, *9*, 112.

(15) Wenk, M. R. *Nat Rev Drug Discov* **2005**, *4*, 594.

(16) Kelkar, D. A.; Chattopadhyay, A. *Biochimica Et Biophysica Acta-Biomembranes* **2007**, *1768*, 2011.

(17) Harold, F. M.; Baarda, J. R. *Journal of Bacteriology* **1967**, *94*, 53.

(18) Moll, G. N.; Vandeneertwegh, V.; Tournois, H.; Roelofsen, B.; Denkamp, J.; Vandeenen, L. L. M. *Biochimica Et Biophysica Acta* **1991**, *1062*, 206.

(19) Fernandez-Lopez, S.; Kim, H. S.; Choi, E. C.; Delgado, M.; Granja, J. R.; Khasanov, A.; Kraehenbuehl, K.; Long, G.; Weinberger, D. A.; Wilcoxen, K. M.; Ghadiri, M. R. *Nature* **2001**, *412*, 452.

(20) Bortner, C. D.; Cidlowski, J. A. *Archives of Biochemistry and Biophysics* **2007**, *462*, 176.

(21) Ketchem, R. R.; Lee, K. C.; Huo, S.; Cross, T. A. *Journal of Biomolecular NMR* **1996**, *8*, 1.

(22) Denise V. Greathouse, R. E. K. I. *Methods in Enzymology* **1999**, *294*, 525.

(23) Shai, Y. *Biopolymers* **2002**, *66*, 236.

(24) Wiegand, I.; Hilpert, K.; Hancock, R. E. W. *Nat. Protocols* **2008**, *3*, 163.

(25) Moll, G. N.; van den Eertwegh, V.; Tournois, H.; Roelofsen, B.; Op den Kamp, J. A.; van Deenen, L. L. *Biochim Biophys Acta* **1991**, *1062*, 206.

(26) Rammelkamp, C. H.; Weinstein, L. *The Journal of Infectious Diseases* **1942**, *71*, 166.

(27) Cherkasov, A.; Hilpert, K.; Jenssen, H.; Fjell, C. D.; Waldbrook, M.; Mullaly, S. C.; Volkmer, R.; Hancock, R. E. *ACS Chem Biol* **2009**, *4*, 65.

(28) Jiang, Z.; Vasil, A. I.; Gera, L.; Vasil, M. L.; Hodges, R. S. *Chem Biol Drug Des* **2011**, *77*, 225.

(29) Meng, H.; Kumar, K. *J Am Chem Soc* **2007**, *129*, 15615.

(30) Bowers, G. N.; Velapoldi, R. A.; (U.S.), N. M. L. **1979**.

(31) Vistica, D. T.; Skehan, P.; Scudiero, D.; Monks, A.; Pittman, A.; Boyd, M. R. *Cancer Research* **1991**, *51*, 2515.

(32) Wimley, W. C.; White, S. H. *Nat Struct Biol* **1996**, *3*, 842.

(33) Tang, M.; Waring, A. J.; Hong, M. *J Am Chem Soc* **2007**, *129*, 11438.

(34) Chen, Y.; Guarnieri, M. T.; Vasil, A. I.; Vasil, M. L.; Mant, C. T.; Hodges, R. S. *Antimicrobial Agents and Chemotherapy* **2007**, *51*, 1398.

(35) Yin, L. M.; Edwards, M. A.; Li, J.; Yip, C. M.; Deber, C. M. *Journal of Biological Chemistry* **2012**, *287*, 7738.

(36) Martin, C.; Zhang, Y. *Nature Review Molecular Cell Biology* **2005**, *6*, 838.

(37) Kouzarides, T. *Cell* **2007**, *128*, 693.

(38) Valkó, K.; Bevan, C.; Reynolds, D. *Analytical Chemistry* **1997**, *69*, 2022.

(39) Lau, S. Y. M.; Taneja, A. K.; Hodges, R. S. *Journal of Chromatography A* **1984**, *317*, 129.

(40) Muller, P. Y.; Milton, M. N. *Nat Rev Drug Discov* **2012**, *11*, 751.

(41) Sakai, N.; Houdebert, D.; Matile, S. *Chemistry – A European Journal* **2003**, *9*, 223.

(42) Hakonen, A.; Hulth, S. *Analytica Chimica Acta* **2008**, *606*, 63.

(43) Sidorov, V.; Kotch, F. W.; Abdrakhmanova, G.; Mizani, R.; Fettinger, J. C.; Davis, J. T. *Journal of the American Chemical Society* **2002**, *124*, 2267.

(44) Brunaldi, K.; Miranda, M. A.; Abdulkader, F.; Curi, R.; Procopio, J. *Journal of Lipid Research* **2005**, *46*, 245.

(45) Arcisio-Miranda, M.; Abdulkader, F.; Brunaldi, K.; Curi, R.; Procopio, J. *Archives of Biochemistry and Biophysics* **2009**, *484*, 63.

(46) Vivian, J. T.; Callis, P. R. *Biophysical Journal* **2001**, *80*, 2093.

(47) Marr, A. K.; Gooderham, W. J.; Hancock, R. E. W. *Current Opinion in Pharmacology* **2006**, *6*, 468.

(48) Goldman, M. J.; Anderson, G. M.; Stolzenberg, E. D.; Kari, U. P.; Zasloff, M.; Wilson, J. M. *Cell* **1997**, *88*, 553.

(49) Fujita, N.; Shinkai, S.; James, T. D. *Chemistry – An Asian Journal* **2008**, *3*, 1076.

(50) Ellis, G. A.; Palte, M. J.; Raines, R. T. *Journal of the American Chemical Society* **2012**, *134*, 3631.

(51) Jin, S.; Cheng, Y.; Reid, S.; Li, M.; Wang, B. *Medicinal Research Reviews* **2010**, *30*, 171.

(52) Springsteen, G.; Wang, B. *Tetrahedron* **2002**, *58*, 5291.

(53) Halo, T. L.; Appelbaum, J.; Hobert, E. M.; Balkin, D. M.; Schepartz, A. *Journal of the American Chemical Society* **2008**, *131*, 438.

(54) Mahalingam, A.; Geonnotti, A. R.; Balzarini, J.; Kiser, P. F. *Molecular Pharmaceutics* **2011**, *8*, 2465.

(55) Springsteen, G.; Wang, B. H. *Chemical Communications* **2001**, 1608.

(56) Afonso, A.; Rosés, C.; Planas, M.; Feliu, L. *European Journal of Organic Chemistry* **2010**, *2010*, 1395.

(57) Duggan, P. J.; Offermann, D. A. *Australian Journal of Chemistry* **2007**, *60*, 829.

(58) Huang, Z.-P.; Du, J.-T.; Zhao, Y.-F.; Li, Y.-M. *Int J Pept Res Ther* **2006**, *12*, 187.